ANALYSIS OF THE F-LATTICE USING SCALE AND MCNP5

BY

STEVEN AARON WEISS

B.S., University of Illinois at Urbana-Champaign, 2007

THESIS

Submitted in partial fulfillment of the requirements
for the degree of Master of Science in Nuclear Engineering
in the Graduate College of the
University of Illinois at Urbana-Champaign, 2008

Urbana, Illinois

Advisers:

Professor Rizwan-uddin
Professor James F. Stubbins

Abstract

ANALYSIS OF THE F-LATTICE USING SCALE AND MCNP5

Steven Weiss, M.S.
Department of Nuclear, Plasma and Radiological Engineering
University of Illinois at Urbana-Champaign, 2008
Rizwan-uddin, Adviser

The current resurgence of interest in the nuclear power industry has led to renewed interest in new reactor designs. The GE Compact Modular Boiling Water Reactor (CM-BWR) is one such reactor. The 350 MWe CM-BWR is designed for small incremental additions to the power grid. A key feature of the CM-BWR is the use of the unique F-Lattice. The F-Lattice employs a staggered row configuration for the control blades. Additionally, the control blades are more than double the width of control blades found in most commercial boiling water reactors today. Increase in blade width and pitch allows for approximately a one-half factor decrease in the number of control blades. Reduction in control blades results in a large reduction in control rod related components. This reduces construction and maintenance costs, as well as reducing the risk of failures within the core. However, before design certification can be completed for the CM-BWR, first the tools needed to design and monitor reactor core performance must be validated.

In this thesis, two versions of the SCALE package are validated to accurately model the F-Lattice by comparing their results against MCNP5 benchmark results. Multiplication factor and flux distribution are compared. The techniques necessary to

analyze the flux calculations on a spatial grid were developed for the SCALE output. To compare flux distributions it was necessary to process the SCALE output and generate flux distributions in the same units as those employed in MCNP. A code is written in Perl to accomplish this task. Limitations of the supplement code, as well as limitations of the SCALE packages are discussed in detail. In addition, parametric studies are performed to determine rod worth and the effect of small and large perturbations to the geometry. Results are obtained for variation in material properties and change in control blade thickness. Suggestions for future work are given.

Acknowledgments

The work done in this thesis was possible thanks to the help and support of many. An important thank you to my advisor, Rizwan-uddin, whose patience and motivation helped guide this project from start to finish. Also, thanks to my girlfriend, Jenny deAngelis, who provided me with clarity and purpose. I would like to acknowledge the SCALE group at Oak Ridge National Lab, specifically Stephen Bowman, for the generous technical help on a variety of topics. And finally, I would like to thank the Nuclear, Plasma and Radiological Engineering department at the University of Illinois for providing an encouraging and enjoyable atmosphere to learn and work, during both my undergraduate and graduate years; and also, for the financial support that the department has provided in the forms of assistantships and fellowships.

Table of Contents

List of Figures

List of Tables

Chapter 1: Introduction

1.1 Introduction

Two key factors for development of new products in the nuclear power industry are safety and cost. With both these issues in mind, any possible modification to a nuclear reactor that can decrease cost while improving, or at the very least maintaining, safety is deemed highly desirable. Many new reactor designs that accomplish these goals have been proposed. Among these is the GE Nuclear Energy Compact Modular Boiling Water Reactor (CM-BWR). The design goal of the CM-BWR is to reduce the complexity, size, cost and number of overall parts in the reactor and reactor building [Fennern et al. 2003]. Further, a modular reactor will depend largely on factory fabrication of many or all parts, which would ideally allow mass production of these. The CM-BWR could be implemented into the smaller power grids of developing countries as part of the Nuclear Fuel Leasing Initiative that was developed as part of the Global Nuclear Energy Partnership (GNEP) [DOE 2007].

Under the GNEP program, nations would be split into supplier nations, referred to as "fuel cycle" states, and into "reactor" states, which would lease fuel from the supplier nations and return the spent nuclear waste for reprocessing or disposal. Reactor states would benefit from the technology of the more developed nations, as well as avoid the financial, environmental and political issues involved in the enrichment and production of nuclear fuel. Fuel cycle states would benefit from the sale and leasing of both nuclear reactors and fuel [Reis et al. 2004]. Most

importantly, the fuel leasing initiative will allow more countries to pursue the financial and environmental benefits of carbon-free nuclear energy while decreasing the proliferation concerns that surround the industry.

Rated at 350 MWe, the CM-BWR could be leased to reactor states that require incremental additions in power supply. Designed with a passive closed loop system that utilizes natural circulation, it is believed to be a very safe and low maintenance reactor. Additionally, the CM-BWR containment vessel is based on an already commercially tested reactor, the GE Advanced Boiling Water Reactor (ABWR) [Fennern et al. 2003]. Thus, no new infrastructure, technology or manufacturing capabilities would be necessary to produce the CM-BWR commercially. Safety, efficiency in construction and maintenance, low cost and the ability to address proliferation concerns make the CM-BWR an ideal candidate for developed, as well as developing countries.

1.2 Objective

A key feature of the CM-BWR is a new core lattice design, known as the Four-Bundle Lattice (F-Lattice). Compared to the current lattice in BWRs, the F-Lattice utilizes an increased control blade width with a staggered row configuration. (A detailed description of the F-Lattice and the reactor is given in Chapter 4.) Increasing the width and staggering the blades allows for a reduction in the total number of control rods needed in the core. Originally designed for the GE Economically Simplified Boiling Water Reactor (ESBWR), the F-Lattice has not yet been built and tested. To expedite the NRC licensing process for the ESBWR, GE decided to return to a more standard control blade and lattice design. However, had

the F-Lattice been retained in the ESBWR design, there would have been nearly half the number of control rods in the core: 137 as opposed to 269 [Challberg 1998].

Fewer control rods also means a reduction in material and manufacturing costs, fewer drives, hydraulic control units and piping. Furthermore, there would have been approximately half the number of control rod related components requiring maintenance or posing the risk of failure. This correlates into a reduction in cost and an increase in safety; the two key goals of all design modifications in a nuclear reactor. While the F-Lattice is no longer a part of the ESBWR, it still remains a key component for the CM-BWR design. Therefore, study and analysis of this new lattice design must be performed before the CM-BWR design can be completed.

The F-Lattice design is investigated in this thesis. The reactor is modeled using the Los Alamos National Lab code, MCNP5, as well as using the SCALE-5 and SCALE-5.1 code packages developed at Oak Ridge National Lab. This thesis is focused on lattice design and analysis codes to analyze the F-Lattice. Simulation codes must be validated before they can be used for design or analysis. As an industry wide standard, the MCNP5 code is chosen for benchmark results. While MCNP can be used for design and analysis, it is computationally intensive. Hence it is desirable to determine if less computationally demanding codes, such as the SCALE packages, can also provide reliable results but in less computational time.

This thesis has two main objectives related to the analysis of the F-Lattice. The first objective is to provide partial validation of the SCALE packages for an F-Lattice reactor by comparing their results with MCNP5 generated benchmark results. Validation of the SCALE packages abilities to calculate accurate effective

multiplication factor and power distribution for the F-Lattice is provided. Additionally, neutron flux distributions are compared and validated. Tools and techniques are developed in this thesis to accurately validate the neutron flux from the SCALE packages on a spatial grid. Complete validation of the codes' other capabilities is left for future work. In the process, conditions under which SCALE-5 and SCALE-5.1 are suitable to model the F-Lattice are detailed. The second objective is to perform parametric design studies of the F-Lattice. Areas of particular interest are the effect of increased blade width and increased control rod pitch, particularly with respect to the neutron fluence throughout the system. To that end, a parametric study of the effects of the control blade is performed. Additionally, the F-Lattice control blade rod worth is determined by analyzing the reactivity effect of instantly removing the control blade and replacing it with a graphite moderator.

1.3 Literature Review

Previous work has been done on the F-Lattice, and to validate the SCALE packages. Only a few papers are available in open literature on the F-Lattice design because it is currently only a design concept with no current production plans. Validation of the SCALE packages has been done extensively for various problems. However, most of these have focused on validating the k-effective calculations. Author has not found any previous work that compares flux or power distributions determined using KENO codes with those obtained using MCNP. Relevant literature on these topics is discussed below.

As a design concept, the F-Lattice has undergone rigorous review at GE Nuclear. Challberg [1998] provided a very detailed approach and motivational reasoning for

the use of the F-Lattice in the ESBWR. The F-Lattice was eventually removed from the ESBWR design but it was later chosen for the CM-BWR design. In 2003, the GE Nuclear Energy and the Japan Atomic Power Company,[Fennern et al. 2003] reported the progress on the design of the CM-BWR. However, Fennern et al. raised several questions that needed to be addressed prior to design certification. Among these issues was the need to develop and validate codes to "accurately predict the performance of the fuel when the F-Lattice with its larger control blades are utilized." This thesis begins that work by validating and analyzing the current tools available. Challberg [1998] and Fennern et al. [2003] are the primary sources of information for the F-Lattice.

The tools available to analyze the F-Lattice include, but are not limited to, the MCNP codes and the SCALE packages. Comparison of SCALE against MCNP benchmarks for the F-Lattice is one of the focus areas of this thesis. Similar validating exercises have been reported earlier for other systems. For example, Johnson and Clarno [2007] provide a systematic approach to compare the results provided by MCNP5 and SCALE-5.1. In this paper, Johnson and Clarno studied a pebble bed reactor which requires addressing the double heterogeneity issues associated with the PBMR fuel. Seven different cases were studied with the two codes and the main focus of validation was comparison of the effective multiplication factor. The approach used by Johnson and Clarno to compare k-effective values will be followed in this thesis.

Previous work on validating codes for new reactor designs have also been used as reference points for this thesis. The Oak Ridge National Laboratory report titled

Code-to-Code Benchmark of Coolant Void Reactivity (CVR) in the ACR-700 Reactor [Clarno et al. 2005] compared four code packages; MCNP5, KENO-VI, NEWT and HELIOS version 1.7. Again the effective multiplication factor was studied closely, this time due to concern related to SCALE's use of the Dancoff factor with respect to pin-to-pin resonance shielding. For the ACR-700, specifically of interest was the Coolant Void Reactivity (CVR). Clarno et al. compared k-effective values for the beginning-of-life, middle-of-life and end-of-life cores.

Additional comparisons for neutron spectrum were made by Johnson and Clarno [2007] to show that discrepancies appear in the thermal energy spectrum due to cross-section differences that result from the use of discrete energy group averaging. Additional differences were found in the 3 eV range as a consequence of the fact that SCALE neglects up-scattering above this energy. In addition to validating the k-effective values, spatial flux or power distributions obtained using the SCALE packages are also compared with those obtained using MCNP in this thesis.

1.4 Thesis Organization

An outline of the thesis is given below.

- Chapter 2: A description of the codes used in this thesis and their input formats is given. The goal of this chapter is to provide a background to allow the comparison between SCALE and MCNP results.

- Chapter 3: This chapter is on testing and analysis of the different code packages. The computational costs involved with the SCALE-5 KENO-Va, SCALE-5.1 KENO-VI and MCNP5 are compared.

- Chapter 4: This chapter outlines the design of the F-Lattice in more detail. The F-Lattice is analyzed for k-effective, as well as the flux distribution using the SCALE and MCNP5 codes. New techniques needed to make flux comparisons possible, along with the explanation of a necessary supplement code script in Perl, FluxParse.pl, are discussed.

- Chapter 5: Results of parametrically varying geometry and material properties within the F-Lattice, including some rod worth results, are reported. This chapter also provides additional, more detailed results of neutron flux profiles for each parametric variation using the capabilities provided by MCNP5.

- Chapter 6: Results are summarized and concluding remarks are given in Chapter 6. Issues to be further researched in the future are also suggested.

Chapter 2: Code Background

This chapter provides a background on the Monte Carlo method and the codes used in this thesis. Limitations to compare the results of the SCALE packages and those obtained using MCNP are discussed.

2.1 Monte Carlo Method

The Monte Carlo Method is a statistical technique for solving problems that are of a probabilistic nature. In this method a sequence of random numbers is employed to simulate the physical process or the problem being analyzed. Probabilities are assigned to all possible outcomes of the specific event being modeled. After the total probability distribution function of events is constructed, the outcomes these probabilities indicate can be assigned to sets of random numbers which are often sampled on the continuous set, 0.0-1.0. This assignment of number sets to specific probabilities and events is known as the cumulative distribution function, which allows for any given process to be simulated through repetition and use of a random number sequence. By repeating a process numerous times with different sequences of random numbers, various statistical conclusions can be drawn about the expected outcome of the process being modeled. Also known as the "Method of Statistical Trials", the Monte Carlo Method can be simply described as a numerical method for solving mathematical problems by means of random sampling [Ragheb 2007].

While it may seem that a technique requiring a high number of repetitions with varying random data sets would be arduous and inefficient, the Monte Carlo Method actually has many advantages over deterministic solution techniques. Deterministic

techniques are often suitable and preferred for problems of low complexities. However, they become cumbersome when applied to complex problems, particularly in the case of modeling atomic interactions on a large scale. In the case of neutronics, deterministic techniques include analytical or numerical solutions of the transport, or diffusion equation. The first limitation is that many systems of interest have no analytical solution. Secondly, approximations and assumptions must then be introduced and the governing equations are solved numerically. In doing this, the physics of the problem can be compromised. An example of the approximations needed in deterministic methods is the need to use homogenized cross sections, particularly for models that have several regions which are separated by less than the system's neutron mean free path. Deterministic approaches, such as finite difference or control volume schemes, are not suitable to properly model the variation in the system geometry without homogenization techniques, which allow different materials to be represented by equivalent homogenized regions. Homogenized cross sections however have their own limitations and cannot capture the variations within the homogenized regions accurately. Monte Carlo techniques allow for highly complicated geometries and nuclear data sets to be modeled in the exact same manner as are much simpler problems. Results are expressed as averages or means of repeated data events and must be accompanied by the appropriate variances and uncertainties. Application of Monte Carlo techniques can be highly computer intensive and require a large amount of time to obtain results with acceptable levels of uncertainties. For these reasons, deterministic techniques are still the preferred approach for design and analysis. However, as computational power drastically increases, and with

the need to model increasingly more complex problems, the Monte Carlo Method is being increasingly used for lattice design.

2.2 MCNP

The Monte Carlo N-Particle (MCNP) code is a Monte Carlo code developed at the Los Alamos National Laboratory for detailed simulations of atomic interactions. MCNP is a general-purpose code that can be used for coupled neutron, photon and electron transport in a system [X-5 Monte Carlo Team 2003]. It is capable of modeling complex 3D geometries and utilizes extensive point-wise cross-section data libraries on a continuous energy spectrum. These data libraries provide the necessary probability distributions for simulating particle interactions through use of random number sampling. The simulations sequentially follow the history of all individual particles from birth to death. Through a large number of repetitions MCNP is capable of determining k-effective, neutron flux, current and many other desired system traits. Increasing the number of system histories utilized, as well as increasing the number of particles tracked in each history, provides more detailed results, though at the expense of higher computational costs. MCNP5 version of the code is used in this thesis.

2.3 MCNP5 Input

MCNP5 is a FORTRAN code. MCNP5 input files are composed of 4 types of cards: a title card, cell cards, surface cards and data cards. The following information and formats can be found in further detail in the MCNP Criticality Primer [Dupree et al. 2003].

The title card is merely the first line of the input file and is used as a label for the system being modeled. It can be up to 80 characters long and is echoed throughout the output file in order to keep track of the file being compiled and run.

Following the title card are the cell cards. Cell cards are used to define the shapes and material composition in physical space being modeled. They are defined by relating various surface cards and material data cards in a manner so that a cell encompasses a fully closed set of space. The format of the cell card is as follows:

```
j          m     d     geom       params
```

j = Cell number, starting in columns 1-5.
m = Material number (0 if cell is a void).
d = Cell material density:
No entry if the cell is a void.
Positive entry = atom density (atoms/b-cm).
Negative entry = mass density (g/cc).
geom = List of all signed surface numbers and Boolean operators that specify a cell.
params = Optional specification of cell parameters.

After the cell cards are the surface cards, which define a specific geometric shape (plane, cylinder, sphere, etc…) and its location in physical space. Its format is:

```
j     a     list
```

j = Surface number, starting in columns 1-5. (1-99999)
a = Surface mnemonic. (plane, sphere, cylinder, etc.)
list = Numbers that describe the surface.
(dimensions, radius, etc., in cm)

The final cards in the input deck are known as data cards. Data cards include material cards, which define the material composition and the data libraries which

contain their material properties. Data cards also specify the type of problem being defined and can be used to define initial particle source locations, as well as criticality convergence requirements. Additional data tally cards can be utilized for desired information, such as flux values. The formats of these respective data cards are:

Material Card

```
                mn zaid1 fraction1 zaid2 fraction2 ….

   mn = Material card name (m) followed immediately by the
        material number (n) on the card.  The mn cards starts
        in columns 1-5.
   zaid = Atomic number followed by the atomic mass of the
        isotope.  Preferably (optionally) followed by the data
      library extension, in the form of .##L (period, two
      digits, one letter).
fraction =  Nuclide fraction
          (+) Atom weight
          (-) Weight fraction
```

Source Card

ksrc x_1 y_1 z_1 x_2 y_2 z_2 ... x_n y_n z_n

ksrc = Card name for initial fission source location. Starts in columns 1-5.

x_k y_k z_k = Location of the k^{th} initial fission source point.

Criticality Card

kcode nsrck rkk ikz kct

kcode = Card name for criticality calculation. Starts in columns 1-5.

nsrck = Number of neutrons per cycle.

rkk = Initial guess for k_{eff}.

ikz = Number of cycles skipped before accumulating data.

kct = Total number of cycles to be run.

Further details and data card types can be found in the MCNP5 Criticality Primer and MCNP5 Manual.

2.4 SCALE

Commissioned by the Nuclear Regulatory Commission in the late 1970s, Software Computer Analyses for Licensing Evaluation (SCALE) was developed by Oak Ridge National Laboratory. It incorporates several code packages in to one module allowing for ease of use of various codes, focusing on applications related to nuclear fuel facilities, and analysis for reactor licensing. SCALE is composed of various packages for cross-section processing: BONAMI, NITAWL, CENTRM, PMC and XSDRNPM. Other packages included are SCALE Material Optimization and REplacement Sequence (SMORES), Tools for Sensitivity and UNcertainty Analysis Methodology Implementation (TSUNAMI) in 1-D and 3-D, STandard Analysis for Reactivity for BUrnup Credit using SCALE (STARBUCS), Criticality Safety Analysis Sequence (CSAS) and the Monte Carlo KENO packages. CSAS6 for KENO-VI is newly introduced to SCALE version 5.1 and provides for problem-dependent cross–section processing and criticality calculations [SCALE: A Modular Code 2005]. KENO-VI allows for more complicated geometry structures than KENO-Va, providing the ability to create any geometry that can be defined by quadratic equations. Furthermore, KENO-VI allows geometry intersections. Of particular interest is the ability to have surfaces that share touching boundaries, a feature not available in KENO-Va. However, the new features in SCALE-5.1 and KENO-VI packages have added costs. Specifically, there is a decrease in detail that can be extracted and there is a significant increase in computational costs. The issue of computational cost associated with KENO-VI is studied in detail in

Chapter 3. Chapter 4 addresses the decreased level of details, specifically involving mesh limitations for flux distributions, which are present in the SCALE packages.

All SCALE packages can be controlled from setup and execution to results and analysis using the Windows Graphical User Interface (GUI) known as Graphically Enhanced Editing Wizard (GeeWiz). GeeWiz is a very user friendly GUI that allows a beginner user of SCALE to quickly develop a model of their system. Through GeeWiz, users are able to specify geometry, material composition, homogenization controls, criticality tests and other useful modeling parameters. Various sample problems are included in the SCALE manual [Scale: A Modular Code 2005] and the KENO-Va Primer for Criticality [Busch and Bowman 2005].

SCALE's advantage is in its ease of use. SCALE is limited by geometries that it can model, as well as by how the modeling can be done. SCALE is limited to composites of rectangular, cylindrical or spherical shapes, though KENO-VI has made advances in this area. Even more limiting is the fact that systems must be modeled with all new shapes encompassing all shapes modeled earlier in the system. This means that no individual shape can stand alone. An example of this is that two cylinders cannot be modeled side-by-side but must instead be modeled inside a larger rectangular shape. This simple model, shown in Figure 2.1, requires a three step approach. First, one of the cylinders must be modeled as an individual geometric unit. Second, the other cylinder is modeled as a region within the rectangular, or cuboid, unit. The second cylinder and the cuboid are grouped as one geometric unit. The final, and third step is that the first cylinder must be inserted (referred to as "hole" in SCALE terminology) into the cuboid unit. This is necessary even if the cuboid unit, shown as blue in Figure 2.1, is vacuum.

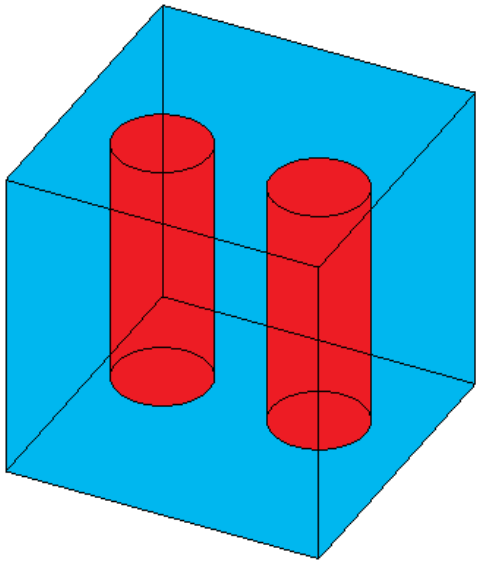

Figure 2.1: Model of two cylinder example.

Another limitation of KENO-VI is that it is a multigroup, stochastic, Monte Carlo transport code with spherical harmonics approximations (P_n) for anisotropic scattering [Clarno et al. 2005]. Since MCNP5 is capable of continuous-energy stochastic transport calculations with exact geometries and specified temperatures, it is expected that MCNP and KENO will lead to somewhat different results. SCALE-5.1 includes improved pin-to-pin resonance shielding as well as improved CENTRM resonance processing methods for AMPX cross sections, allowing for more accurate multigroup cross sections [Scale: A Modular Code 2005]. MCNP and KENO depend on different cross-section libraries for some isotopes and interactions, particularly for the initial generation, so variation in results is expected. SCALE contains a 238-energy-group neutron cross-section library based on ENDF/B-V and ENDF/B-VI, as well as a 44-group library collapsed from ENDF/B-V [Scale: A Modular Code 2005].

A simple example problem is solved in the following chapter to compare the computational cost of MCNP and the SCALE packages. This is important because cost

and efficiency must also be considered when choosing the tools needed to accurately model the F-Lattice.

Chapter 3: Computational Cost Comparisons

The computational cost associated with MCNP5 and the SCALE packages is investigated in this chapter using a simple model of a core with plate fuel. The goal is to determine the simulation conditions (mesh size, geometry, etc) under which one code is more efficient than the other code. Sample input files for a SCALE-5.1/KENO-VI, SCALE-5 KENO-Va and MCNP5 are provided in Appendix A.

3.1 Computational Time Comparisons

The SCALE packages are intended for ease of use and low computational cost. However this comes at the loss of accuracy and limitations on geometries that can be faithfully modeled. On the other hand, MCNP is intended for accurate simulations of complex problems. It however, does not provide as user friendly an environment for development as SCALE. Moreover, it is considered to have a very large computational cost. The computational cost of the three codes is investigated as the model complexity is increased. The following tests were performed.

Simulations for only basic k-effective calculations, as well as simulations for flux, along with k-effective, calculations are carried out. Flux calculations require more detailed evaluations in order to keep track of neutron fluence throughout the system. These more detailed simulations are more computationally intensive than the simulations for only k-effective calculations, but they provide additional, pertinent information. The computational costs of simulations for only k-effective calculations are however important because a large fraction of design and analysis simulations are for k-effective only.

The system modeled is the central assembly in a core with plate fuel. Four fuel plates are contained within a light water container. The dimensions of the entire system are 45 cm in the x-direction, 30 cm in the y-direction and 110 cm in the z-direction. The dimensions of each fuel plate are 5 cm in the x-direction, 20 cm in the y-direction and 100 cm in the z-direction. There is a 5 cm spacing between each plate and the edge plates and the boundaries. A cross-sectional view of the system is given in Figure 3.1 and in Figure 3.2. These images were generated using the MCNP visual editor, VisEd. Mirror boundaries conditions were imposed in the x and y directions, assuming perfect reflection of all neutrons. Particles are allowed to leak out of the system in either the negative or positive z direction.

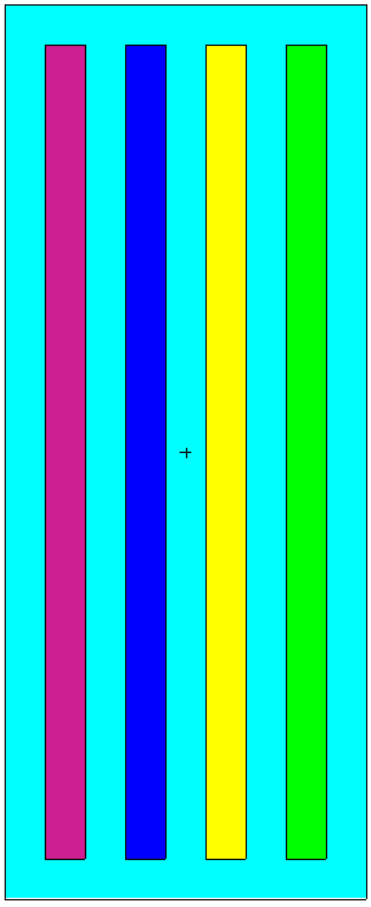

Figure 3.1: A cross-sectional view of the x-z plane for a simplified plate fuel reactor.

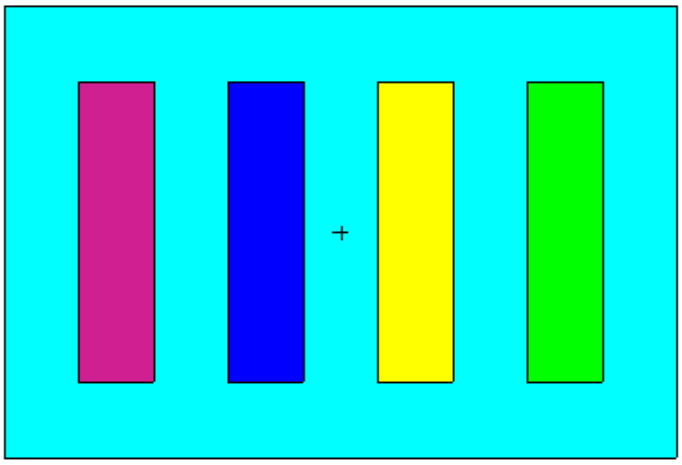

Figure 3.2: A cross-sectional view of the x-y plane for a simplified plate fuel reactor.

Each fuel plate is composed of enriched UO_2 fuel. The enrichment levels, in weight percent, are 2%, 3%, 4% and 5%, respectively for each plate, increasing in the x-direction (for Figure 3.2, purple represents a 2% enrichment level, green a 5% enrichment).

Flux calculations require the use of a mesh, which divides the model into different cells. (The individual "cell" of the mesh should not be confused with a unit "fuel cell", which describes the grouping of fuel, gap, clad and surrounding water as one geometric unit) Flux results are then averaged within each cell. A more refined mesh leads to smaller cells, which reduces the effect of averaging. Smaller cells lead to more accurate flux distributions. The flux, or power, distribution can be determined with the average flux results for each cell. A superimposed mesh is independent of the model and geometric or material properties. A superimposed mesh is not necessary for k-effective.

Here, the goal is to determine the neutron flux distribution, and in so doing, determine the effect of increasing mesh refinement on the computational efficiency of the two codes.

A superimposed mesh that covers only desired specific locations in the model can be specified in MCNP5. Mesh cell size can be varied for each individual direction and different size meshes can be placed in different parts of the system. The SCALE-5.1 package does not allow for a superimposed mesh. Instead, flux values are reported for each geometry unit. This means that in order to obtain more spatially detailed results, the model must be broken up into smaller constituent geometry units even if geometric units are materially alike [Busch and Bowman 2005]. Additionally, fluxes are reported for all units since there is no option to indicate only specific geometry units of the model where flux results are desired.

Mesh refinement is introduced in the z-direction only. For MCNP5, this is a simple task of increasing the mesh size in each fuel blade as the number of desired mesh cells increases. For SCALE-5.1, this requires that smaller and smaller blocks of fuel be used in the z direction. These smaller blocks are then stacked on top of each other to develop a "mesh" of the complete fuel plate. These tests are carried out for KENO-Va and KENO-VI inside the SCALE-5.1 package. [The importance of comparing KENO-Va and KENO-VI is that KENO-VI was specifically developed for enhanced abilities to handle more complex geometries.] The time required for each simulation is compared. Increased CPU time indicates that more computer resources are needed for the simulation.

It is important to note that the SCALE-5 package does allow superimposing a mesh over the entire system. However, this mesh must have equal spacing in all dimensions (uniform) and cannot be localized to specific locations. Due to the inability to specify non-uniform mesh, or to define the mesh over only specific parts of the model,

a direct comparison of the SCALE-5 package cannot be made to the SCALE-5.1 package for this model. Therefore a second set of tests were performed to directly compare the performance of KENO-Va (within the SCALE-5 package) with MCNP5. Identical mesh sizes are used in both codes, again with the objective of determining the computational cost as a function of the grid size.

3.2 Efficiency Tests: MCNP5 and SCALE-5.1 (KENO-Va and KENO-VI)

These tests were performed using a 2 GHz Intel Core2 CPU processor with 2 GB of RAM. Simulations were carried out for 1, 2, 5, 10, 50 and 100 mesh cells in the z direction, and with 1,000 and 10,000 particles. The 1, 2, 5, 10, 50 and 100 mesh cells correlate to mesh sizes of 100 cm, 50 cm, 20 cm, 10 cm, 2 cm and 1 cm, respectively in the z direction. The reported flux were averaged over the entire x-y plane of each individual fuel plate (5 cm by 20 cm rectangle), the cross-sectional image shown in Figure 3.2. Examples of the meshes, in the z direction, for 5 cells (20 cm) and 10 cells (10 cm) are shown in Figure 3.3 and Figure 3.4, respectively. Computational costs are compared for the two codes in Fugre 3.5 and Figure 3.6.

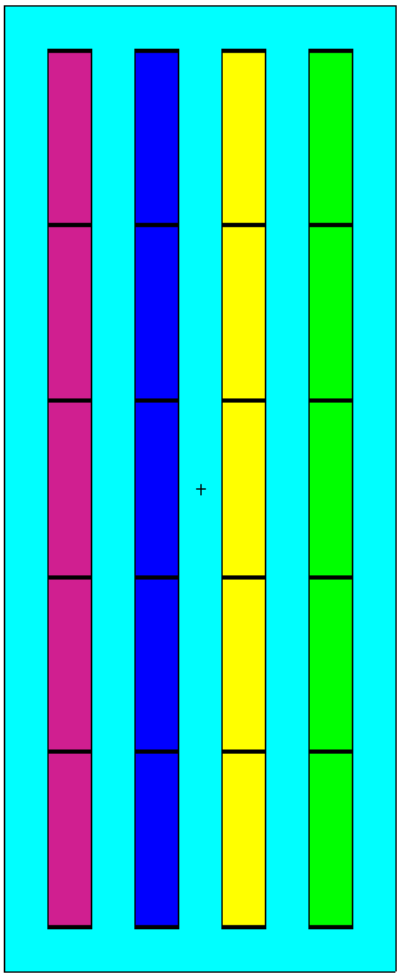

Figure 3.3: 5 cell (20 cm) mesh in the z direction.

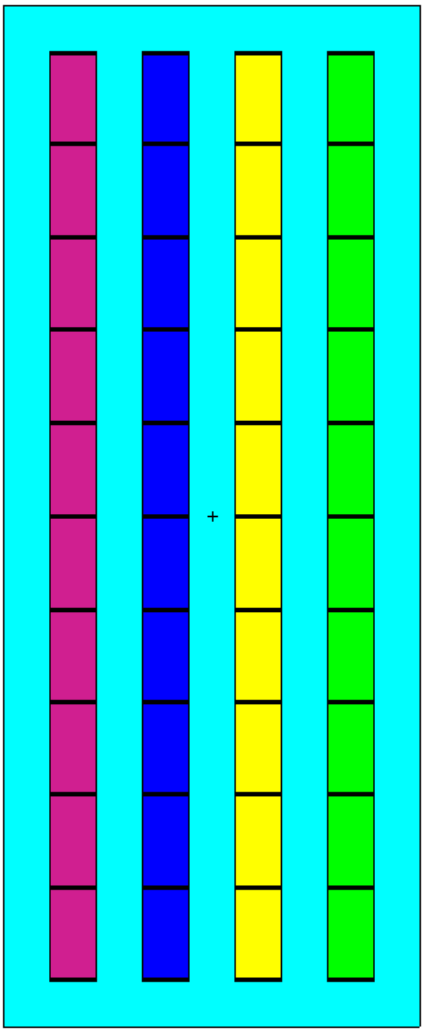

Figure 3.4: 10 cell (10 cm) mesh in the z direction

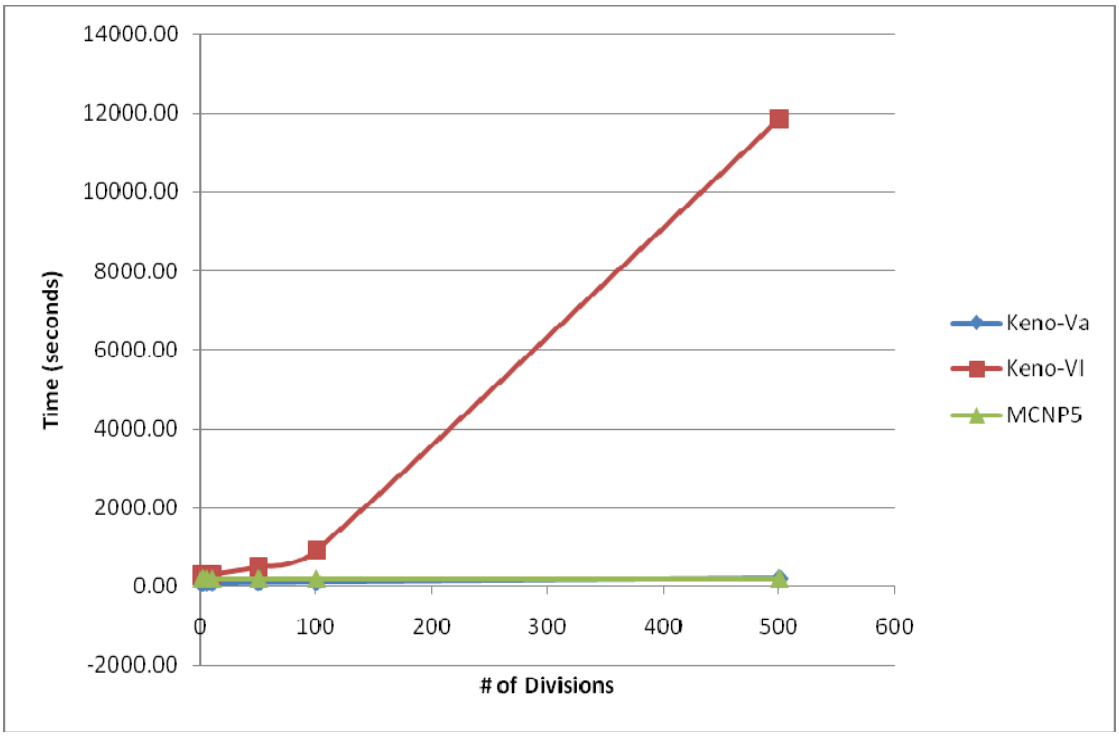

Figure 3.5: Results of computational efficiency tests with 1,000 particles and up to 500 cells.

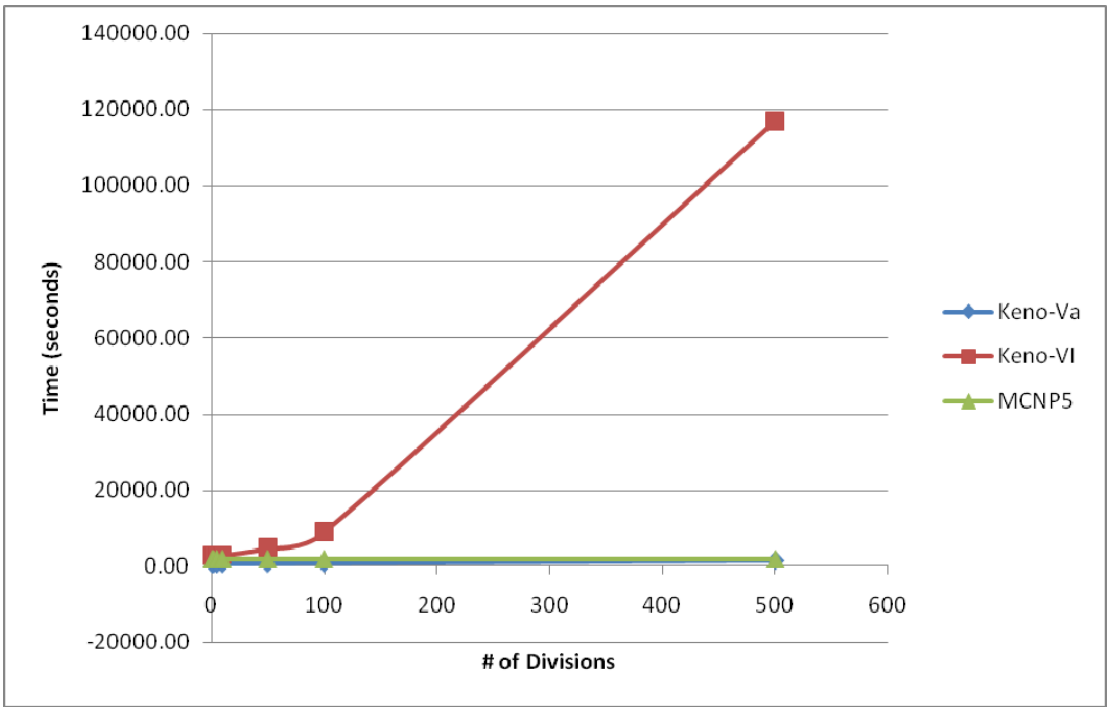

Figure 3.6: Results of computational efficiency tests with 10,000 particles and up to 500 cells.

Results show that CPU time for MCNP5 remains essentially constant as mesh is refined. KENO-Va shows a very slight increase in CPU time requirements as mesh refinement is increased but remains less costly than MCNP5. Most interesting result is that KENO-VI is the most computationally expensive even for coarse mesh, showing a dramatic increase in CPU time as the number of cells increases. For a more relative comparison of the two KENO codes, Figure 3.7 shows the ratio of the CPU time for the two codes as a function of number of cells.

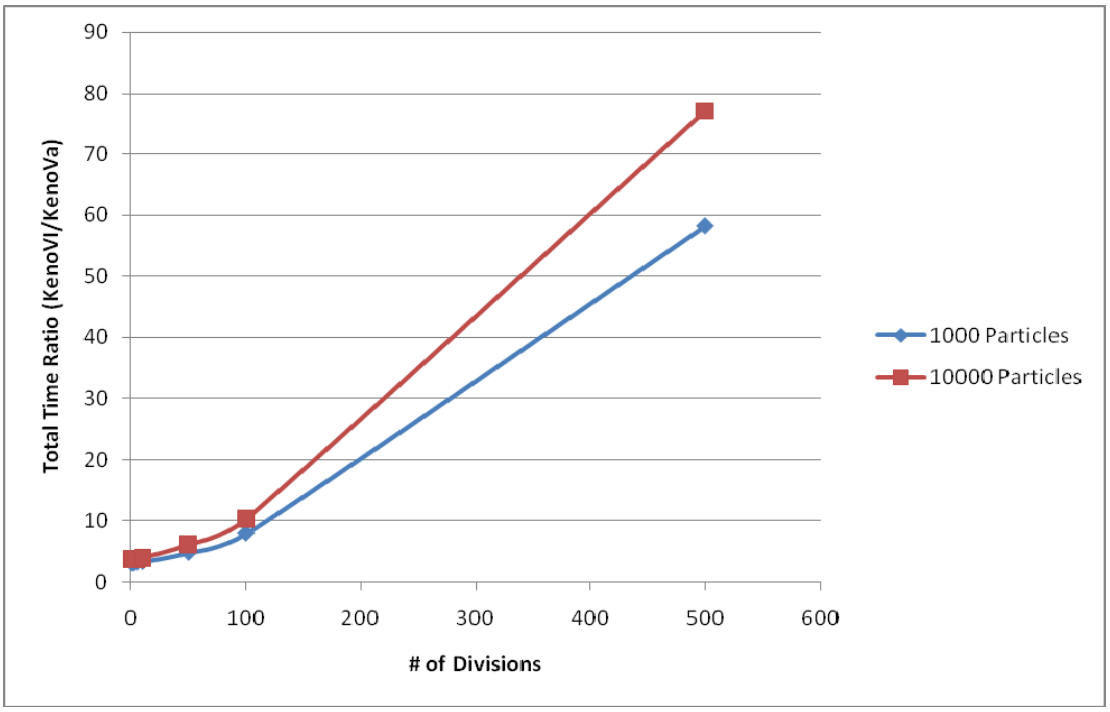

Figure 3.7: CPU time ratio for KENO-VI relative to KENO-Va

Figure 3.7 shows that KENO-VI is approximately a factor of 3-4 slower than KENO-Va for up to about 100 cells. As the number of cells increases KENO-VI can be up to 80 times slower when used with 10,000 particles or 60 times slower with 1000 particles than KENO-Va. Table 3.1 shows the relative CPU times for the 1,000 particle and the 10,000 particle cases respectively.

Mesh Cells	CPU KENO-VI / CPU KENO-Va
1	3.14
2	3.19
5	3.26
10	3.40
50	4.88
100	7.98
500	58.18

(a) 1,000 particles

Mesh Cells	CPU KENO-VI / CPU KENO-Va
1	3.84
2	3.86
5	3.91
10	4.09
50	6.20
100	10.42
500	77.10

(b) 10,000 particles

Table 3.1: CPU time for KENO-VI relative to KENO-Va.

The effect of increased problem complexity, without flux calculations, was also studied by comparing the CPU time for different systems. CPU times for four systems were compared for KENO-Va and KENO-VI. Only the basic criticality calculations are performed. [Additional calculations, such as for flux, were not performed.] The most basic system analyzed was a homogeneous cube of UO_2 with 5 weight percent enriched U-235. The cube is twenty centimeters in each direction. One thousand particles were used for the k calculation. The next system studied was the slab geometry system discussed previously in this section, but without the flux calculations. Results for the 1,000 particle case are reported. Both the 4-bundle and 16-bundle F-Lattice cases are also studied for increasing complexity. [A detailed description of these systems is provided in Chapter 4.] The F-Lattice systems were run with 10,000 particles. All cases were run for 600 total generations with 200 inactive cycles. The results are shown in Table 3.2.

System	SCALE-5 KENO-Va Time (s)	SCALE-5.1 KENO-VI Time (s)	VI/Va Total Time
Cube	148.24	201.51	1.36
Slabs	137.93	278.8	2.02
4-bundle	1155.94	5676.29	4.91
16-bundle	1336.01	6345.09	4.75

Table 3.2: CPU time comparisons for KENO-Va and KENO-VI for criticality only calculations.

The results shown in Table 3.2 further support those shown in Table 3.1. They show that as complexity increases, the CPU time for KENO-VI relative to KENO-Va continues to grow even when only k-effective is being calculated. The 16-bundle case shows a slight decrease in relative time compared to the 4-bundle case. However, as described later in Section 4.3, the geometric complexity of the KENO-Va model actually increases more significantly from the 4-bundle case to the 16-bundle case than it does for the KENO-VI model. This is due to the advanced modeling capabilities of KENO-VI to allow overlapping geometric boundaries. The overall conclusion can still be drawn that KENO-Va is significantly less computationally intensive than KENO-VI, and the relative CPU time continues to grow with system complexity. In the following section the computational costs of KENO-Va (within the SCALE-5 package) and MCNP5 with superimposed meshes for flux calculations are compared for the plate fuel reactor.

3.3 Efficiency Tests: MCNP5 and SCALE-5/KENO-Va

This section investigates the effect of superimposed mesh refinement on computational cost (CPU time). The system studied is the simple reactor with plate fuel described in Section 3.1 and shown in Figure 3.1 and Figure 3.2. These tests were performed using a 2 GHz Intel Core2 CPU processor with 2 GB of RAM. A uniform,

superimposed mesh is imposed for k-effective and flux calculations. The mesh is over the entire system and has equal spacing in all directions. Mesh refinement was performed with 50 cm, 20 cm, 10 cm, 5 cm, 2 cm and 1 cm cell size spacing used in all directions. As cell size is decreased, the number of mesh points increases, providing a more accurate analysis of the system. Figure 3.8 shows the computational cost of these tests.

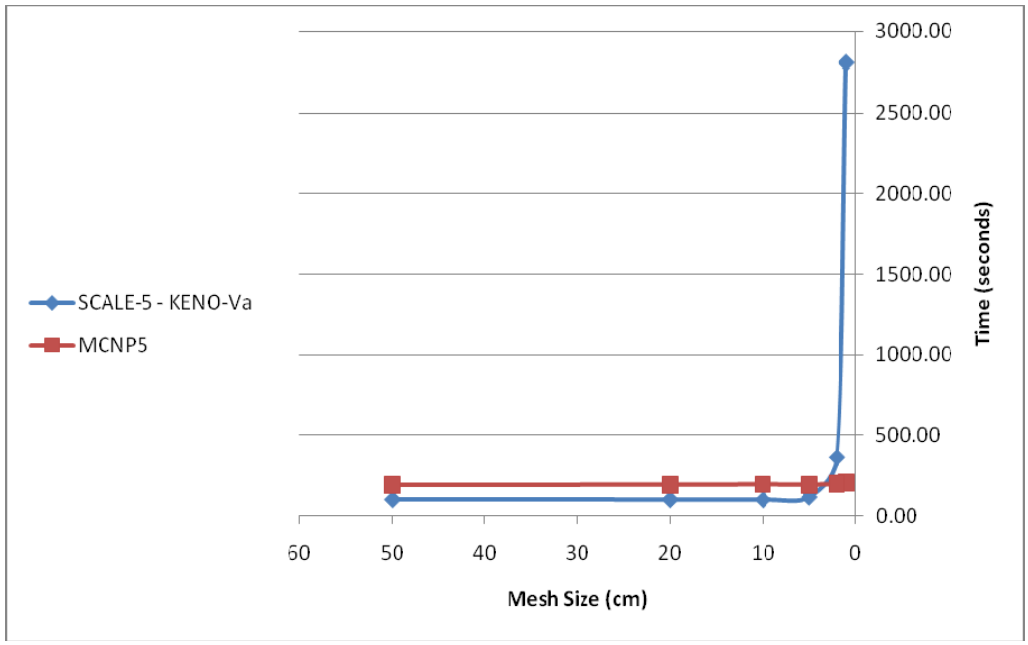

Figure 3.8a: CPU time for MCNP5 and SCALE-5/KENO-Va with superimposed mesh, 1,000 particles.

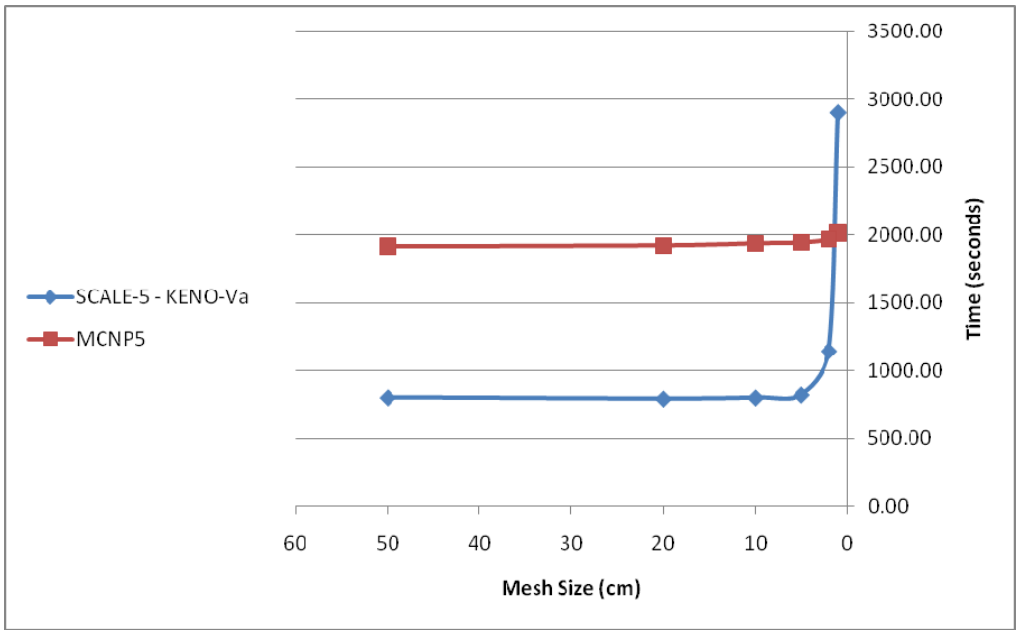

Figure 3.8b: CPU time for MCNP5 and SCALE-5/KENO-Va with superimposed mesh, 10,000 particles.

All tests showed good accuracy in calculated multiplcation factors. The 1,000 particle simulations resulted in a k of 0.9388 for KENO-Va and 0.9321 for MCNP5. The 10,000 particlue simulations resulted in a k of 0.9436 for KENO-Va and 0.9319 for MCNP5 (Results are not affected by mesh size). The accuracy, as determined by Equation 4.2 in Section 4.7, of the k-effective values is within 0.71% and 1.26% for the 1,000 particle and 10,000 particle simulations, respectively. The techniques necessary to compare the results of the flux calculations of the two codes are given in Chapter 4. With strong agreement in results, the important feature of these tests is the variation in computational cost. Figure 3.8a (1,000 particles) and Figure 3.8b (10,000 particles) both show that CPU time for KENO-Va, in SCALE-5, for very coarse meshes is shorter than that for MCNP5. It is when the mesh starts to become highly refined that SCALE-5 begins to dramatically increase in computational cost. Figure 3.8a shows that with 1,000 particles MCNP5 becomes more efficient at a cell size of 2 cm. Figure 3.8b shows that

for a higher number of particles, 10,000 particles per generation, KENO-Va remains more efficient than MCNP5 for a 1 cm or larger mesh. The dramatic increase in CPU time is a result of temporary memory (RAM) limitations. A large increase in computational cost, or increase in run-time, occurs when the computer must utilize the harddrive as virtual memory. [Virtual memory allows for the use of additional temporary memory when it is required beyond the storage capacity of the RAM.] The effect of using virtual memory can be an increase as large as an order of magnitude for runtime [Landau et al. 2007], as illustrated in Figure 3.8.

It is important to note that it is because of the output format of the SCALE-5 mesh file that RAM space quickly gets used up and harddrive must be used as virtual memory. At a 1 cm cell, this simple model produced an output text file that was over 2 GB in size. No standard text editor was able to open this size text file and it was neccesary to use a program called “Large Text File Viewer 4u” [SwiftGear 2005] to read the output. Additionally, for the 1 cm mesh case, the code was unable towrite all the information and close the files, and hence the criticality information was not ouputted, leaving out crucial data in this simulation. Mesh refinement could not be carried any further due to these limitations.

3.4 Efficiency Tests Conclusions

The efficiency tests for MCNP5, KENO-Va in SCALE-5.1 and KENO-VI in SCALE-5.1 provided very clear results. With the ability to provide localized, well-defined meshes, MCNP5 is able to maintain a near constant computational cost as more spatially refined detailed information is desired. Computational cost for KENO-VI in SCALE-5.1 dramatically increases as geometric complexity increases. This is due to the

generalized nature of the code, which quickly negates the benefits of more complex geometry features. The computational cost for KENO-Va in SCALE-5.1 only slightly increases with geometric complexity but remains below that of MCNP5. These results suggest that KENO-Va is the most cost-effective code for this type of simulation.

Perhaps most interesting is the information provided in Figure 3.5. The SCALE manual states that a system that can be modeled in both KENO-Va and KENO-VI will "typically run twice as long in KENO-VI as in KENO-Va" [SCALE: A Modular Code 2005]. It suggests using KENO-VI only for systems that cannot be modeled in KENO-Va. However, Figure 3.7 shows that the CPU time for KENO-VI relative to KENO-Va grows with finer mesh, eliminating any advantage in using KENO-VI, especially when MCNP5 can be utilized for greater detail. A significant increase in CPU time for basic k-effective calculations was also shown in Table 3.2.

The MCNP5 and KENO-Va (within SCALE-5) tests further verified that KENO-Va is less computationally intensive for coarse mesh calculations. A dramatic increase in computing time was seen once the mesh refinement reached a certain point that overtaxed the temporary memory available. The rapid increase in computing time seen with KENO-Va (within SCALE-5) was most likely due to the code's needs exceeding the available 2 GB RAM. These limits were reached with meshes that were still fairly coarse. This was because of the inability to: 1) Specify non-uniform mesh; 2) Specify the mesh only in regions where the flux or power distribution is needed.

These efficiency tests show that KENO-Va within the SCALE package should only be used when quick basic results, including relatively coarse meshes for flux calculations, are desired. However, for very complex geometries and analysis that calls

for detailed flux information, it would be computationally cost effective to utilize MCNP5.

The following chapter provides a detailed background on the F-Lattice. Additionally, the accuracy of KENO-VI (within SCALE-5.1) and KENO-Va (within SCALE-5) are evaluated by comparing their results to those obtained using MCNP5.

Chapter 4: The F-Lattice

First, a detailed description of the main features of the F-Lattice design is given. The F-Lattice is then modeled and analyzed using MCNP5, SCALE-5.1/KENO-VI and SCALE-5/KENO-Va. The ability to accurately calculate the system's effective multiplication factor using the KENO codes is validated in this chapter. The necessary steps to compare the results of the neutron flux calculations are developed and the results for SCALE-5/KENO-Va and MCNP5 are compared.

4.1 The F-Lattice

The Four-Bundle Lattice, known as the F-Lattice, is an innovative design that reduces the total number of control blades employed in the reactor design. Standard lattice designs, sometimes referred to as the N-Lattice, have control blades located every other fuel bundle. While the width of each control blade varies with design, they are smaller than bundle pitch. An earlier modification, known as the K-Lattice, employed a staggered row configuration. The result is that each individual fuel bundle is effectively enclosed by control blades on all four sides [Challberg 1998]. The K-Lattice is intended to improve control rod worth, a concern in some early GE BWR designs that utilized stainless steel clad. The K-Lattice also implemented an increased control rod pitch and larger fuel assembly. It was seen that the K-Lattice was most beneficial with increased fuel assembly size, a larger pitch and wider control blades. Increasing the size of the fuel assemblies, pitch and control blade width helped reduce power peaking that resulted from the staggered row configuration [Challberg 1998]. The F-Lattice was adapted directly from the K-Lattice with these ideas in mind.

The F-Lattice also utilizes a staggered row configuration for the control blade; however, unlike the K-Lattice, the width of the control blade is now increased by a factor of 2.2. This increased width allows each control blade to cover two bundles in each direction, resulting in four bundles, or one assembly, to be entirely enclosed by two control blades; thus the name, Four-Bundle Lattice [Challberg 1998]. The evolution of the standard lattice design to the K-Lattice and finally the F-Lattice design is shown in Figure 4.1, taken from Challberg [1998].

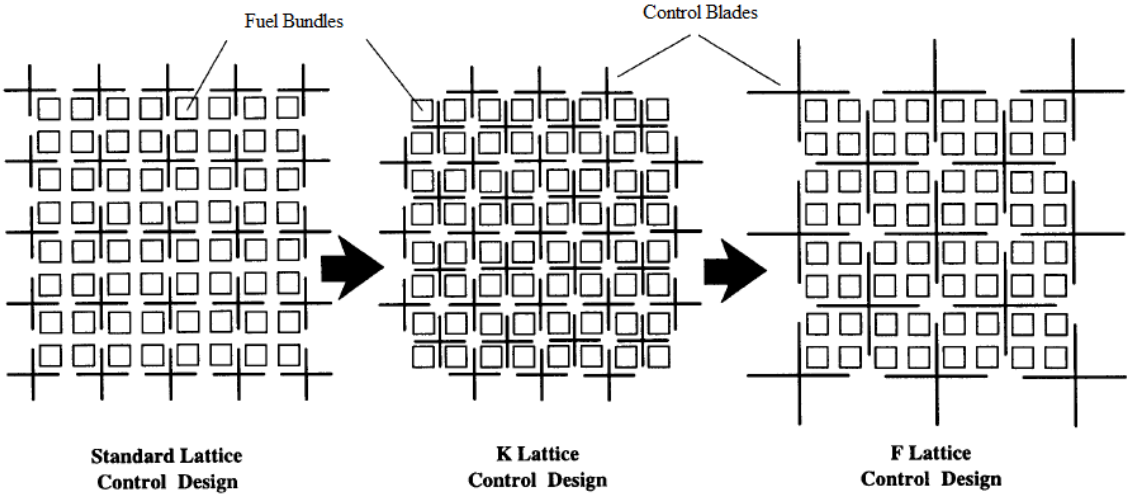

Figure 4.1: Evolution of lattice designs [Challberg 1998].

The main features of the F-Lattice can be clearly seen in Figure 4.1. Larger width control blades in staggered row configuration allow for a reduction in half of the number of control blades in the reactor. As mentioned in Chapter 1, a reduction in the number of control blades correlates to a dramatic reduction of parts that require maintenance. With a reduction in the number of parts, the risk of failure also decreases. Figure 4.2, also from Challberg [1998], shows the core configuration for four assemblies, or sixteen bundles, with one complete center control blade and sections of four outer-corner control

blades. Figure 4.3 is an additional view of this configuration when modeled with MCNP5.

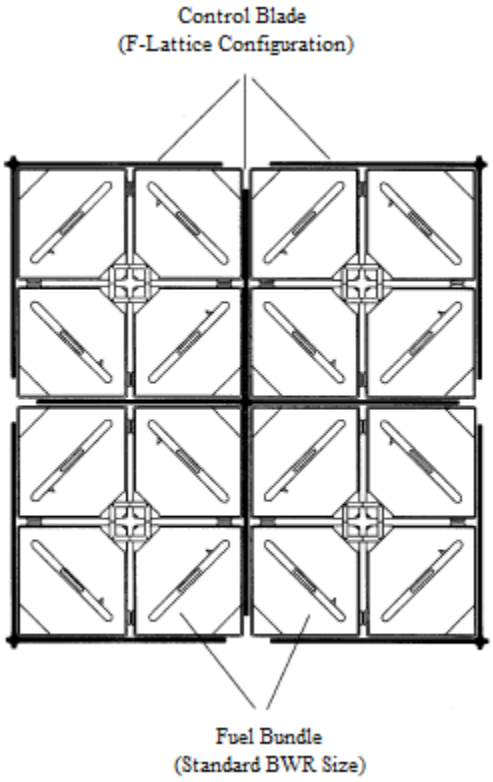

Figure 4.2: 16-bundle F-Lattice core configuration [Challberg 1998].

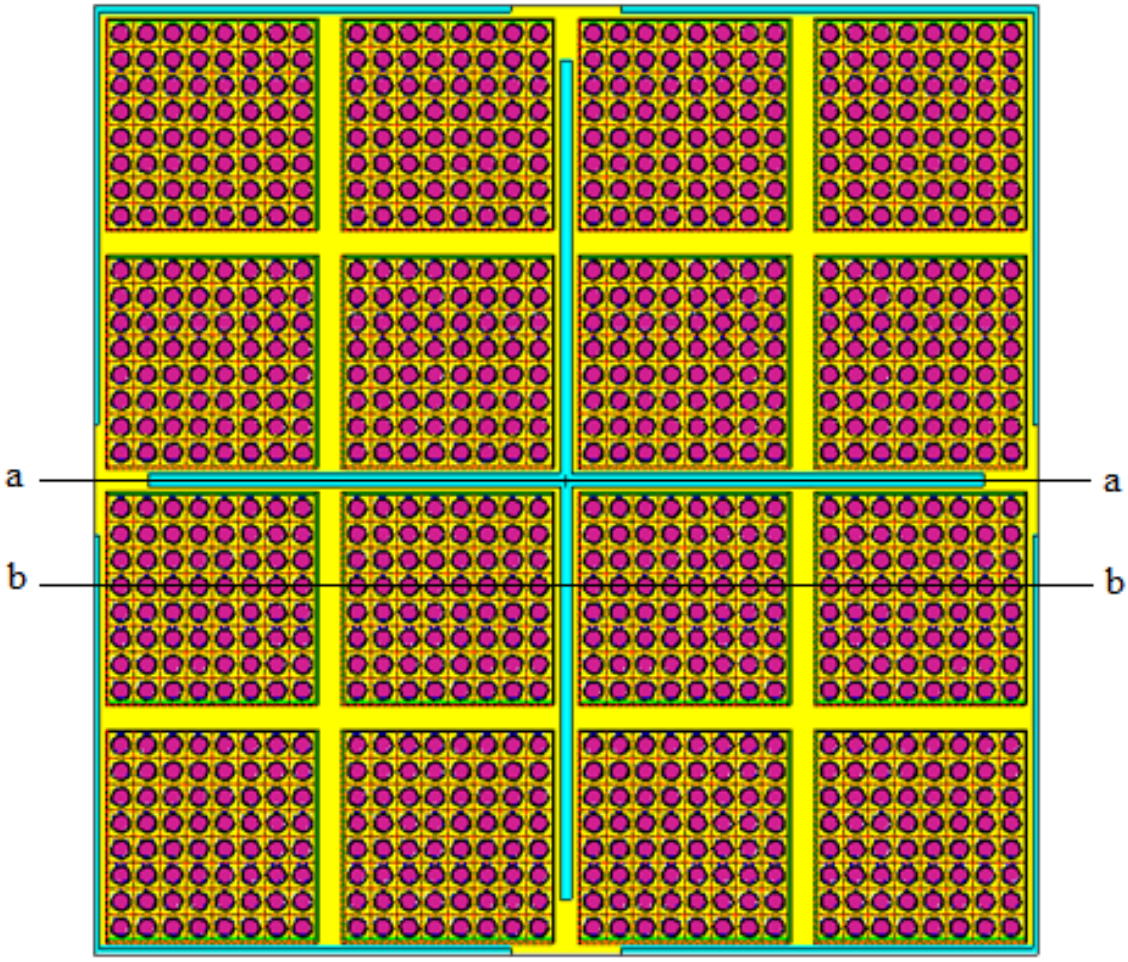

Figure 4.3: 16-bundle cell F-Lattice core configuration modeled in VisEd for MCNP5.

This 16 bundle configuration, henceforth referred to as the 16-bundle cell, is the basic F-Lattice design that is modeled and analyzed in this thesis. The 16-bundle cell is repeated periodically throughout the reactor for a total of 408 bundles, or 102 assemblies [Fennern et al. 2003]. A smaller section of the 16-bundle cell can also be used to represent the F-Lattice. Using only 4 bundles, which are fully encapsulated by two control blades, with mirror boundary conditions allows for a smaller model to be analyzed. This configuration, shown in Figure 4.4, will be referred to as the 4-bundle cell. The important feature of the 4-bundle cell is the fact that it is not repeated periodically, but actually is a mirror image of the 4-bundle cells that it neighbors in all

directions. Therefore, Figure 4.5 is provided as another possible representation of the 4-bundle cell. The results will not differ however for the two cases with different orientation because 100% reflection, or mirror boundary conditions are implemented. However, for consistency, the orientation shown in Figure 4.4 is modeled and analyzed throughout this thesis.

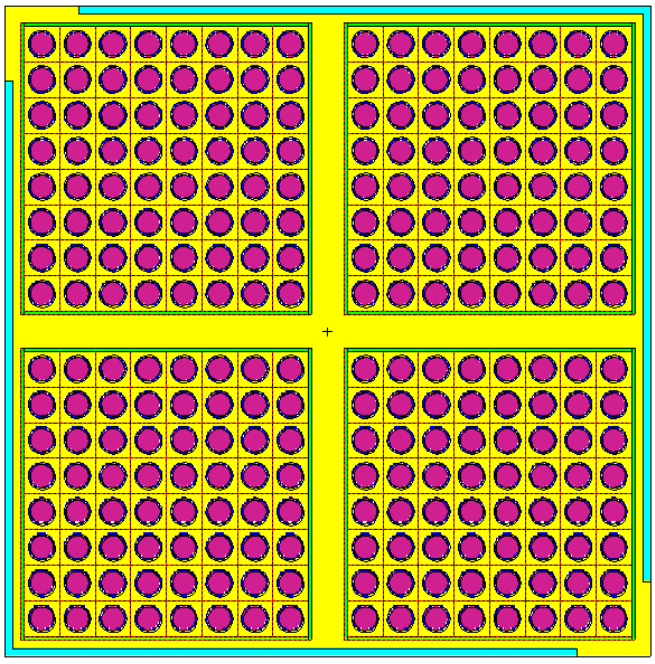

Figure 4.4: 4-bundle cell F-Lattice core configuration (orientation 1) used for analysis.

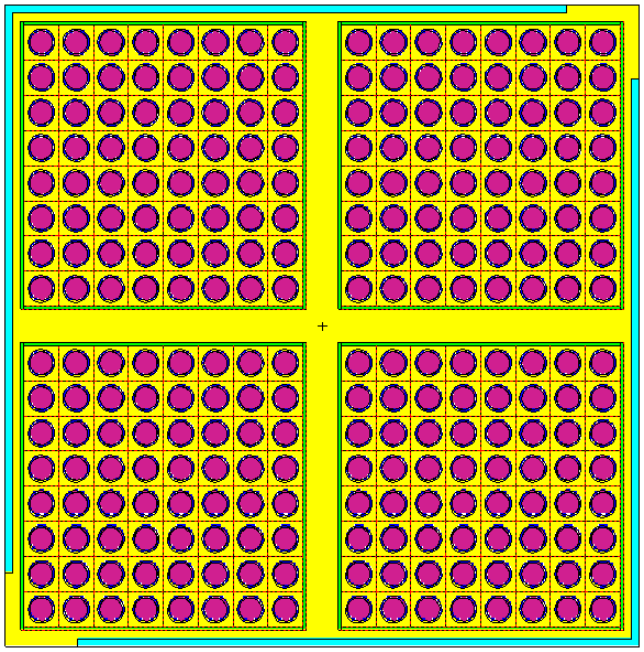

Figure 4.5: 4-bundle cell F-Lattice core configuration; orientation 2.

The design analyzed in this thesis is adapted from Challberg [1998] and Fennern et al. [2003]. It was necessary to combine the description of the F-Lattice originally intended for the ESBWR with the description of the CM-BWR provided by Challberg [1998]. Additional details on fuel size and composition were taken from Duderstadt and Hamilton [1976], following specifications for the BWR/6, which Fennern et al. [2003] discuss in relation to the ESBWR. Core specifications relevant to this analysis are given in Table 4.1.

Parameter	CM-BWR
Power (MWt)	1000
Power (MWe)	350
Number of Fuel Bundles	408
Active Fuel Height (cm)	274.3
Active Poison Length (cm)	259.1
Control Rod Width (cm)	54.8
Control Rod Thickness (mm)	8.3
Control Rod Material	B_4C
Moderator/Coolant	H_2O
Fuel-Element Array	8 x 8
Assembly Pitch (cm)	30.98
Assembly Dimension (cm)	13.915 x 13.915
Canister Material	SS-304
Canister Thickness (mm)	1.535
Clad Material	Zircaloy-4
Clad Thickness (cm)	0.09072
Fuel-Pellet Diameter (cm)	1.1088
Pellet-Clad Gap (cm)	0.0084
Fuel-Element Pitch (cm)	1.701
Fuel	UO_2
Fuel Enrichment (w%)	2.5

Table 4.1: Reactor core parameters used in the F-Lattice analysis.

The following sections explain the methodology used to model the system using the MCNP5 code and the SCALE packages. Results for the F-Lattice design obtained using the two codes are compared. Discussion of the results follows.

4.2 MCNP5 Methodology

The MCNP input file used for analysis is included in Appendix B. The lattice was modeled as a collection of unit cells. A unit fuel cell composed of the fuel, gap, clad and surrounding moderator was first modeled. This unit fuel cell was then repeated using the MCNP "lattice fill" option To create an 8 x 8 unit bundle. A SS304 canister was then modeled around the unit bundle. This unit bundle was then repeated four times with

moderator spacing between them. This was done using the "like m but" command in MCNP. This command allows a unit to be repeated with slight changes in material or physical location. The control rods were then modeled around the four bundles. This completed the 4-bundle cell. The 4-bundle cell was then repeated, as well as rotated as needed, to create the 16-bundle cell.

The source used was the "ksrc", which allows the user to define specific locations for the initial sources to be located. Sources were placed in the center of several different fuel rods throughout the system. MCNP5 automatically expands its source locations with each generation history, using information from each previous history to better approximate the next. Finally, the F4 tally was utilized for the flux analysis. As discussed in Chapter 3, MCNP5 allows a user-defined superimposed mesh for the flux calculations (The F4 tally). Energy levels can also be specified with the F4 tally [X-5 Monte Carlo Team 2003]. Thermal, epithermal, fast and total neutron fluxes were monitored. The energy groups were 0 - 0.225 eV for thermal neutrons, 0.225 eV – 0.1 MeV for epithermal neutrons and 0.1 MeV and above for fast neutrons. The F4 flux tally results are outputted in a second file different from the standard output. Normalization techniques are discussed in Section 4.6.

4.3 SCALE-5.1/KENO-VI Methodology

The SCALE input code used for analysis is included in Appendix B. As discussed in Chapter 2 and Chapter 3, the SCALE package requires that each geometric unit be built surrounding the previous units. Thus, the initial approach to model the F-Lattice using SCALE-5.1/KENO-VI is similar to that for the MCNP5 code. A unit fuel cell composed of fuel, gap, clad and water moderator is first created. The SCALE

package utilizes arrays, filled with geometric units, to repeat the structures. This allows the unit fuel cell to be repeated in an 8 x 8 array, which can then be encapsulated in the stainless steel canister, creating a unit bundle. The unit bundle can then be repeated in an array four times. The SCALE package allows for additional geometric units, referred to as "holes", to be inserted as desired into the system. As discussed in Chapter 2, KENO-VI allows for these holes to have overlapping boundaries with other geometric units. This allows for the 4-bundle cell, and eventually the 16-bundle cell, to be modeled directly in the same fashion as in MCNP. The 4-bundle cell can then be repeated and rotated in a 2 x 2 array to create the 16-bundle cell. It is important to note that rotating the 4-bundle cell orientation actually requires an entirely new 4-bundle to be modeled, since there is no command available to rotate or "flip" a geometric unit; this is also the case in MCNP5.

While modeled fairly simply using KENO-VI, it is important to keep in mind the limitations discussed in Chapter 3. KENO-VI cannot evaluate fluxes with a user-defined superimposed mesh. In order to determine the local reaction rates, geometric units must be broken down (when the geometry is built) in to smaller and smaller units, which increasingly become more computationally expensive. The SCALE-5.1 package slows down (compared to MCNP5) when more spatially detailed flux distributions are desired. As an example, the 4-bundle cell case was developed that used 100 divisions along the z-axis only within the fuel cells. That is the control blades were still treated as a single unit. This corresponds to a coarse mesh of 2.743 cm in just the z-direction and only within the fuel cells. However, the time required to complete this run was 116642.12 seconds (over 1 day and 8 hours). On the other hand, MCNP5, using a superimposed

mesh, yields extremely refined levels of detail in 7 and 16 hours for 4-bundle cell and 16-bundle cell, respectively. However, as shown in Chapter 3, KENO-Va still maintains a computational advantage over MCNP5 for most levels of detail. Therefore, it is desirable to develop techniques to use the SCALE-5/KENO-Va package to model the system.

4.4 SCALE-5/KENO-Va Methodology

KENO-Va is capable of calculating fluxes with a user-defined superimposed mesh but has limitations in modeling systems that involve geometric units that have overlapping boundaries. To overcome this difficulty, it was necessary to break the 4-bundle cell and 16-bundle into smaller pieces which could then be combined together in multiple sets of arrays. This approach is much more difficult and complicated compared to the KENO-VI approach. For the 4-bundle case, the number of geometric units required increases from 5 units and 1 array to 25 units and 5 arrays. The 16-bundle case increases from 7 units and 2 arrays to 32 units and 8 arrays. Sample input files for both KENO-VI and KENO-Va are included for the 4-bundle and 16-bundle cases in Appendix B.

The advantages that KENO-Va provides in both computational cost, as outlined in Chapter 3, as well as the ability to utilize a superimposed mesh for flux calculations far outweigh the relative disadvantages in geometry modeling. The mesh level flux results are included in the standard SCALE output file broken down by unit, region and energy. Also, when comparing flux values it is important to keep in mind that the SCALE-5 superimposed mesh is over the entire model and cannot be uniquely defined for each dimension. The SCALE-5 mesh extends beyond the boundaries of the model if part of a unit is present in the cell. An example is a mesh size of 10 cm for a model that is 10.10

cm long in one of the dimensions. SCALE-5 will have 2 cells in the mesh despite the fact that the second cell is 99% void. For comparison, it is necessary to adjust the MCNP5 mesh accordingly to be the same as that for the SCALE output. The techniques required to compile and compare flux values with MCNP5 results are detailed in the following section.

4.5 Flux Output and Perl

A literature search found no previous work on the SCALE-5/KENO-Va flux calculations using a superimposed mesh. Superimposed mesh has been used to evaluate leakage rates or for increased accuracy in perturbation studies [SCALE: A Modular Code 2005]. Moreover, when fluxes were reported, they were in per unit lethargy units [Johnson and Clarno 2007]. For this reason, SCALE-5/KENO-Va spatial flux results have not previously been compared to results obtained with another code, such as MCNP5. The necessary approach to make such a comparison for SCALE-5 and MCNP5 are developed in this section.

The KENO-Va flux results file is very large. Moreover, the flux results are broken down by geometric units, regions, energy and cell in the mesh. A single unit fuel cell that has four regions (fuel, gap, clad and moderator) and only one cell of the superimposed mesh is a good example of the output's complexity. Even though only one cell in the mesh contains the entire unit fuel cell, each region is reported individually for that cell. With 238 energy levels this results in 952 flux values (4 regions multiplied by 238 energy groups) reported for a single cell. The output is further complicated by the fact that some cells can include multiple units. Results for the same cell are then reported in multiple locations in the output file. Additionally, the output is reported in

mesh grid locations, despite being defined by mesh cell size in centimeters. These mesh grid locations must be transformed to the Cartesian grid to allow comparison with MCNP5 results. The final difficulty related to the mesh flux values are the reported units. As discussed in Section 4.5, MCNP5 reports flux values normalized to "per starting particle." However, the SCALE-5 values are normalized to "per unit volume per starting particle" [SCALE: A Modular Code 2005]. "Unit volume" refers to the geometric "region" within the unit that is within the specific cell for which the flux value is reported. In the SCALE-5 terminology, a "region" is a geometric shape that is contained within a larger "unit." The approach followed here is to normalize the SCALE-5 flux values to "per starting particle", which are then scaled to the proper units of neutrons per centimeter squared per second following Equation 4.1, described in Section 4.6.

With a very complicated and seemingly disorganized output file, it becomes necessary to develop an efficient way to organize and sum all the flux values in order to obtain a single total flux for each individual cell of the mesh.

Practical Extraction and Report Language (Perl) is a scripting language that is used for parsing large data sets into more manageable and easier to analyze results [Lemey and Colburn 2002]. Perl can be used on all major operating systems with no changes necessary to the input file. It is an open source scripting language that can be obtained free of charge from many online locations; the main provider being www.ActiveState.com. Its ease of programming and ability to quickly parse data sets provide ideal abilities to extract desired results from the KENO-Va output. The script, FluxParse.pl, was written in Perl to analyze the output file for any arbitrary sized mesh

for any geometry modeled in SCALE-5/KENO-Va. FluxParse.pl is included in Appendix C along with simple test case results for verification. The comments in FluxParse.pl explain the one-line command necessary to run the script from the OS command line (DOS for Windows).

The script, FluxParse.pl, sums all the flux values for a single cell together to report a single total neutron flux value. To address the issue of "per unit volume" discussed above, it is necessary to first extract the total volume for each region as calculated by SCALE-5. Total volume information is reported in the "sum of mesh volumes for each region" table in the output file. An "average volume" (per cell) is then evaluated by dividing the total volume by the number of times each region appears in the model. An example of how the "sum of mesh volumes for each region" table appears in the output file is shown in Figure 4.6.

sum of mesh volumes for each region

unit	uses	region	mixture	total volume	meshes used
1	256	1	1	6.78059E+04 cm**3	252
		2	0	2.07029E+03 cm**3	252
		3	2	2.43425E+04 cm**3	252
		4	4	1.08958E+05 cm**3	448
2	4	1		2.03177E+05 cm**3	448
		2	4	1.38670E-02 cm**3	196
		3	3	9.27084E+03 cm**3	420
3	2	1	4	1.20232E+04 cm**3	112
4	2	1	4	1.20232E+04 cm**3	112
5	1	1	4	6.80436E+02 cm**3	28
6	1	1	5	1.49623E+03 cm**3	54
		2	4	1.51911E+03 cm**3	56
7	1	1	5	1.69354E+02 cm**3	27
		2	4	1.71944E+02 cm**3	28
8	1	1	5	1.19569E+03 cm**3	54
		2	4	1.81964E+03 cm**3	84
9	1	1	5	1.49623E+03 cm**3	54
		2	4	1.51911E+03 cm**3	56
10	1	1	5	1.69354E+02 cm**3	27
		2	4	1.71944E+02 cm**3	28
11	1	1	5	1.19569E+03 cm**3	54
		2	4	1.81964E+03 cm**3	84
12	1	1	5	1.49623E+03 cm**3	81
		2	4	1.51911E+03 cm**3	84
13	1	1	5	1.69355E+02 cm**3	27
		2	4	1.71944E+02 cm**3	28
14	1	1	5	1.19570E+03 cm**3	54
		2	4	1.81965E+03 cm**3	56
15	1	1	5	1.49623E+03 cm**3	81
		2	4	1.51911E+03 cm**3	84
16	1	1	5	1.69355E+02 cm**3	27
		2	4	1.71944E+02 cm**3	28
17	1	1	5	1.19570E+03 cm**3	54
		2	4	1.81965E+03 cm**3	56
18	2	1	4	3.42382E+02 cm**3	56
19	2	1	5	8.92472E+01 cm**3	54
		2	4	5.23565E+00 cm**3	4
20	2	1	5	8.06450E+01 cm**3	54
		2	4	4.73100E+00 cm**3	4
21	2	1	5	8.06450E+01 cm**3	54
		2	4	4.73100E+00 cm**3	4
22	2	1	4	7.71469E+01 cm**3	56
23	1	1		1.71191E+02 cm**3	28
24	1	1		1.71191E+02 cm**3	28

***** restart data has been written on unit 35 *****

Figure 4.6: The output file for the "Sum of Mesh Volumes for Each Region" table for 4-bundle cell, with a 10 cm mesh.

As the flux values are added together for each cell, they are first multiplied by the "average volume of the region per cell" to account for the "per unit volume" normalization. All the values for a single cell added together are then divided by the

mesh block volume (1000 cm^3 for a 10 cm mesh). A separate tab delimited text file, Flux.txt, is then created containing results normalized to "per starting particle", the same as the MCNP5 flux tallies. Flux.txt can be opened by a spreadsheet editor, such as Excel. The output is organized in the same, increasing (x, y, z) order format that is used by the MCNP5 mesh output. Transformation to a Cartesian grid system can then be carried out manually. However, if a similarly sized mesh is used in an MCNP5 run, then the MCNP5 grid will be the same and can be used directly for both codes for comparison. (The Perl script can easily be modified to incorporate the transformation to the Cartesian grid if desired.)

Error is introduced in this process due to the use of the average volume of each region per cell. Depending on the system being modeled and the mesh size utilized, each cell contains different fractions of "region volume". Using the average volume assumes that the same amount of "region volume" appears in each cell that the region is in. More accurate analysis would take the varying "region volumes" in to account for each specific cell. However, since "region volume" is not reported for each cell of the mesh, the average values are used, leading to a volume averaging error. To eliminate this error would require a manual calculation of "region volume" for each specific model and mesh size, a task that would be very tedious. Section 4.7 and Section 4.8 provide further discussion of how this averaging error manifests itself in the results.

4.6 Flux Normalization

The flux output for MCNP5 is normalized with "per starting particle" and must be converted into "real" fluxes. The SCALE-5 values in Flux.txt are also normalized with

"per starting particle". Flux with the units of number of neutrons per centimeter squared per second is computed as [Tari 1994].

$$Neutron\ Flux\ \frac{\#}{cm^2\ \sec} = Tallied\ Quantity \times \frac{P}{Q} \cdot \frac{1}{q} \cdot \frac{\upsilon}{k_{eff}} \qquad (4.1)$$

- P = Thermal reactor power in MW (1000 MWt)
- Q = Energy released per fission, MeV (200 MeV)
- q =1.602x10^{-19} joules per eV, conversion factor
- υ = Average number of neutrons released per fission, determined by MCNP/SCALE
- k_{eff} = Effective neutron multiplication number, determined by MCNP/SCALE

4.7 MCNP & SCALE Comparison Results

The 4-bundle and 16-bundle cases were run using MCNP5, SCALE-5.1/KENO-VI and SCALE-5/KENO-Va. The results of the three codes are compared. Relative percent differences are reported,

$$Relative\ \%\ Difference = \frac{(x_{SCALE\_results} - x)}{x}\ x\ 100\% \qquad (4.2)$$

where the absolute value is not taken in order to preserve the positive or negative correlations. Fluxes are reported in the units of number of neutrons per centimeter squared per second as dictated by Equation 4.1. The variance and standard deviation between the flux values are normalized to the unit interval, following Equation 4.3 and Equation 4.4:

$$\textit{Variance } \sigma^2 = \sum_{i=1}^{N} \frac{(\Phi_i - \Phi_{i\,test})^2}{N} \tag{4.3}$$

$$\textit{Standard Deviation } \sigma = \sqrt{\sum_{i=1}^{N} \frac{(\Phi_i - \Phi_{i\,test})^2}{N}} \tag{4.4}$$

where N is the total number of cells in the mesh and i sums over all cells. All codes were run for an acceptably small standard deviation of the effective multiplication factor, always less than 0.001. The 16-bundle MCNP5 case was run with 50,000 particles for 250 inactive cycles and 350 active cycles. The 4-bundle MCNP5 case used 100,000 particles for 250 inactive cycles and 550 active cycles. More particles and histories were used in the 4-bundle case for evaluation of the flux distribution, which requires more information than the k-effective calculations. Flux distributions were not analyzed in the 16-bundle case. The SCALE-5.1/KENO-VI cases were both run with 10,000 particles for 200 inactive cycles and 400 active cycles. The SCALE-5/KENO-Va cases were all run with 10,000 particles for 250 inactive cycles and 550 active cycles. More histories were used for KENO-Va than KENO-VI to guarantee accurate flux calculations. An additional test of a single unit fuel cell is included to give basis of comparison for the more complicated F-Lattice. These trials were run in the SCALE packages with 1000 particles for 3 inactive cycles and 200 active cycles. The unit fuel cell case was run in MCNP5 using 500 particles for 100 inactive cycles and 200 active cycles.

The results, including standard deviation, for the unit fuel cell are shown in Table 4.2. The unit fuel cell results are included to show the level of agreement between the SCALE packages results and MCNP5 results for a simple system. Similar agreement is desirable for the F-Lattice simulations.

Model	MCNP		Scale-5.1 Keno-VI		% Error Relative to MCNP	% Error Relative to SCALE-5 KENO-Va	(KENO-MCNP)/σ_{max}
	Keff	σ	Keff	σ			
1 Unit Fuel Cell	1.34148	0.00166	1.3346	0.0012	0.5129	-0.3459	-4.14

(a)

Model	MCNP		Scale-5 Keno-Va		% Error Relative to MCNP	(KENO-MCNP)/σ_{max}
	Keff	σ	Keff	σ		
1 Unit Fuel Cell	1.34148	0.00166	1.3300	0.0012	0.8558	-6.92

(b)

Model	MCNP		Scale-5.1 Keno-Va		% Error Relative to MCNP	% Error Relative to SCALE-5/KENO-Va	% Error Relative to SCALE-5.1/KENO-VI	(KENO-MCNP)/σ_{max}
	Keff	σ	Keff	σ				
1 Unit Fuel Cell	1.34148	0.00166	1.3326	0.0015	0.6620	-0.1955	0.1499	-5.35

(c)

Table 4.2: K-effective results for the unit fuel cell.

The unit fuel cell was also tested using SCALE-5.1/KENO-Va. Table 4.2 shows that KENO-Va leads to different results when operated within SCALE-5 than within SCALE-5.1. KENO-Va within the SCALE-5.1 package is not used for the F-Lattice mainly because it does not provide the ability to use a superimposed mesh for flux calculations. Also, SCALE-5.1 has a higher computational cost associated with it than does SCALE-5. SCALE-5.1/KENO-VI lead to 0.5129% error compared to MCNP5 (Table 4.2a, third column). SCALE-5/KENO-Va has 0.8558% error compared to MCNP5 (Table 4.2b, third column). Both results are below one percent error, which, for this thesis, is the maximum acceptable error for k-effective. Table 4.2c is included because it also has less than one percent error compared to MCNP5, 0.6620% (third

column). This is less than 0.20% error compared to SCALE-5/KENO-Va (Table 4.2c, fourth column) and SCALE-5.1/KENO-VI (Table 4.2c, fifth column). The last columns of Table 4.2a-c is the absolute difference of the k-effective values divided by the maximum standard deviation of MCNP5 and the SCALE/KENO package tested. All results are less than 10.0 (absolute value), which is in agreement with the results of Johnson and Clarno [2007].

The effective multiplication factor results for the F-Lattice, simulated in MCNP5 and SCALE-5.1/KENO-VI, are shown in Table 4.3. Variation between the 4-bundle and 16-bundle cases is shown to be below 1% for MCNP5 and only 0.037% for SCALE-5.1.

Model	MCNP5		Relative % Variation to 16-Bundle Case	Scale-5.1 Keno-VI		Relative % Variation to 16-Bundle Case	% Error Relative to MCNP	(KENO - MCNP) /σ_{max}
	Keff	σ		Keff	σ			
16-Bundle	0.94857	0.00016	0.0000	0.94306	0.00033	0.0000	-0.5809	-16.70
4-Bundle	0.93944	0.00009	-0.9625	0.94341	0.00032	0.0371	0.4226	12.41

Table 4.3: K-effective results for the F-Lattice (MCNP5 and SCALE-5.1/KENO-VI).

K-effective results varied by less than one percent between the 16-bundle and 4-bundle cases for both MCNP5 and SCALE-5.1/KENO-VI. The 16-bundle and 4-bundle models both accurately represent the F-Lattice but some variation in results is expected due to each code's approach to material and cross-section processing. Less than one percent variation is within the desired agreement. The absolute difference of the k-effective values divided by the higher of standard deviations for MCNP5 and SCALE-5.1/KENO-VI was included for more direct comparison to the work done by Johnson and Clarno [2007]. Their work also reported relative differences but were defined as the

negative of what is used in this thesis. These results agree with that of Johnson and Clarno [2007] in that the relative difference between the MCNP5 and KENO-VI cases are all less than 0.7%. The result for the absolute difference divided by the maximum of the standard deviation, shown in Table 4.3 (last column), are slightly higher than that seen in Johnson and Clarno [2007], where they report a maximum absolute value of 11.4. However, these values are misleading because very similar effective multiplication factors could have been achieved with larger standard deviations if fewer trials or fewer particles had been used. Johnson and Clarno [2007] did not report the number of trials or histories used. The relative percent error is also on the same order as for the simple unit fuel cell case shown in Table 4.2.

The effective multiplication factor results for the F-Lattice, simulated using MCNP5 and SCALE-5/KENO-Va, are given in Table 4.4.

Model	MCNP5		Scale-5 Keno-Va		Relative % Variation to 16-Bundle Case	% Error Relative to MCNP	(KENO-MCNP)/σ_{max}
	Keff	σ	Keff	σ			
16-Bundle	0.94857	0.00016	0.94120	0.00029	0.0000	-0.7770	-25.41
4-Bundle	0.93944	0.00009	0.94173	0.00032	-0.0563	0.2438	7.16

Table 4.4: K-effective results for the F-Lattice (MCNP5 and SCALE-5/KENO-Va.)

The relative difference between MCNP5 and KENO-Va is again shown to be below one percent. The percent error for the 4-bundle case is 0.244% (Table 4.4, fourth column), compared to 0.423% error with KENO-VI (Table 4.3, fifth column). The 16-bundle case leads to error of 0.777% compared to MCNP5 (Table 4.4, fourth column). KENO-VI, compared to MCNP5, lead to 0.581% error (Table 4.3, fifth column) for the

16-bundle case. The absolute difference over the maximum standard deviation is rather large for the 16-Bundle case at -25.41. However, this value for the 4-bundle case (7.16) is within an acceptable range of variation between MCNP5 and SCALE-5 KENO-Va. Results of the flux analysis for the 4-bundle model are presented below.

Flux calculations were performed for the 4-bundle case using the F4 tally in MCNP5, and in KENO-Va using the MFX and MSH options located under the TSUNAMI-3D Parameters tab, which is a subset of 'Parameter Data' only found in SCALE-5. As discussed in Section 4.5 and Section 3.3, only cubic meshes that have equal spacing in all directions can be defined in SCALE-5. This results in very large output files, taxing available memory and hard drive space. Thus, the meshes studied (10 cm, 5 cm and 3cm) are rather coarse for the system. Memory limitations are also the reason as to why the 4-bundle case was used and not the larger 16-bundle system. Additionally, SCALE-5 produces different results depending on how the Global Unit is defined, where the Global Unit is the final (largest) geometric unit that contains all other units and where the boundary conditions are applied. The Global Unit can be defined as an array or it can be defined as a cuboid that is of the same size as the array and contains that array. The results for the array-defined Global Unit are given in Table 4.5, and the results for the cuboid-defined Global Unit are included in Table 4.6. Reported values for k-effective and flux calculations vary depending on which type of Global Unit is used. This is an effect of how the initial calculations are performed for the volume weighted averaging integrals that SCALE uses for its calculations [SCALE: A Modular Code 2006]. The cuboid-defined Global Unit case leads to more accurate results when compared to the MCNP5 results than the array-defined Global Unit case and thus, is the

focus of discussion in this thesis. The k-effective results in Table 4.4 are from the cuboid-defined Global Unit. Simulations using the array-defined Global Unit produced a k-effective of 0.94267 with a standard deviation of 0.00028 for the 4-bundle case. Compared to MCNP5 benchmark results, this is a 0.344% error, whereas the cuboid-defined Global Unit had a smaller error of 0.244%. In Table 4.5 and Table 4.6 the location of the peak flux value is given; the origin (0, 0, 0) is defined at the bottom left corner, and z = 0, of the 4-bundle cell shown in Figure 4.4.

3 cm Mesh								Unit Normalized	
	X (cm)	Y (cm)	Z (cm)	Peak Flux (n/cm^2-s)	% Error Relative to MCNP	Average Flux (n/cm^2-s)	% Error Relative to MCNP	Variance From MCNP	Standard Deviation From MCNP
MCNP	16.5	16.5	115.5	2.3114E+16	0.00	9.5298E+15	0.00	0.0000	0.0000
SCALE	16.5	13.5	106.5	2.8754E+16	24.40	9.2224E+15	-3.23	0.0238	0.1544

5 cm Mesh								Unit Normalized	
	X (cm)	Y (cm)	Z (cm)	Peak Flux (n/cm^2-s)	% Error Relative to MCNP	Average Flux (n/cm^2-s)	% Error Relative to MCNP	Variance From MCNP	Standard Deviation From MCNP
MCNP	17.5	17.5	117.5	2.2026E+16	0.00	8.5026E+15	0.00	0.0000	0.0000
SCALE	12.5	17.5	107.5	2.1658E+16	-1.67	8.1305E+15	-4.38	0.0118	0.1084

10 cm Mesh								Unit Normalized	
	X (cm)	Y (cm)	Z (cm)	Peak Flux (n/cm^2-s)	% Error Relative to MCNP	Average Flux (n/cm^2-s)	% Error Relative to MCNP	Variance From MCNP	Standard Deviation From MCNP
MCNP	15	15	115	2.1510E+16	0.00	6.3936E+15	0.00	0.0000	0.0000
SCALE	15	15	105	1.8577E+16	-13.63	5.8211E+15	-8.95	0.0108	0.1040

Table 4.5: Flux results for the array-defined Global Unit in SCALE-5/KENO-Va.

3 cm Mesh								Unit Normalized	
	X (cm)	Y (cm)	Z (cm)	Peak Flux (n/cm^2-s)	% Error Relative to MCNP	Average Flux (n/cm^2-s)	% Error Relative to MCNP	Variance From MCNP	Standard Deviation From MCNP
MCNP	16.5	16.5	115.5	2.3114E+16	0.00	9.5298E+15	0.00	0.0000	0.0000
SCALE	1.5	31.5	1.5	3.4485E+16	49.20	9.2383E+15	-3.06	0.0398	0.1995

5 cm Mesh								Unit Normalized	
	X (cm)	Y (cm)	Z (cm)	Peak Flux (n/cm^2-s)	% Error Relative to MCNP	Average Flux (n/cm^2-s)	% Error Relative to MCNP	Variance From MCNP	Standard Deviation From MCNP
MCNP	17.5	17.5	117.5	2.2026E+16	0.00	8.5026E+15	0.00	0.0000	0.0000
SCALE	17.5	17.5	102.5	2.2021E+16	-0.02	8.1483E+15	-4.17	0.0128	0.1132

10 cm Mesh								Unit Normalized	
	X (cm)	Y (cm)	Z (cm)	Peak Flux (n/cm^2-s)	% Error Relative to MCNP	Average Flux (n/cm^2-s)	% Error Relative to MCNP	Variance From MCNP	Standard Deviation From MCNP
MCNP	15	15	115	2.1510E+16	0.00	6.3936E+15	0.00	0.0000	0.0000
SCALE	15	15	105	1.8965E+16	-11.83	5.8407E+15	-8.65	0.0117	0.1080

Table 4.6: Flux results for the cuboid-defined Global Unit in SCALE-5/KENO-Va.

Flux distributions were synthesized from the SCALE-5/KENO-Va output using the FluxParse.pl script discussed in Section 4.5, and scaled to real flux values using Equation 4.1. The SCALE-5/KENO-Va average flux values are within close agreement with the MCNP5 results. The 3 cm mesh produced the smallest error at 3.06%, followed by the 5 cm mesh with 4.17% and the 10 cm mesh with 8.65%. As the mesh is refined further, it is very likely that the results will agree even better with those obtained using MCNP5; however, due to memory limitations, further refinement was not carried out.

The error in peak flux results showed an unexpectedly large error for the 3 cm mesh. The 3 cm mesh lead to a 49.20% difference for the SCALE-5/KENO-Va results compared to the MCNP5 results, whereas the 5 cm mesh only differed by 0.02% (Table 4.6, fifth column). Additionally, as shown in Table 4.6, the difference in peak flux location is rather significant for the 3 cm mesh. To explore the discrepancy in these results, three-dimensional contour plots for MCNP5 and SCALE-5 are shown in Figure 4.7 – Figure 4.10.

Figure 4.7 and Figure 4.8 are the xy-plane surface contour plots for z = 115.5 cm, the location of the MCNP5 peak flux value of 2.3114e+16 neutrons per centimeter squared per second. Figure 4.9 and Figure 4.10 are the xy-plane surface contour plots for z = 1.5 cm, the location of the SCALE-5 peak flux value of 3.4485e+16 neutrons per centimeter squared per second. SCALE-5 results in less smooth contour plot for both Figure 4.8 and Figure 4.10. This is a result of some of the approximations discussed in Chapter 2, the difference in approaches that each code system uses and also probably more importantly, the volume averaging error mentioned in Section 4.3 which is introduced in scaling the flux values to the same units as the MCNP5 values.

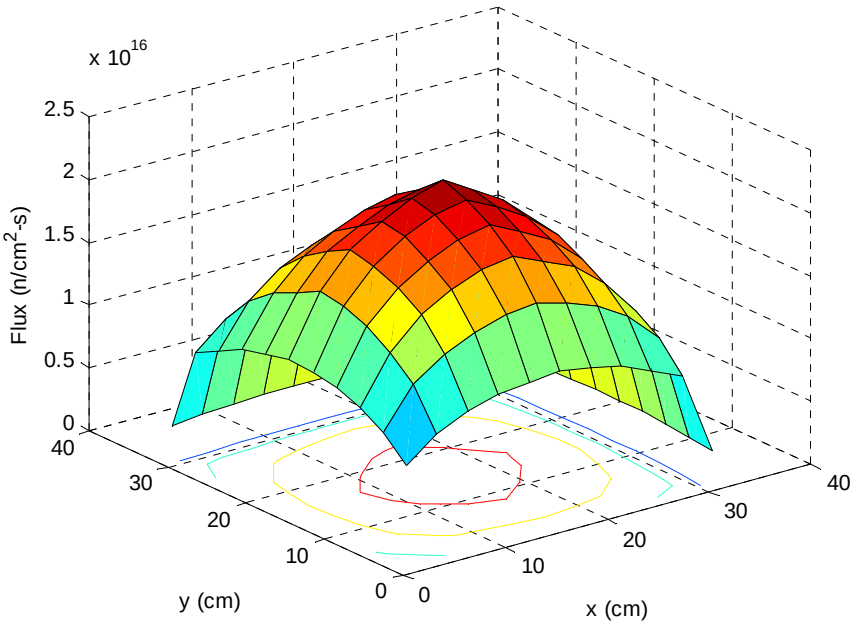

Figure 4.7: MCNP5 flux distribution over the xy-plane at z = 115.5cm using a 3 cm mesh.

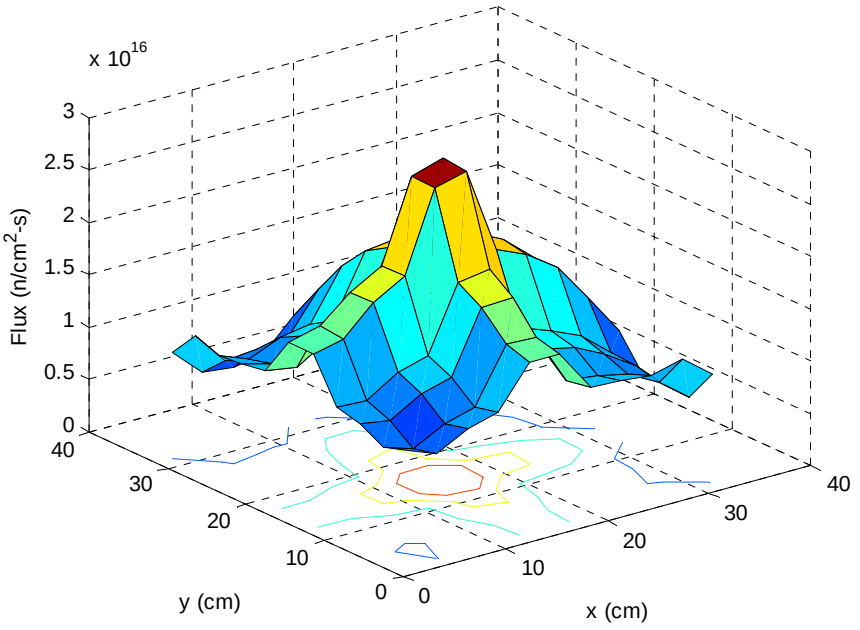

Figure 4.8: SCALE-5 flux distribution over the xy-plane at z = 115.5cm using a 3 cm mesh.

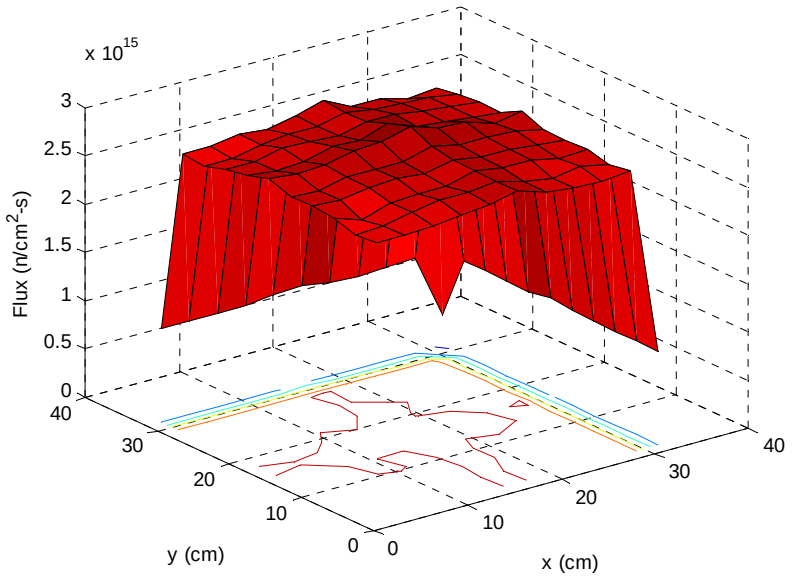

Figure 4.9: MCNP5 flux distribution over the xy-plane at z = 1.5cm using a 3 cm mesh.

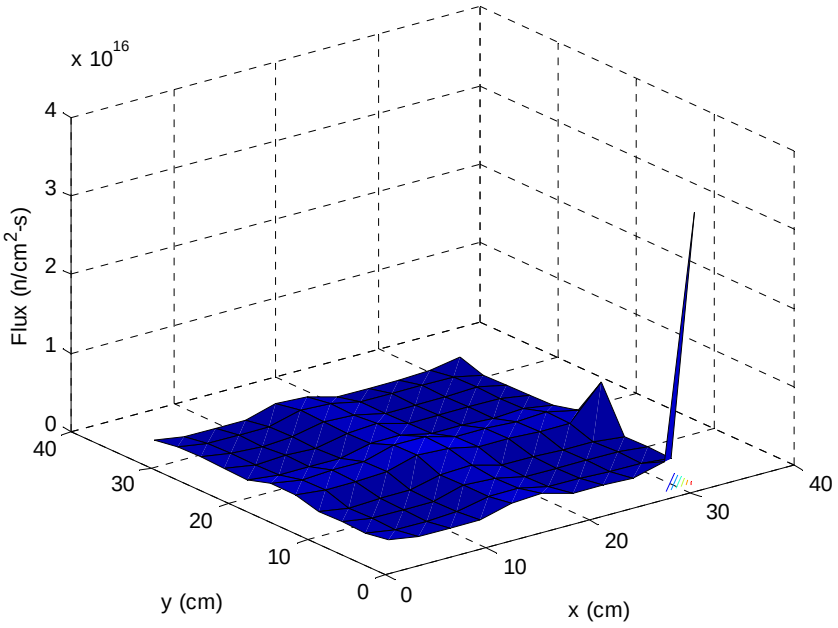

Figure 4.10: SACLE-5 flux distribution over the xy-plane at z = 1.5cm using a 3 cm mesh.

The volume averaging error has the effect of overweighting or underweighting different cells in the mesh, depending on the system geometry and mesh size used; the effect of which is seen in the contour plots. The effect of these can be seen in the non-

smooth (wrong curvature) nature of Figure 4.8. It is clear that due to this averaging error, specific location or magnitude of the flux cannot be accurately compared. Due to the nature of this error, further refinement of the mesh can result in additional error when specific cell comparisons are made (as shown by the peak value comparisons). The overall increase in error in cell to cell comparison is also the reason for the slight increase in the normalized variance and standard deviation values with increased mesh refinement shown in Table 4.6 and Table 4.5. However, the average flux values do show better agreement with mesh refinement because averaging the values helps cancels out, though not completely, the volume averaging error introduced in normalizing the flux to "per starting particle".

Figure 4.9 and Figure 4.10 show the flux distributions at a height of 1.5 cm from the bottom of the system, the z plane at which SCALE-5 shows the maximum flux. The sharp drop-off along the outer boundaries of the model in Figure 4.9 is due to the mesh size. The outer cells contain almost all control blade material and void (see Figure 4.11). Therefore, when the flux is evaluated for the outer boundary cells, there is a significantly smaller flux than compared to the cells (containing fuel) next to the boundaries. The location of the SCALE-5 peak flux value can be seen to be an anomaly (Figure 4.10), and is caused by the volume averaging error. The SCALE-5 peak is a data spike in a cell near the boundary of the model. Most of that cell is void, due to the way the mesh is defined in SCALE-5 (as discussed in Section 4.3). With a cell that is mostly void, multiplying the flux result for that location by an average "region volume" (described in Section 4.5) results in a very large overestimation of the flux in that region. Taking this into

consideration, the next largest flux value in the SCALE-5 results is a more reliable peak value, given in Table 4.7.

3 cm Mesh					
	X	Y	Z	Peak Flux (n/cm^2-s)	% Error Relative to MCNP
MCNP	16.5	16.5	115.5	2.3114E+16	0.00
SCALE	16.5	16.5	115.5	2.9830E+16	29.06

Table 4.7: Alternate peak value results for cuboid-defined Global Unit 3 cm mesh.

The difference in peak values is reduced, though 29.06% is still considerably large. However, the peak value is now found to be at the same location for the MCNP5 and SCALE-5 calculations, showing better agreement than the 5-cm or 10-cm mesh cases. Overall, the flux results are reasonable, especially the average flux comparisons. The following section explains the volume averaging error in more detail.

4.8 Volume Averaging Error

The model geometry and chosen mesh size has a large effect on the flux calculations. To better understand the cause of the volume averaging error discussed in the previous sections, it is necessary to understand how varying the mesh size affects the results. Figures 4.11-4.13 are provided as visual representations of the mesh patterns, in the xy-plane, for the 4-bundle case utilizing a 3 cm, 5 cm and 10 cm mesh, respectively.

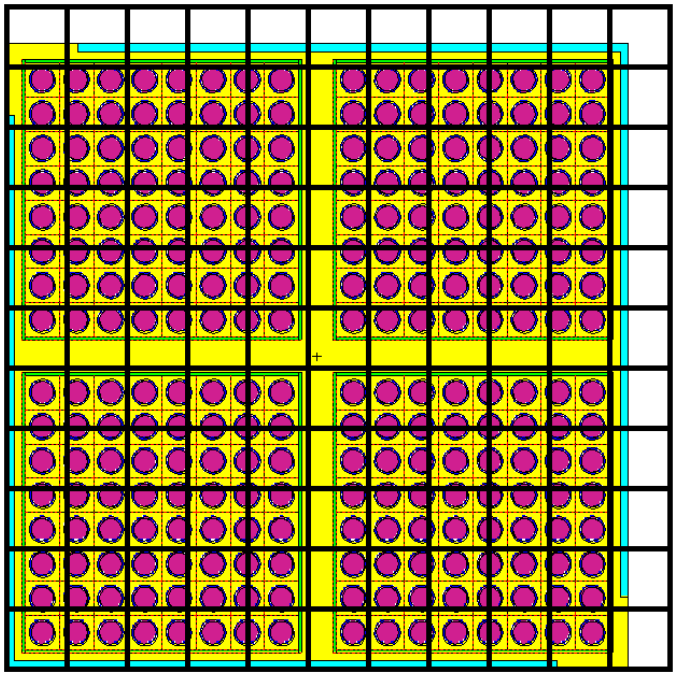

Figure 4.11: 3 cm mesh pattern superimposed on the 4-bundle case.

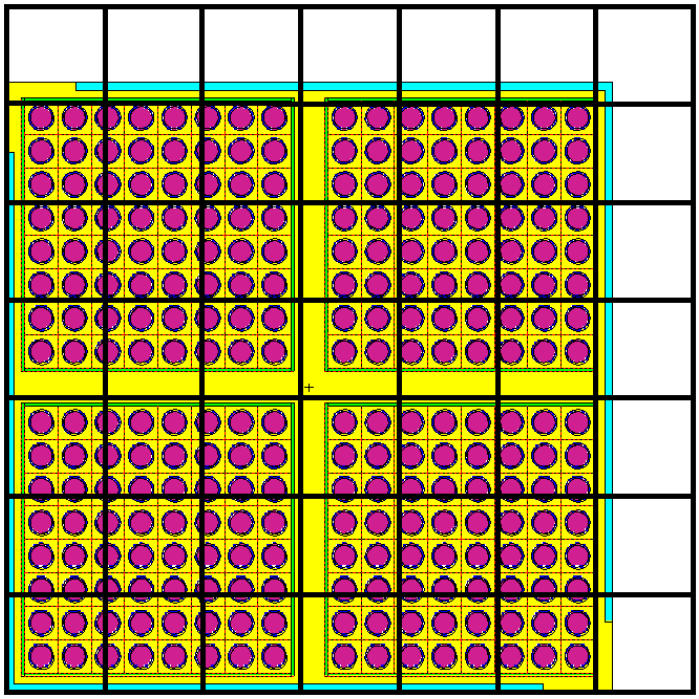

Figure 4.12: 5 cm mesh pattern superimposed on the 4-bundle case.

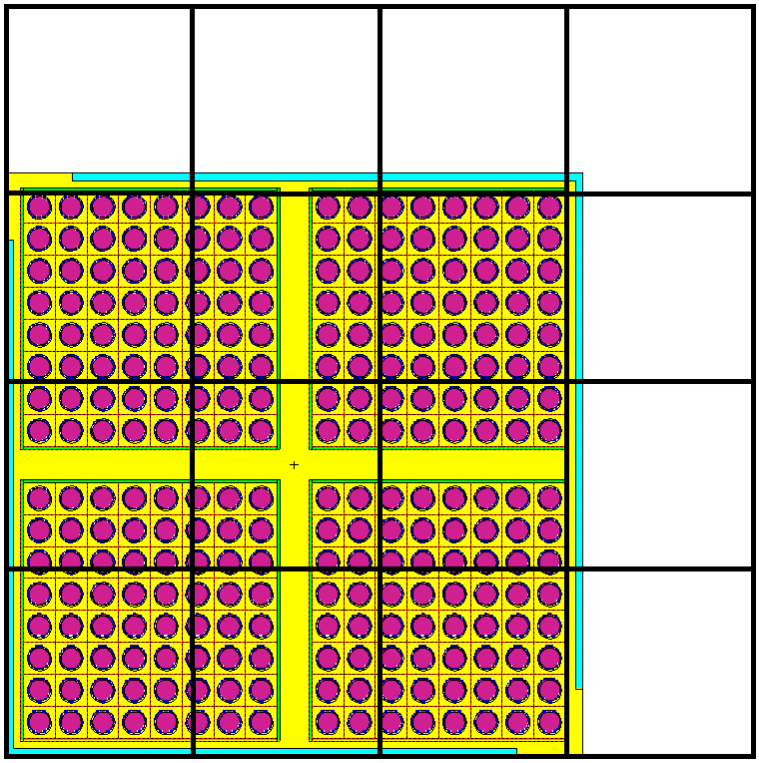

Figure 4.13: 10 cm mesh pattern superimposed on the 4-bundle case.

Varying the mesh size greatly alters the amount of material and geometry that is present in each individual cell in the mesh. Additionally, the large amount of void space present in various cells can vary drastically from the 3 cm mesh to the 10 cm mesh. When the flux values are scaled, via FluxParse.pl, to "per starting particle" the average volume, per cell, is used in the transformation. This average volume is determined from the "Sum of Mesh Volumes for Each Region" table shown in Figure 4.6. For all three mesh sizes and for each cell in the mesh, the volume of each geometric unit in a cell differs from every other cell. As an example, in the 3 cm mesh case, some cells have almost four complete "unit fuel cells" while others only have part of one "unit fuel cell", where a fuel cell refers to the grouping of the fuel, gap, clad and surrounding water as one unit. In Figure 4.11, the cell in the first row, first column (bottom left corner of the model) contains one entire fuel cell, along with parts of the canister, water gap and

control blade. The cell in second row, second column contains parts of four different "unit fuel cells". Considering just the fuel for this example, there is approximately a factor of four more fuel present in the second row, second column cell than there is in the first row, first column cell. However, the volume averaging technique in FluxParse.pl assumes that if fuel is present in any cell, the fuel volume in the cell is equal to the total volume of fuel in the model divided by the number of cells (the average volume). Each cell clearly contains a different volume of fuel (and other materials). The use of an average volume for all cells results in the large difference when specific cell values are directly compared to MCNP5 results. (FluxParse.pl multiplies all flux values by the volume of the geometric unit present in the cell for which the flux is reported. This is done to transfrom the flux normalization from "per unit volume per starting particle" to "per starting particle". See Section 4.5) Calculating "region volumes" that are not averaged cannot be automated, as discussed in Section 4.5. Therefore, manual calculation of the volume of each geometric unit within specific cells is required to eliminate the volume averaging error.

To determine how large an effect the volume averaging has on the flux calculations, it is necessary to perform manual "region volume" calculations for specific cells. As mentioned in Section 4.3, this would be extremely difficult and very intensive due to the fact that each cell requires unique "region volume" calculations. Therefore, only the cells of the peak flux values determined by MCNP5 (as reported in Table 4.6) are explored in greater detail here. Figure 4.14, Figure 4.15 and Figure 4.16 are enlarged views of the cells being analyzed.

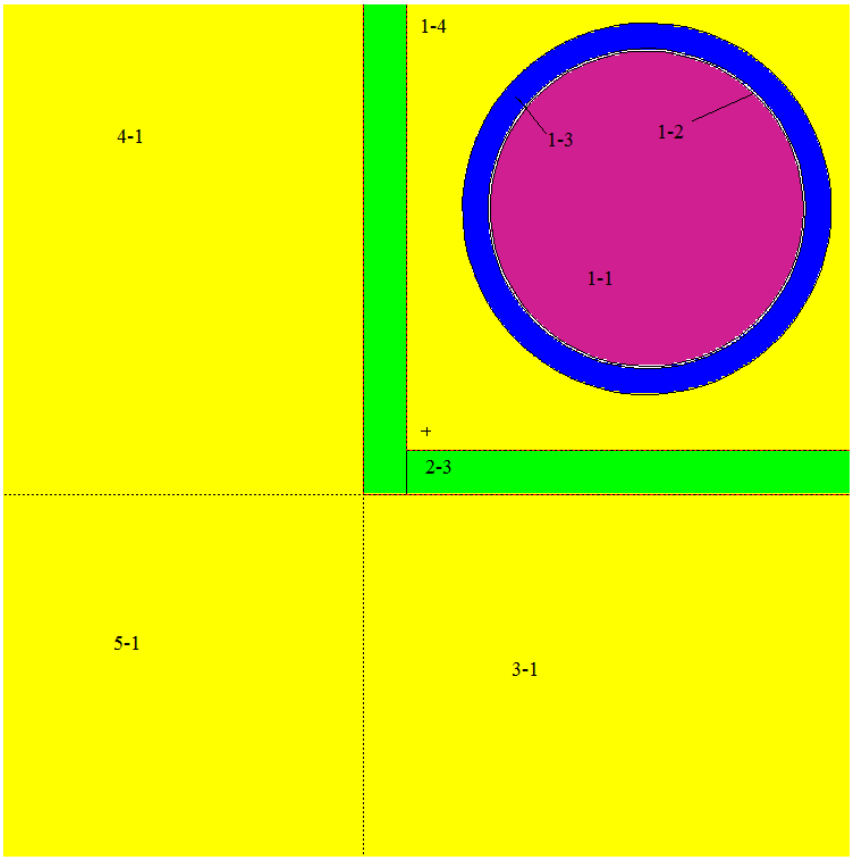

Figure 4.14: 3 cm cell containing the MCNP5 calculated peak flux location (Table 4.6).

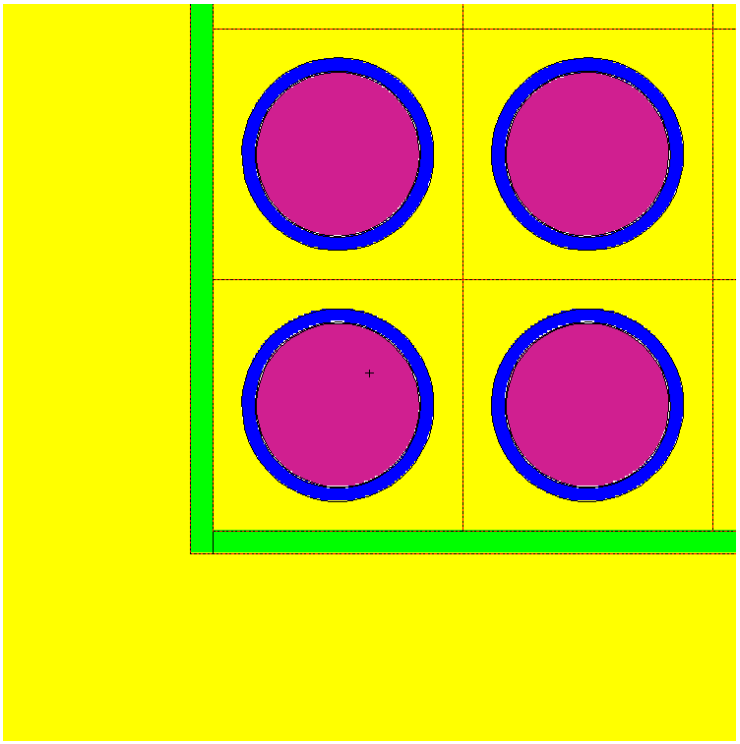

Figure 4.15: 5 cm cell containing the MCNP5 calculated peak flux location (Table 4.6).

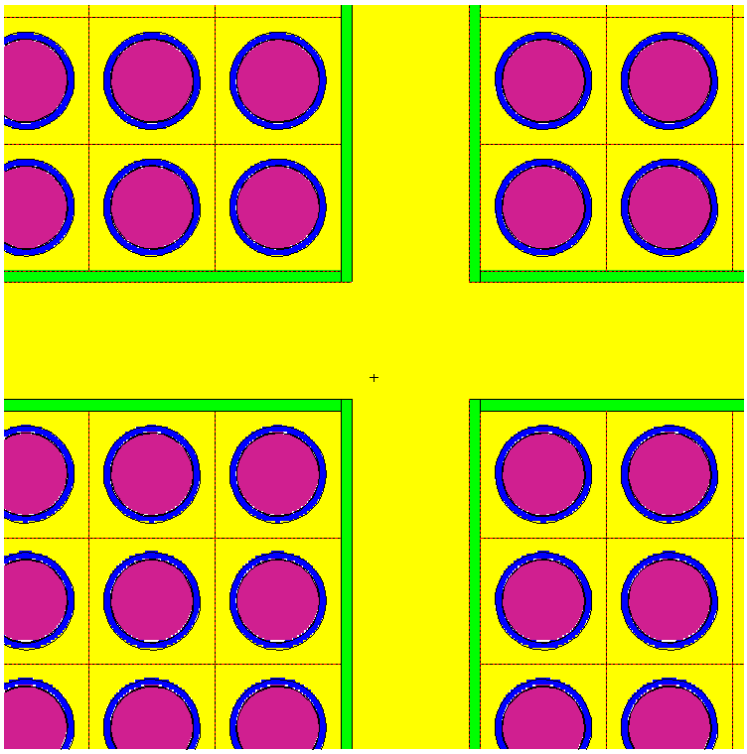

Figure 4.16: 10 cm cell containing the MCNP5 calculated peak flux location (Table 4.6).

The manually calculated volumes are shown alongside the averaged volumes in Table 4.8 for all three mesh sizes. The unit and region (first two columns of Table 4.8) are identified in Figure 4.14 as (Unit-Region). The relative errors are not reported because these values are only valid for the specific cell that the volumes were calculated for and do not represent the overal error in using averaged volumes.

3 cm Mesh				
Unit	Region	Unit - Region Description	Manually Calculated Volume for MCNP5 Peak Flux Cell (cm^3)	Averaged Volume for the Entire Model (cm^3)
1	1	Fuel	2.89679372	7.370565
1	2	Gap	0.08844664	0.225045
1	3	Clad	3.93676661	2.645891
1	4	Water	0.46327603	9.787549
2	3	Canister	1.51573575	1.399583
3	1	Water	6.60148125	5.940316
4	1	Water	6.60148125	5.940316
5	1	Water	4.89601875	1.849011

(a)

5 cm Mesh				
Unit	Region	Unit - Region Description	Manually Calculated Volume for MCNP5 Peak Flux Cell (cm^3)	Averaged Volume for the Entire Model (cm^3)
1	1	Fuel	19.3119581	34.24581
1	2	Gap	0.58964427	1.045611
1	3	Clad	26.2451107	12.29414
1	4	Water	17.5420919	40.42968
2	3	Canister	5.59622625	4.214018
3	1	Water	23.7774688	15.61455
4	1	Water	23.7774688	15.61455
5	1	Water	8.16003125	3.092891

(b)

Table 4.8: Manually calculated and averaged volumes at the MCNP5 calculated peak flux mesh location.

10 cm Mesh				
Unit	Region	Unit - Region Description	Manually Calculated Volume for MCNP5 Peak Flux Cell (cm^3)	Averaged Volume for the Entire Model (cm^3)
1	1	Fuel	226.321582	269.071
1	2	Gap	6.42153836	8.215437
1	3	Clad	47.0348786	96.59722
1	4	Water	359.328811	243.2098
2	2	Water	19.91243	7.08E-05
2	3	Canister	50.78701	22.07343
3	1	Water	132.69375	107.35
4	1	Water	132.69375	107.35
5	1	Water	24.80625	24.30129

(c)

Table 4.8: (continued)

The flux results scaled to neturons per centimeter squared per second, evaluated using the manually calculated volumes are reported in Table 4.9. Table 4.10 is provided as a summary of the pertinent results fromTable 4.6, which are based on the averaged volumes.

	3 cm Mesh	5 cm Mesh	10 cm Mesh
MCNP (n/cm^2-s)	2.3114E+16	2.2026E+16	2.1510E+16
SCALE (n/cm^2-s)	2.328E+16	2.182E+16	2.1224E+16
% Error Relative to MCNP	0.7109	-0.9533	-1.3294

Table 4.9: Peak flux comparisons based on manually calculated, location specific, volumes.

	3 cm Mesh	5 cm Mesh	10 cm Mesh
MCNP (n/cm^2-s)	2.3114E+16	2.2026E+16	2.1510E+16
SCALE (n/cm^2-s)	3.4485E+16	2.2021E+16	1.8965E+16
% Error Relative to MCNP	49.1968	-0.02166	-11.8282

Table 4.10: Peak flux comparisons based on system averaged volumes, shown in more detail in Table 4.6.

Table 4.9 shows a dramatic reduction in the difference between the SCALE-5/KENO-Va and MCNP5 calculated flux values when the proper "region volumes" for the cell are used. These results suggest that MCNP5 and SCALE-5/KENO-Va are capable of producing flux values that differ from each other by about one percent when the volume averaging error in the KENO-Va calculation is eliminated. Percent difference in peak flux values decreases with mesh refinement, and is likely to continue to decrease if computing resources were available for further mesh refinement. While the 5 cm mesh case shows a smaller relative difference in the volume averaged case it is important to note that, as shown in Table 4.6, these values are not located at the same mesh location and thus are not suitable for a direct comparison. A fortuitous cancellation of errors is most likely the reason for the smaller error shown in Table 4.10.

The flux results show that SCALE-5/KENO-Va and MCNP5 lead to less than one percent difference in peak flux values when cell "region volumes" are appropriately taken into account. Additionally, if the volume averaging error could be eliminated in all cells it would be expected that the average flux values would show even closer agreement.

4.9 MCNP & SCALE Comparison Conclusions

Chapter 4 explored the F-Lattice in detail and provides preliminary validation of SCALE packages using MCNP5 results as benchmarks. It was shown that the SCALE

results, both for SCALE-5.1/KENO-VI and SCALE-5/KENO-Va, are within one percent of the MCNP5 results. This is in agreement with the work reported by Johnson and Clarno [2007]. However, since SCALE-5/KENO-Va provides accurate results, allows for a superimposed mesh for flux calculations and is less computationally intensive than SCALE-5.1, SCALE-5.1/KENO-VI can be quickly ruled out for use for the F-Lattice.

Additionally, this chapter explored SCALE-5/KENO-Va to report flux distributions; a use not found in literature. A Perl script was written to extract the large and "disorganized" flux values from the SCALE-5 output files. The Perl script was written so that it can be used with any arbitrary system or mesh size. Average flux values were shown to be highly accurate, within 3.06%, and would most likely improve in accuracy as the mesh is further refined. Specific values however cannot be trusted with complete accuracy due to a volume averaging error in normalizing the SCALE-5 flux values to "per starting particle." The effect of the volume averaging error on the flux calculations was quantified in Section 4.8. An approach to eliminate this error is discussed in Section 6.2: Future Work.

Having developed the tools, and then using them to compare flux values and validating their results, along with more general k-effective calculations, SCALE-5/KENO-Va is considered reliable for modeling the F-Lattice. SCALE-5 is compared with MCNP5 for some parametric studies of the F-Lattice in the next chapter. Rod worth calculations are performed for the F-Lattice control blades. Additionally, MCNP5 is used more extensively to analyze the effects that geometry and material changes have on the neutron flux profiles of the system.

Chapter 5: Parametric Studies

The effects of varying material properties and geometry within the F-Lattice are investigated in this chapter. The effective rod worth of the standard B_4C control blades is determined by comparing reactivity change when B_4C is replaced by pure graphite blades. Geometric effects on rod worth are also investigated by varying the thickness of the control blades. Thickness changes affect rod worth directly in terms of volume of control material present, as well as a slight effect on the control blade surface area. Additionally, the water moderator gap is altered by changes in control blade thickness because pitch is kept constant. The changes in the effective multiplication factor, as well as pertinent neutron flux values, are studied using both MCNP5 and SCALE-5/KENO-Va to assess the capabilities of KENO-Va to model the variations in the F-Lattice. Additionally, neutron flux profiles are analyzed for each case by MCNP5.

5.1 Material Change: Graphite

The key feature of the F-Lattice is the increased width of the control blades and the staggered row configuration. The nominal case of B_4C control rods with a thickness of 8.3 mm was analyzed in Section 4.7. The rod worth of the F-Lattice control blades is studied by replacing the blades by a moderator. The B_4C control rods are replaced by pure graphite. Graphite, or carbon, primarily scatters neutrons while Boron, present in B_4C, acts as a strong absorber [Duderstadt and Hamilton 1976]. Therefore, the control (absorption) material has been completely removed and replaced by a moderating material. In terms of rod worth, this represents an instantaneous reactivity change. Rod worth is evaluated as [Lamarsh 1966]:

$$\rho_w = \frac{k - k_o}{k} \tag{5.1}$$

Where k_o is the multiplication factor with control rods inserted in, and k is the multiplication factor with the control rods pulled out and replaced with pure graphite. When B_4C is replaced by graphite, neutron absorption dramatically decreases, causing an increase in neutron population, increase in flux and a larger effective multiplication factor. (Standard rod worth analysis is performed by replacing the control rods with the system's moderator material, which is light water for the F-Lattice. However, rod worth is determined by replacing B_4C with graphite to additionally study the effect of a significant material change.) The results of SCALE-5/KENO-Va, compared to the benchmark MCNP5 results, are presented in the following section to quantify the effect of this material change.

5.2 Material Change Results: Rod Worth

The SCALE-5/KENO-Va simulations were run for both the 4-bundle case and the 16-bundle case with 10,000 particles for 250 inactive cycles and 550 active cycles. MCNP5 simulations were carried out with 50,000 particles for 250 inactive cycles and 350 active cycles for the 16-bundle case. The MCNP5 4-bundle case used 100,000 particles for 250 inactive cycles and 550 active cycles. The 4-bundle case was run with more particles and histories to ensure accurate flux results. It is not necessary to run the 16-bundle case, which has a very large computational cost, for higher accuracy because results from the 4-bundle and 16-bundle case differ negligibly. The resulting effective

multiplication factors for the F-Lattice analyzed with SCALE-5/KENO-Va and MCNP5 are given in Table 5.1.

Model	MCNP5		Rod Worth	Scale-5 Keno-Va		% Error Relative to MCNP	Rod Worth	(KENO-Va-MCNP)/ σ_{max}
	Keff	σ	ρ_w	Keff	σ		ρ_w	
4-Bundle Nominal (B4C)	0.9394	0.00009	0.00	0.9417	0.00032	0.2438	0.00	7.16
4-Bundle Graphite	1.2174	0.00007	0.2284	1.2077	0.00026	-0.7911	0.2203	-37.04
16-Bundle Nominal (B4C)	0.9486	0.00016	0.00	0.9412	0.00029	-0.7770	0.00	-25.41
16-Bundle Graphite	1.2172	0.00013	0.2207	1.2092	0.00024	-0.6564	0.2216	-33.29

Table 5.1: K-effective and rod worth results for the F-Lattice (MCNP5 and SCALE-5/KENO-Va) with material change in control blades.

Rod worth of the B_4C control blades was determined by MCNP5 to be 0.2284 for the 4-bundle case and 0.2207 for the 16-bundle case. The SCALE-5/KENO-Va results lead to a calculated rod worth of 0.2203 for the 4-bundle case and 0.2216 for the 16-bundle case. Overall, a rod worth of about 0.22 indicates that the B_4C control blades (fully inserted) have a very strong effect on the core reactivity. This is beneficial to overall core life, indicating that a gradual removal of the control blades from the core will allow for a prolonged fuel burn. A preliminary study of isotopic burn-up for the model is provided in Appendix D.

The change to pure graphite control blades lead to MCNP5 results for an effective multiplication factor of 1.2174 for the 4-bundle case and 1.2172 for the 16-bundle case. SCALE-5/KENO-Va results remained within one percent error, compared to the MCNP5 results, with a k-effective of 1.2077 for the 4-bundle case and 1.2092 for the 16-bundle

case. The error is still within the acceptable range of less than one percent and actually presented a decrease from the nominal 16-bundle case, 0.66% from 0.78%. The absolute difference, between MCNP5 and SCALE-5/KENO-Va results, divided by the maximum standard deviations increased, dramatically for the 4-bundle case, when compared to the nominal B_4C case. This can be attributed to the increase, by a factor of three, in the relative difference, which correlates to a larger absolute difference. The 16-bundle case's absolute difference over standard deviation also increased despite a decrease in relative difference. However, a decrease in relative difference does not necessarily correspond to a decrease in absolute difference. There is a 28% increase in k-effective for the 16-bundle case but only an 8% increase in absolute difference, -0.0074 for the nominal B_4C 16-bundle case to -0.008 for the graphite 16-bundle case. Additionally, the decrease in the maximum standard deviation, 0.00024 from 0.00029 in the nominal case, contributes to an increased absolute difference over maximum standard deviation. While the absolute difference over the maximum standard deviation is relatively large, the small relative difference still confirms the results to be accurate for SCALE-5/KENO-Va.

Flux calculations were also compared for the 4-bundle models. The SCALE-5 models used a cuboid-defined Global Unit as it leads to better agreement with MCNP5 results, as discussed in Chapter 4 when compared to the array-defined Global Unit. The flux results, compared to MCNP5 benchmark results, using a 3 cm mesh, are given in Table 5.2.

Graphite C.B. 3 cm Mesh								Unit Normalized	
	X	Y	Z	Peak Flux (n/cm^2-s)	% Error Relative to MCNP	Average Flux (n/cm^2-s)	% Error Relative to MCNP	Variance From MCNP	Standard Deviation From MCNP
MCNP	16.5	16.5	139.5	1.5701E+16	0.00	8.3218E+15	0.00	0.0000	0.0000
SCALE	1.5	1.5	139.5	2.1350E+16	35.98	8.3441E+15	0.27	0.049771	0.223095

Table 5.2: Flux results for 4-bundle case with control blades replaced with graphite (SCALE-5/KENO-Va and MCNP5)

The average flux values for the two codes are in very close agreement, 0.27%, which is smaller than the 0.79% difference seen for the k-effective values. Similar to the flux results in Chapter 4, there is a relatively large difference in peak flux between the two codes, as well as variation in the location of the peak. However this is again due to the volume averaging error previously discussed.

Flux profiles were also analyzed on the 16-bundle cases using more advanced meshing abilities of MCNP5, discussed in Section 4.2. Neutron flux was tracked in the x-direction with a fine mesh (0.02 cm mesh spacing in the x-direction, with 1 cm mesh spacing for both the y-direction and z-direction). Due to symmetry, flux profiles in the y-direction would produce similar results. The flux profile along the x-direction was analyzed near the middle of the reactor, centered at z = 136.9 cm, and in two different y-locations for all simulations. These two locations were chosen to monitor the effect the larger control rods have on neutron population, within the control blade and through a section of fuel. The first set of flux profiles shown are along a line parallel and through the center of the main, center control blade present in the 16-bundle case (shown in Figure 4.3 as line "a"). The second set of flux profiles are along a line that is perpendicular to, and crosses the main, center control blade. This line is centered through the midpoint of the fourth fuel cell below the main center control blade, 6.894 cm from the center of the parallel running control blade (shown in Figure 4.3 as line "b"). The F4 tally was used specifying flux calculation by energy group, as described in Section 4.2. The energy grouping was 0 - 0.225 eV for thermal neutrons, 0.225 eV – 0.1 MeV for epithermal neutrons and 0.1 MeV and above for fast neutrons. Total neutron flux was also evaluated. All flux values are scaled to units of the number of neutrons per

centimeter squared per second, as dictated by Equation 4.1, to a power level of 1000 MWt.

Flux calculations that run parallel through the center of the main control blade are presented first. Thermal neutron flux is shown in Figure 5.1 and provides the most poignant example of the model's rod worth. The strong absorber, B_4C results in near zero thermal neutron flux through the center of the control blade. The locations where the nominal thermal flux dramatically increases correspond to the edges of the control blades and beginning of the light-water moderator section of the core. The stronger moderator, graphite, is shown to maintain a high thermal neutron flux throughout the blade, which is directly related to the significantly larger k-effective associated with the graphite system.

Figure 5.2 is a plot of the epithermal neutron flux. The graphite system presents a larger flux profile through the blade than the B_4C system. This is expected as more of the fast neutrons are slowed down via interactions with the graphite than are by B_4C. Figure 5.3 provides the flux profile for the fast neutrons. As expected, the graphite system again presents larger flux values, though it is not as significant as it is in the epithermal or thermal cases. Slightly more fast neutrons are present in the graphite case due to the increase in overall fission reactions that are taking place compared to the B_4C control rod system.

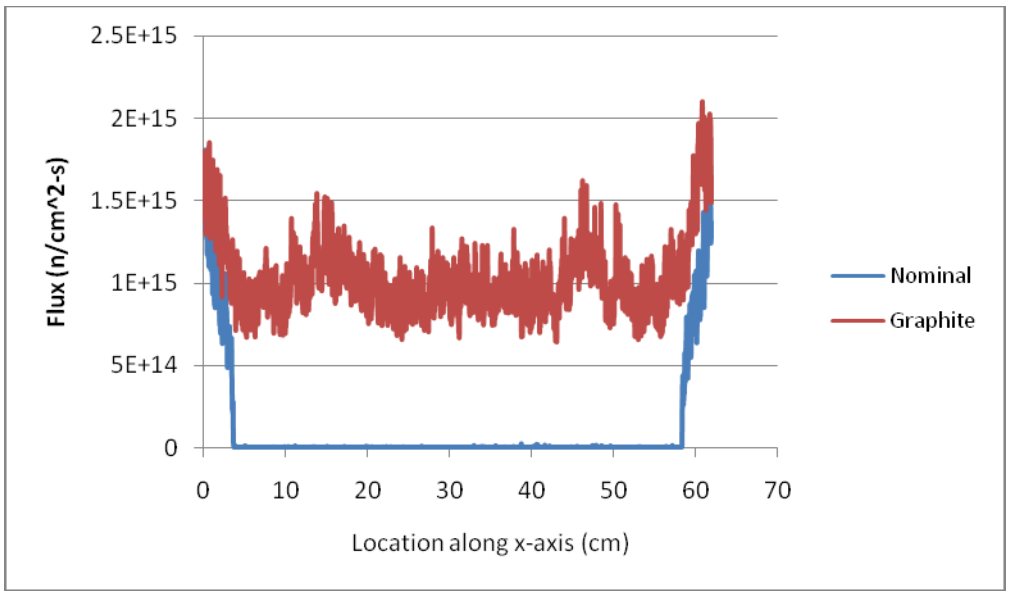

Figure 5.1: Thermal neutron flux through center control blade (graphite and B_4C).

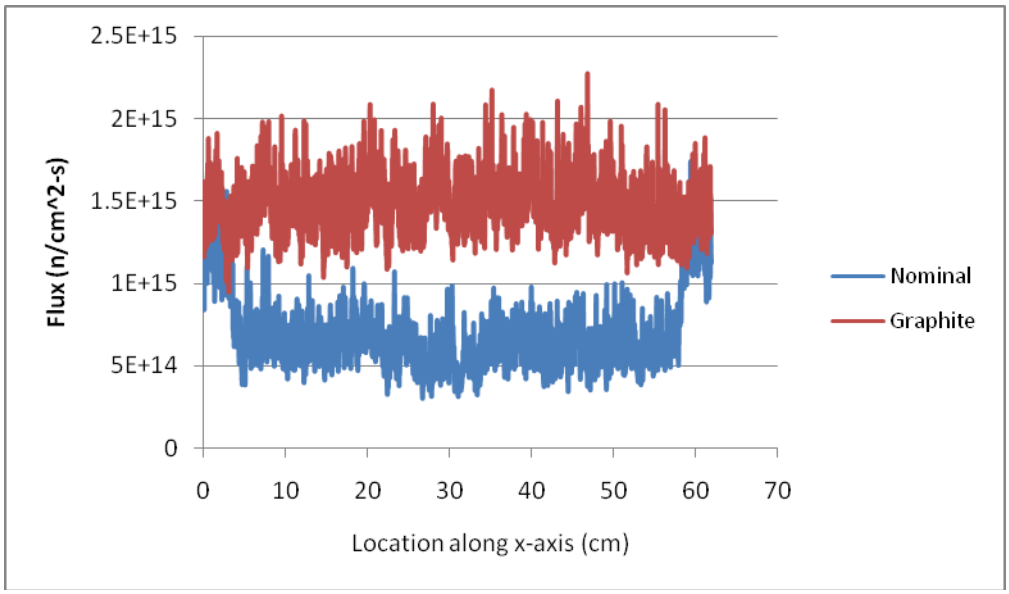

Figure 5.2: Epithermal neutron flux through center control blade (graphite and B_4C).

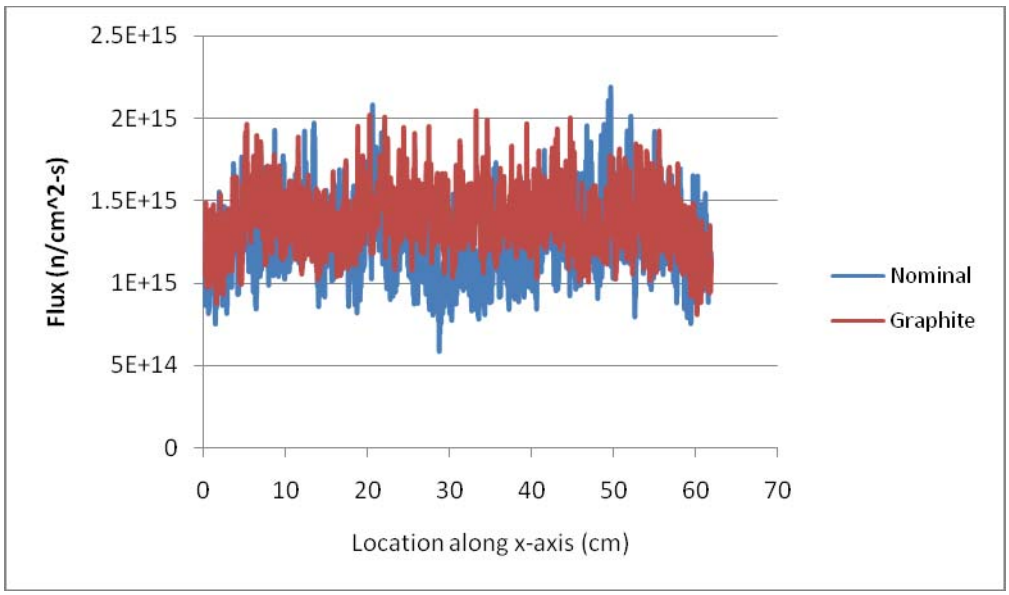

Figure 5.3: Fast neutron flux through center control blade (graphite and B_4C).

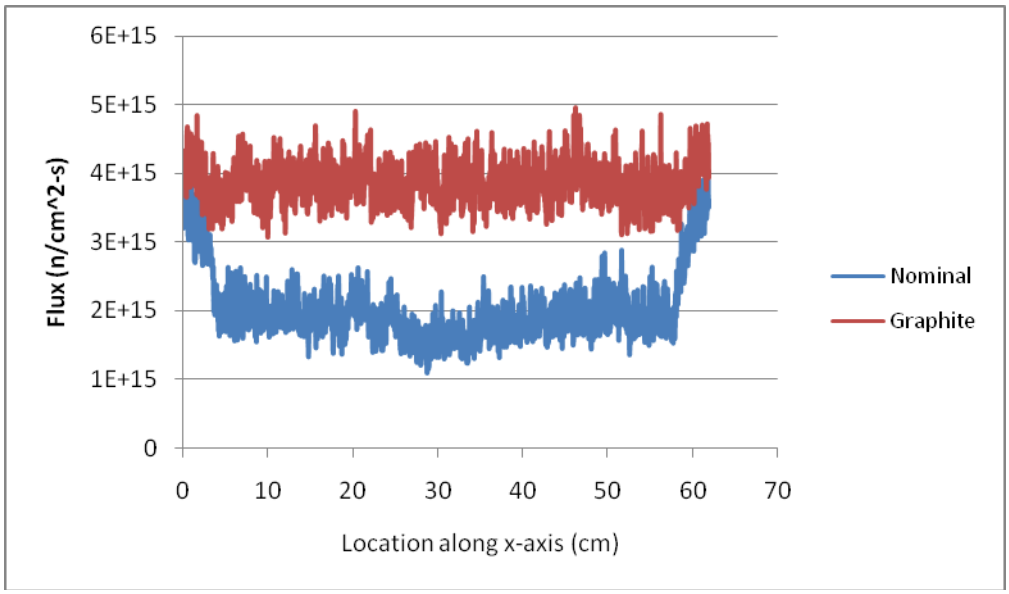

Figure 5.4: Total neutron flux through center control blade (graphite and B_4C).

There is significant difference in the total neutron flux (Figure 5.4) between the graphite blade model and the nominal B_4C blade model, mostly due to the increase in the thermal and epithermal neutron population shown in Figures 5.1 - 5.3.

Table 5.3 provides pertinent numerical flux results for the mesh that runs parallel through the center of the control blade.

Thermal						Normalized	
	Peak Flux Location in X-dimension (cm)	Peak Flux (n/cm^2-s)	Peak Relative % Variation	Average Flux (n/cm^2-s)	Average Relative % Variation	Variance From Nominal	Standard Deviation From Nominal
B4C	0.15	1.8093E+15	0.00	1.0741E+14	0.00	0.0000	0.0000
Graphite	60.85	2.0965E+15	15.87	1.0188E+15	848.58	0.1970	0.4439

Epithermal						Normalized	
	Peak Flux Location in X-dimension (cm)	Peak Flux (n/cm^2-s)	Peak Relative % Variation	Average Flux (n/cm^2-s)	Average Relative % Variation	Variance From Nominal	Standard Deviation From Nominal
B4C	59.43	1.7335E+15	0.00	6.7478E+14	0.00	0.0000	0.0000
Graphite	46.83	2.2751E+15	31.24	1.4691E+15	117.72	0.0892	0.2987

Fast						Normalized	
	Peak Flux Location in X-dimension (cm)	Peak Flux (n/cm^2-s)	Peak Relative % Variation	Average Flux (n/cm^2-s)	Average Relative % Variation	Variance From Nominal	Standard Deviation From Nominal
B4C	49.67	2.1858E+15	0.00	1.2277E+15	0.00	0.0000	0.0000
Graphite	33.23	2.0461E+15	6.39	1.3624E+15	10.97	0.0257	0.1602

Total						Normalized	
	Peak Flux Location in X-dimension (cm)	Peak Flux (n/cm^2-s)	Peak Relative % Variation	Average Flux (n/cm^2-s)	Average Relative % Variation	Variance From Nominal	Standard Deviation From Nominal
B4C	0.45	4.0621E+15	0.00	2.0099E+15	0.00	0.0000	0.0000
Graphite	46.23	4.9559E+15	22.00	3.8504E+15	91.57	0.0955	0.3091

Table 5.3: Flux profile results through center control blade (graphite and B_4C).

The largest effect on the system was on the thermal and epithermal neutrons, as expected by the significant 0.22 rod worth of the B_4C control blades.

Results for the flux calculations along the line that runs through the center of fuel cells and perpendicularly intersect the center control blade are presented in Figures 5.5 – Figure 5.8. Both flux profiles are normalized, following Equation 4.1, to a power level of

1000 MWt. Flux magnitudes are determined by this normalization technique. However, with no other changes, replacing B_4C with graphite would actually result in a larger power level, and also larger flux values. 1000 MWt was maintained in both cases to allow for a direct comparison of the effect the material change has on the flux distribution. The constant power normalization is the reason that the peak flux values in the thermal flux (Figure 5.5) are larger for the nominal case, compared to the graphite case.

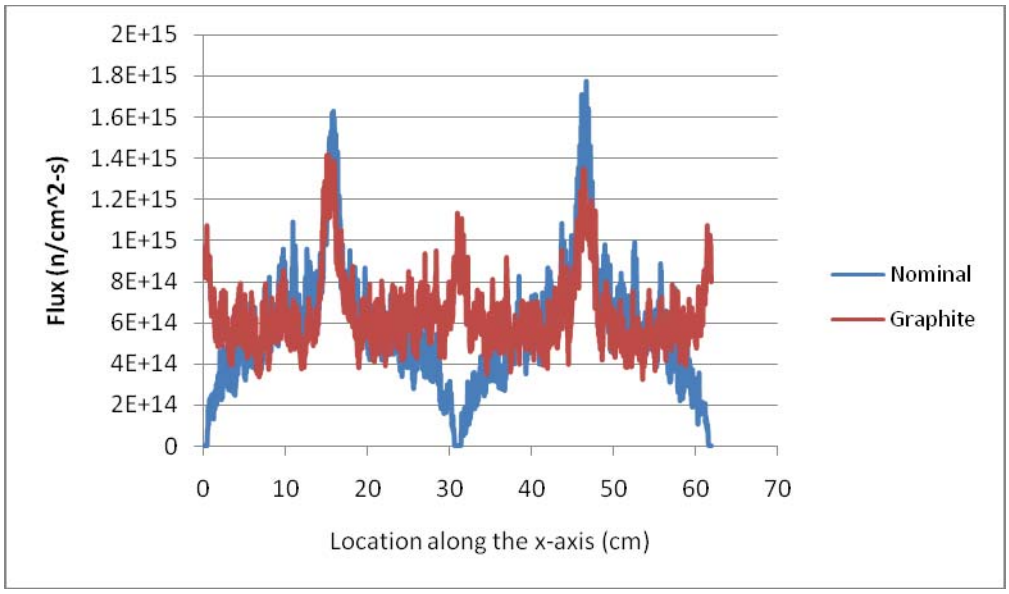

Figure 5.5: Thermal neutron flux along a line that runs through fuel and perpendicularly intersects the center blade (graphite and B_4C).

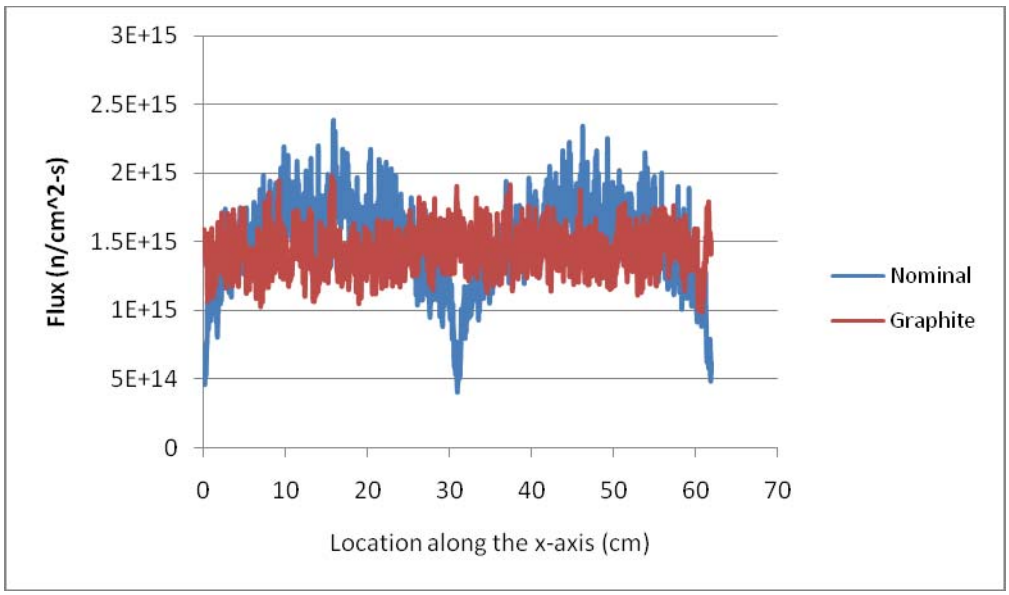

Figure 5.6: Epithermal neutron flux along a line that runs through fuel and perpendicularly intersects the center blade (graphite and B_4C).

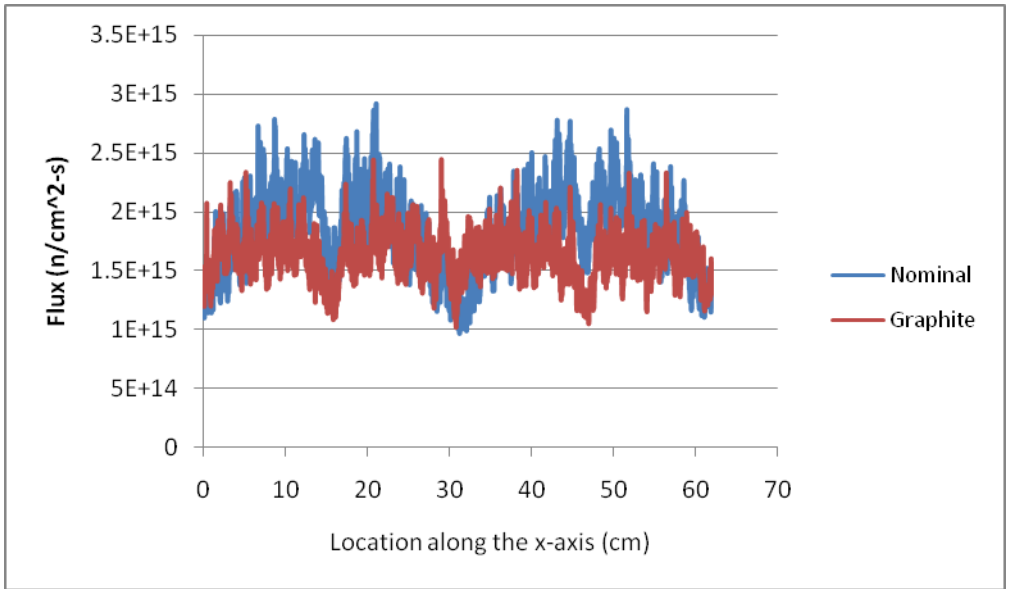

Figure 5.7: Fast neutron flux along a line that runs through fuel and perpendicularly intersects the center blade (graphite and B_4C).

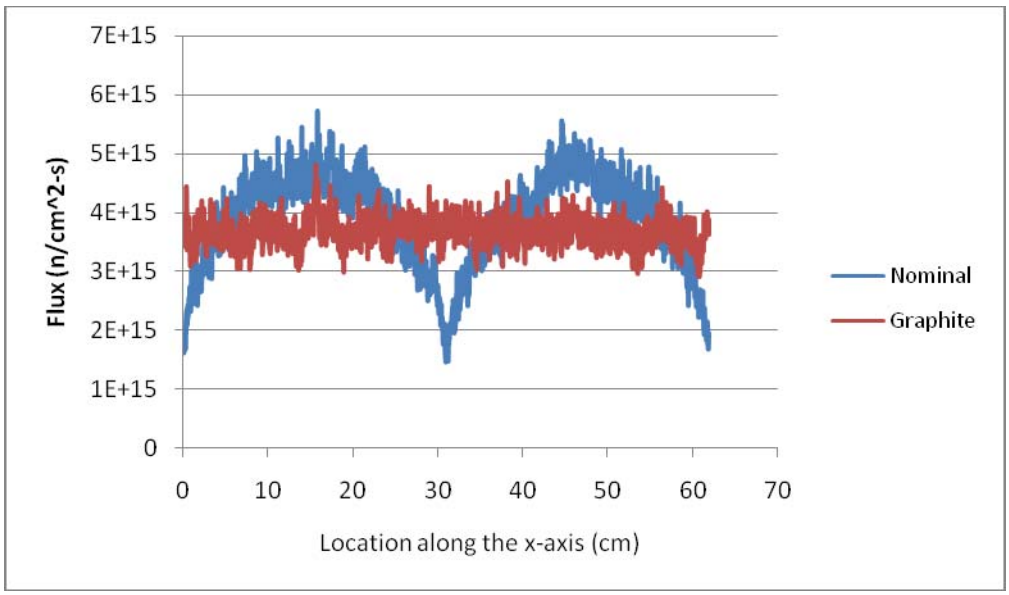

Figure 5.8: Total neutron flux along a line that runs through fuel and perpendicularly intersects the center blade (graphite and B_4C).

Again, the graphite rods have a dramatic effect on the thermal nuetron population. Additional peaks are located near the graphite control blades, where in the B_4C system the control blades have sharp decreases in thermal neutrons. Total flux is essentially flat for the graphite system. Table 5.4 provides the pertinent data for the flux calculations. The average total flux only differs by 5.24% in the fuel region, but by a significant 91.57% at the blade location for the graphite results compared to the B_4C blade results. This is due to the strong effect the material of the control blade has, especially in the central locations near the blades.

Thermal						Normalized	
	Peak Flux Location in X-dimension (cm)	Peak Flux (n/cm^2-s)	Peak Relative % Variation	Average Flux (n/cm^2-s)	Average Relative % Variation	Variance From Nominal	Standard Deviation From Nominal
B4C	46.69	1.7719E+15	0.00	5.4523E+14	0.00	0.0000	0.0000
Graphite	15.01	1.4123E+15	20.30	6.2985E+14	-15.52	0.0441	0.2100

Epithermal						Normalized	
	Peak Flux Location in X-dimension (cm)	Peak Flux (n/cm^2-s)	Peak Relative % Variation	Average Flux (n/cm^2-s)	Average Relative % Variation	Variance From Nominal	Standard Deviation From Nominal
B4C	15.81	2.3876E+15	0.00	1.4830E+15	0.00	0.0000	0.0000
Graphite	15.61	1.9810E+15	17.03	1.4110E+15	4.86	0.0311	0.1764

Fast						Normalized	
	Peak Flux Location in X-dimension (cm)	Peak Flux (n/cm^2-s)	Peak Relative % Variation	Average Flux (n/cm^2-s)	Average Relative % Variation	Variance From Nominal	Standard Deviation From Nominal
B4C	21.03	2.9111E+15	0.00	1.8308E+15	0.00	0.0000	0.0000
Graphite	20.69	2.4427E+15	16.09	1.6159E+15	11.74	0.0160	0.1264

Total						Normalized	
	Peak Flux Location in X-dimension (cm)	Peak Flux (n/cm^2-s)	Peak Relative % Variation	Average Flux (n/cm^2-s)	Average Relative % Variation	Variance From Nominal	Standard Deviation From Nominal
B4C	15.81	5.7218E+15	0.00	3.8591E+15	0.00	0.0000	0.0000
Graphite	15.61	4.8079E+15	15.97	3.6567E+15	5.24	0.0285	0.1687

Table 5.4: Flux results along a line that runs through fuel and perpendicularly intersects the center blade (graphite and B_4C).

The rod worth of the model was determined to be 0.22 (when replaced by pure graphite blades). The abilities for KENO-Va (within SCALE-5) to accuratly calculate k-effective and flux distributions for the F-Lattice, compared to MCNP5, were not affected despite significant variations in the neutron population.

As the last validation test, the abilities of SCALE-5/KENO-Va are assessed when only slight modifications are made in the model from the nominal case. The control blade geometry is modified and its impact on k and flux results is analyzed in the following section.

5.3 Geometry Change: +/-10% in Thickness of Control Blade

Section 5.2 confirmed that SCALE-5/KENO-Va is capable of calculating the effective multiplication factor with less than one percent error (MCNP5 benchmarks results) for the F-Lattice after a large change in reactivity in rod worth calculations. Additionally, the flux capabilities developed in Chapter 4 were tested for rod worth calculations.

Less dramatic changes can be studied by varying the thickness of the control blades. The pitch remains constant but the thickness of the control blade is varied by +/-10%, thus affecting the size of the water gap between the fuel and the control blade. Altering the thickness of the control blades also results in a significant change in quantity of control material present in the system. While rod worth is directly proportional to the ratio of control blade surface area to fuel volume (control rod worth will increase as this ratio increases [Duderstadt and Hamilton 1976]) the change in surface area is negligible due to small variations in control rod thickness. (Rod worth calculations were carried out because of the significant increase or decrease in control material volume.) Reactivity changes are expected to be small due to the fact that the control blades' absorption cross-section, the control blade surface area and the fuel volume (the three main components of rod worth [Duderstadt and Hamilton 1976]) are not significantly affected in this parametric study.

The three cases of nominal control blade thickness of 8.3 mm, 10% thicker (9.13 mm) and 10% thinner (7.47 mm) are studied with KENO-Va (within SCALE-5) and MCNP5. Additionally, comparisons of the flux results similar to those presented in Section 5.2 are provided.

5.4 Results for Three Different Control Blade Thicknesses

The two new cases were run in MCNP5 with 50,000 particles for 250 inactive cycles and 350 active cycles for both the 4-bundle and 16-bundle cases. The KENO-Va cases were both run with 10,000 particles for 250 inactive cycles and 550 active cycles. Results for the nominal test cases are the same as those presented in Section 5.2. Table 5.5a provides the k-effective results for these trials. Results for change in reactivity are given in Table 5.5b.

Model	MCNP5		% Variation Relative to MCNP Nominal Case	Scale-5 Keno-Va		% Error Relative to MCNP	% Variation Relative to Scale-5 Nominal Case	(KENO-Va-MCNP)/σ_{max}
	Keff	σ		Keff	σ			
4-Bundle Nominal	0.9394	0.00009	0.0000	0.9417	0.00032	0.2438	0.0000	7.16
4-Bundle 10% Thinner	0.9430	0.00009	0.3832	0.9460	0.00028	0.3086	0.3345	6.52
4-Bundle 10% Thicker	0.9365	0.00009	-0.3119	0.9392	0.00028	0.2915	-0.2644	9.75
16-Bundle Nominal	0.9486	0.00016	0.0000	0.9412	0.00029	0.7770	0.0000	-25.41
16-Bundle 10% Thinner	0.9520	0.00017	0.3605	0.9452	0.00029	0.7122	0.4261	-23.38
16-Bundle 10% Thicker	0.9452	0.00016	-0.3511	0.9373	0.00028	0.8368	-0.4112	-28.25

Table 5.5a: K-effective results for control blade thickness changes (MCNP5 and SCALE-5/KENO-Va).

Model	MCNP5	Reactivity Change	Scale-5 Keno-Va	Reactivity Change
	Keff	$\Delta\rho_w$	Keff	$\Delta\rho_w$
4-Bundle Nominal	0.9394	0	0.9417	0
4-Bundle 10% Thinner	0.943	0.0038	0.946	0.0045
4-Bundle 10% Thicker	0.9365	-0.0031	0.9392	-0.0027
16-Bundle Nominal	0.9486	0	0.9412	0
16-Bundle 10% Thinner	0.952	0.0036	0.9452	0.0042
16-Bundle 10% Thicker	0.9452	-0.0036	0.9373	-0.0042

Table 5.5b: Reactivity results for control blade thickness changes (MCNP5 and SCALE-5/KENO-Va).

The 10% thinner cases lead to an increase in the effective multiplication factor between 0.33% - 0.43% from nominal. The 10% thicker cases all produced a decrease on a similar scale, 0.26% - 0.41%. The (+/-) 10% thickness changes lead to overall reactivity changes of about (+/-) 0.004 (Table 5.5b). Relative error for KENO-Va compared to MCNP5 remained below one percent for this variation; however, a maximum relative error of 0.84% occurred in the 16-bundle 10% thicker case. Very little change in reactivity occurred because only control material volume, and not surface area, was altered.

A 3 cm mesh was imposed for flux distributions, for all three blade thickness cases, using MCNP5 and SCALE-5/KENO-Va. A cuboid-defined Global Unit was used in the KENO-Va cases and all calculations were performed for the 4-bundle case. Results are shown in Table 5.6 and Table 5.7 for the 10% thinner blade and 10% thicker blade cases, respectively.

These tests provide the final validation for the flux calculation abilities of SCALE-5/KENO-Va. The average flux percent error for KENO-Va, compared to MCNP5, remained around 3 percent, 3.08% for the 10% thinner case and 3.21% for the 10% thicker case, where the nominal case had 3.23% error (Table 4.5). The volume averaging error is present again but the overall results provide acceptable agreement between the two code packages.

10% Thinner C.B. 3 cm Mesh								Unit Normalized	
	X	Y	Z	Peak Flux (n/cm^2-s)	% Error Relative to MCNP	Average Flux (n/cm^2-s)	% Error Relative to MCNP	Variance From MCNP	Standard Deviation From MCNP
MCNP	16.5	16.5	103.5	2.287E+16	0.00	9.4960E+15	0.00	0.0000	0.0000
SCALE	16.5	16.5	124.5	2.838E+16	24.06	9.2033E+15	-3.08	0.0251	0.1586

Table 5.6: Flux results for 4-bundle model with 7.47 mm thick control blade (SCALE-5/KENO-Va and MCNP5).

10% Thicker C.B. 3 cm Mesh								Unit Normalized	
	X	Y	Z	Peak Flux (n/cm^2-s)	% Error Relative to MCNP	Average Flux (n/cm^2-s)	% Error Relative to MCNP	Variance From MCNP	Standard Deviation From MCNP
MCNP	16.5	16.5	118.5	2.312E+16	0.00	9.5623E+15	0.00	0.0000	0.0000
SCALE	16.5	16.5	91.5	2.872E+16	24.20	9.2553E+15	-3.21	0.0246	0.1567

Table 5.7: Flux results for 4-bundle model with 9.13 mm thick control blade (SCALE-5/KENO-Va and MCNP5).

Flux distribution results for the three MCNP5 cases are reported for the same location and energy grouping as described in Section 5.2 for the rod worth studies. The results for the mesh parallel with and through the center of the main control blade are presented in Figure 5.9 - Figure 5.12. Little to no variation can be detected between all three cases, as would be expected considering that there is less than 0.45% variation in the three models' k-effective values.

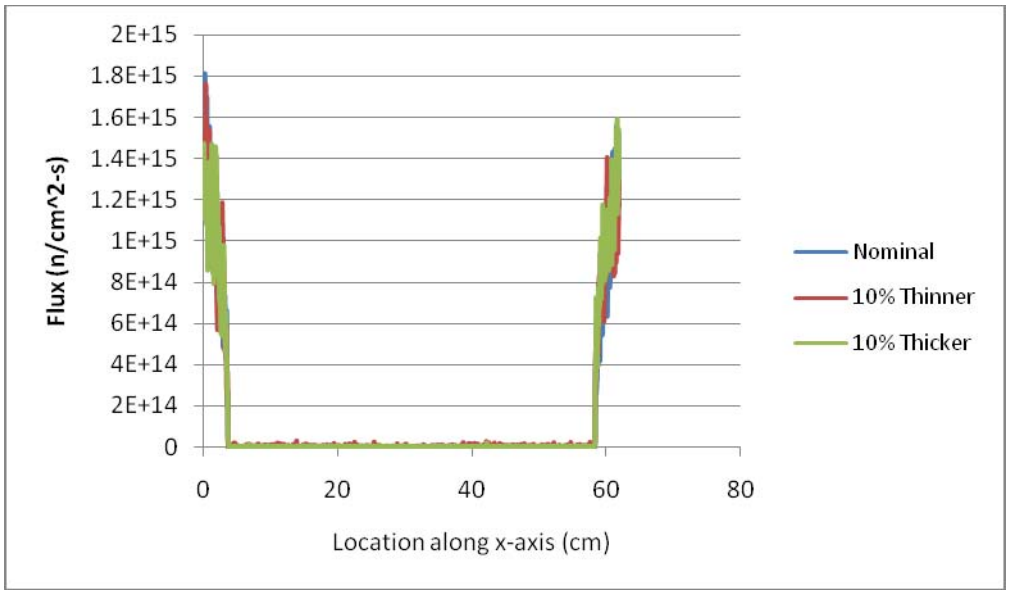

Figure 5.9: Thermal neutron flux through the center of the main control blade for three different control blade thicknesses.

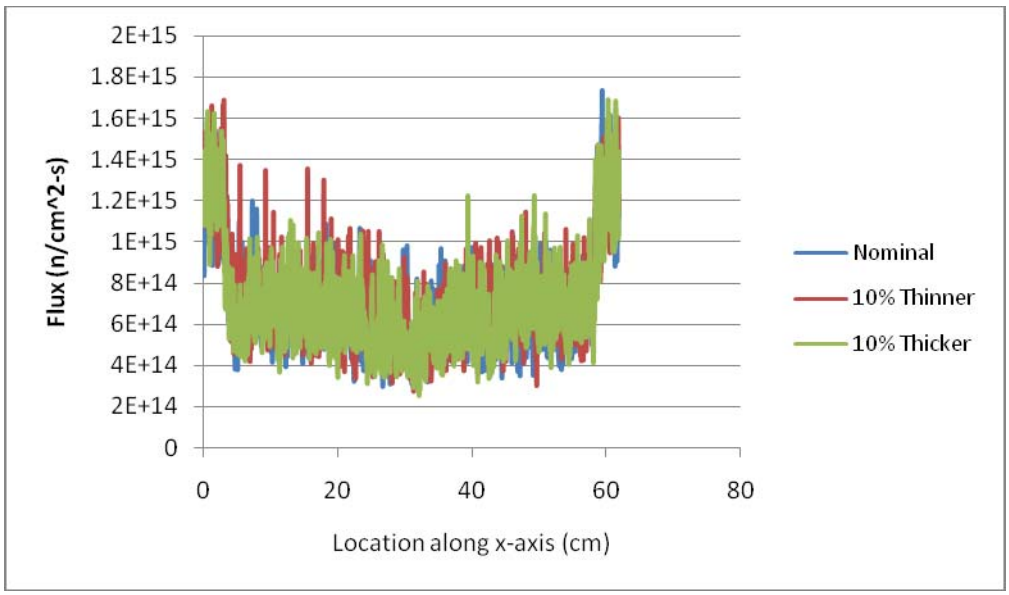

Figure 5.10: Epithermal neutron flux through the center of the main control blade for three different control blade thicknesses.

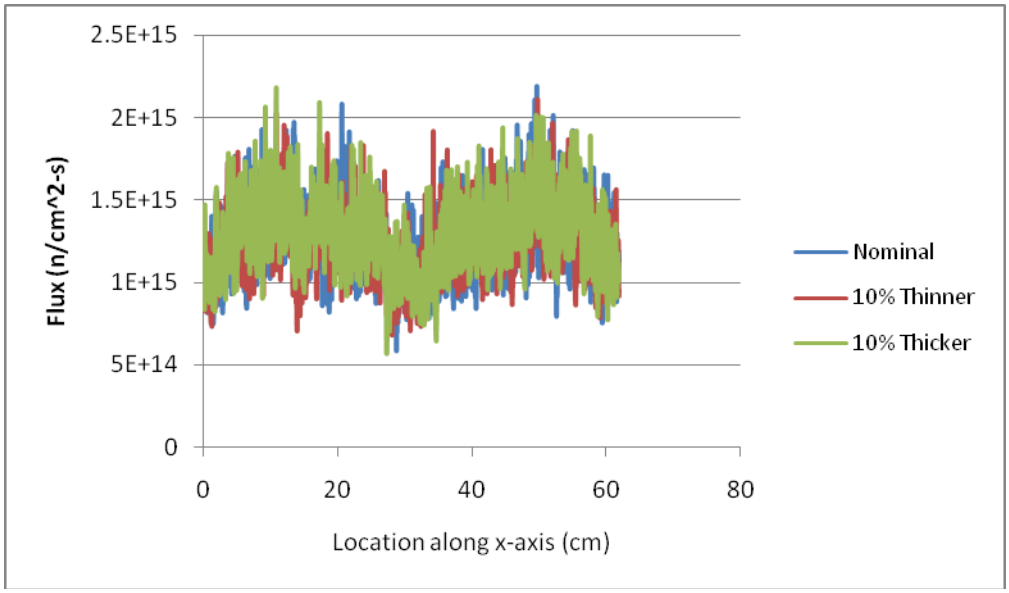

Figure 5.11: Fast neutron flux through the center of the main control blade for three different control blade thicknesses.

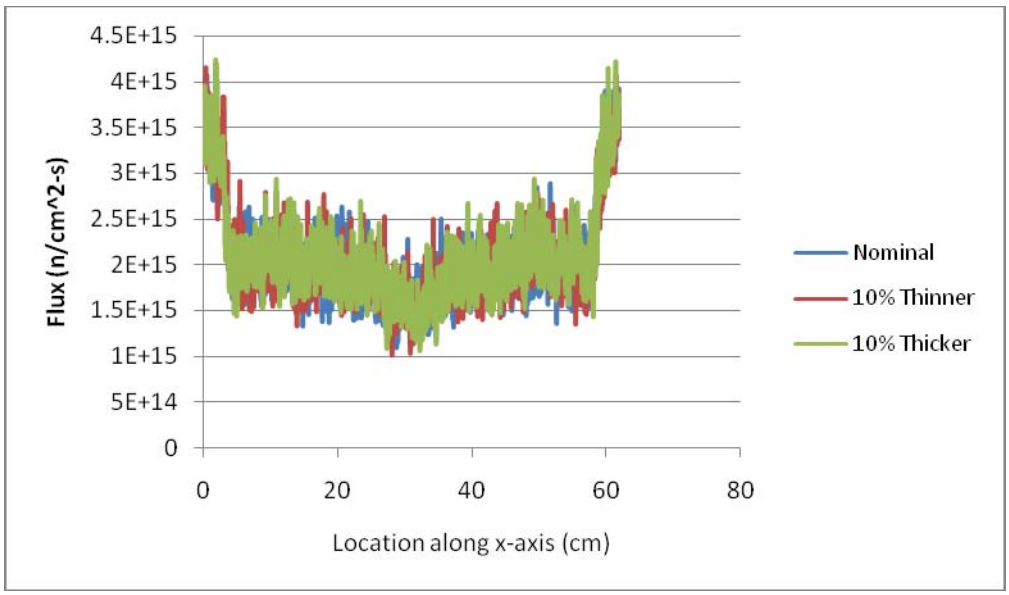

Figure 5.12: Total neutron flux through the center of the main control blade for three different control blade thicknesses.

The numerical values for comparisons between the flux results are given in Table 5.8. Total relative variation for the three cases remained below 5% for all energy groups. The average variation for the total neutron flux was 1.05% for the 10% thinner model. The 10% thicker model showed a 2.06% variation in total nuetron flux compared to the nominal case results. (All cases showed an increase in average flux from the nominal case except for the fast neutron group in the 10% thinner case. This is due to the fact that all three cases are scaled to the same power level of 1000 MWt, as dictated by Equation 4.1.)

Thermal						Normalized	
	Peak Flux Location in X-dimension (cm)	Peak Flux (n/cm^2-s)	Peak Relative % Variation	Average Flux (n/cm^2-s)	Average Relative % Variation	Variance From Nominal	Standard Deviation From Nominal
Nominal	0.15	1.8093E+15	0.00	1.0741E+14	0.00	0.0000	0.0000
10% Thinner	0.25	1.7627E+15	-2.58	1.0987E+14	2.29	0.0016	0.0395
10% Thicker	61.67	1.5906E+15	-12.09	1.1031E+14	2.70	0.0026	0.0511

Epithermal						Normalized	
	Peak Flux Location in X-dimension (cm)	Peak Flux (n/cm^2-s)	Peak Relative % Variation	Average Flux (n/cm^2-s)	Average Relative % Variation	Variance From Nominal	Standard Deviation From Nominal
Nominal	59.43	1.7335E+15	0.00	6.7478E+14	0.00	0.0000	0.0000
10% Thinner	2.99	1.6851E+15	-2.79	7.0647E+14	4.70	0.0114	0.1066
10% Thicker	60.31	1.6890E+15	-2.56	6.7866E+14	0.57	0.0119	0.1089

Fast						Normalized	
	Peak Flux Location in X-dimension (cm)	Peak Flux (n/cm^2-s)	Peak Relative % Variation	Average Flux (n/cm^2-s)	Average Relative % Variation	Variance From Nominal	Standard Deviation From Nominal
Nominal	49.67	2.1858E+15	0.00	1.2277E+15	0.00	0.0000	0.0000
10% Thinner	49.79	2.1080E+15	-3.56	1.2237E+15	-0.33	0.0141	0.1188
10% Thicker	10.79	2.1806E+15	-0.24	1.2624E+15	2.83	0.0138	0.1174

Total						Normalized	
	Peak Flux Location in X-dimension (cm)	Peak Flux (n/cm^2-s)	Peak Relative % Variation	Average Flux (n/cm^2-s)	Average Relative % Variation	Variance From Nominal	Standard Deviation From Nominal
Nominal	0.45	4.0621E+15	0.00	2.0099E+15	0.00	0.0000	0.0000
10% Thinner	0.29	4.1468E+15	2.08	2.0401E+15	1.50	0.0057	0.0753
10% Thicker	1.75	4.2313E+15	4.16	2.0514E+15	2.06	0.0062	0.0788

Table 5.8: Flux results through the center of the main control blade for three different control blade thicknesses.

The results for the flux distributions along a line through the fuel section and perpendicular to the center control blade are shown in Figure 5.13 – Figure 5.16.

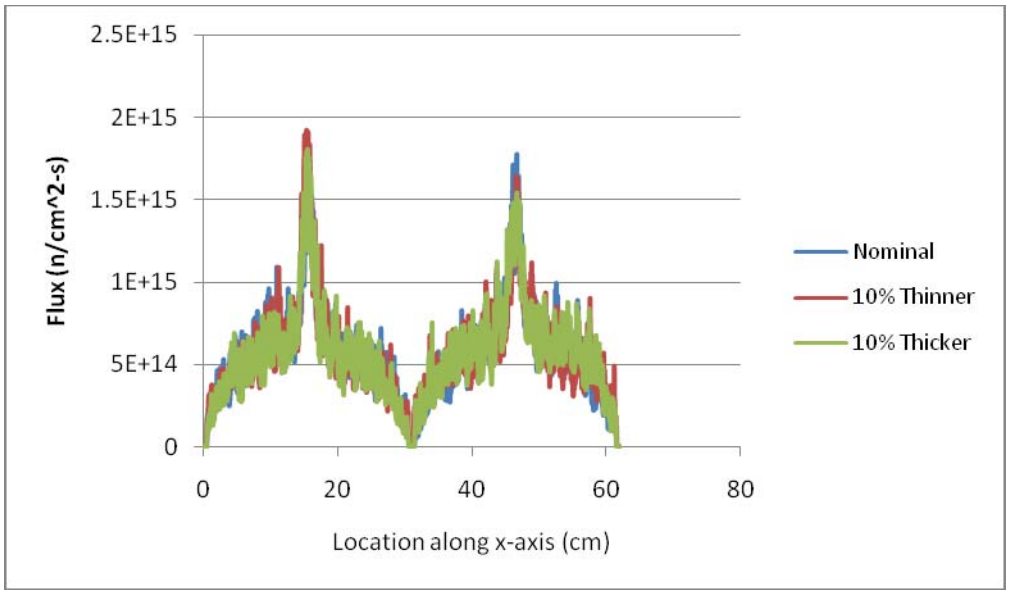

Figure 5.13: Thermal neutron flux along a line that runs through fuel and perpendicularly intersects the center blade for all three control blade thicknesses.

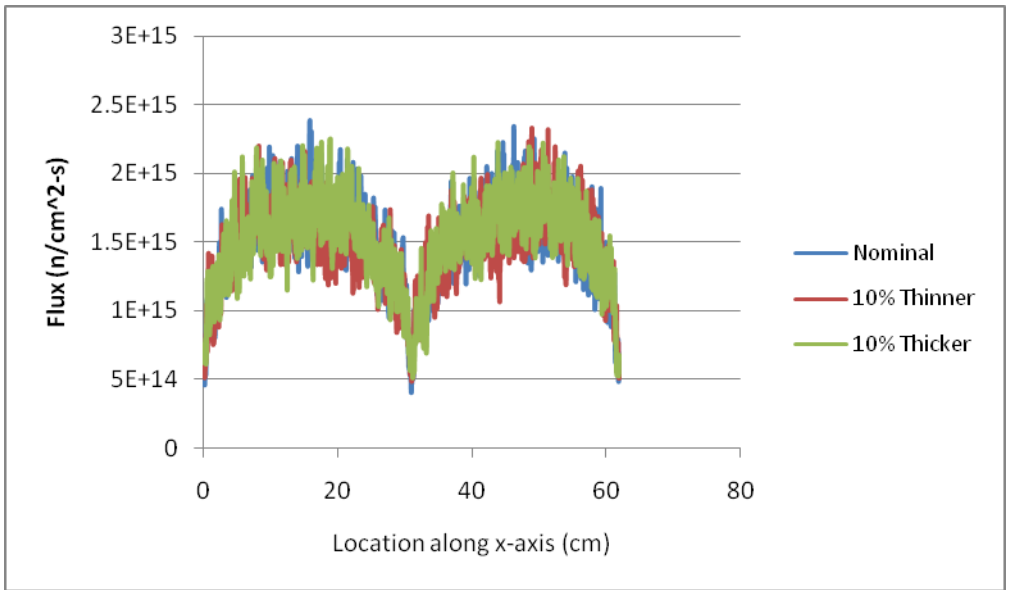

Figure 5.14: Epithermal neutron flux along a line that runs through fuel and perpendicularly intersects the center blade for all three control blade thicknesses.

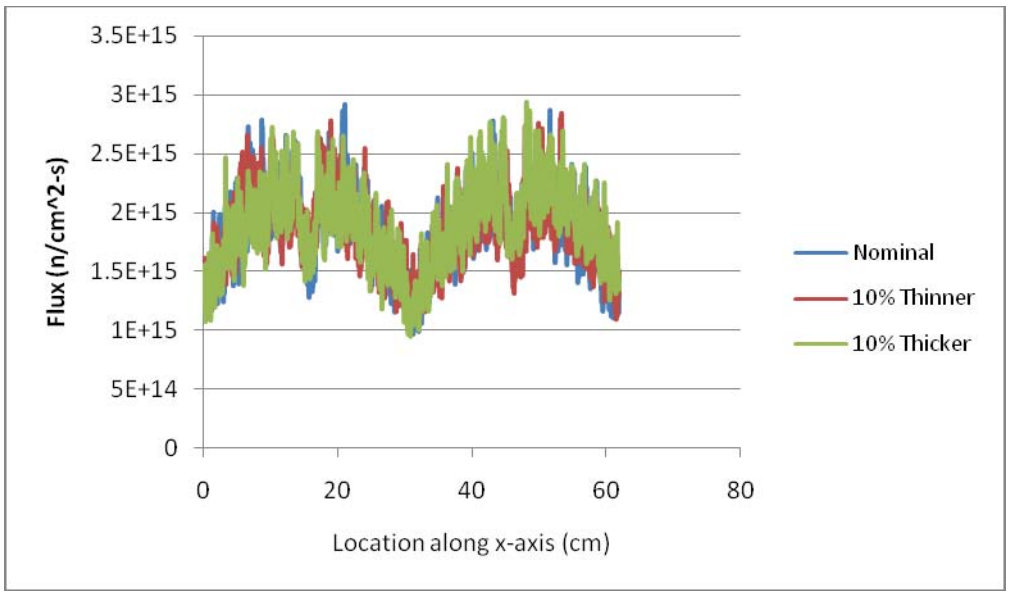

Figure 5.15: Fast neutron flux along a line that runs through fuel and perpendicularly intersects the center blade for all three control blade thicknesses.

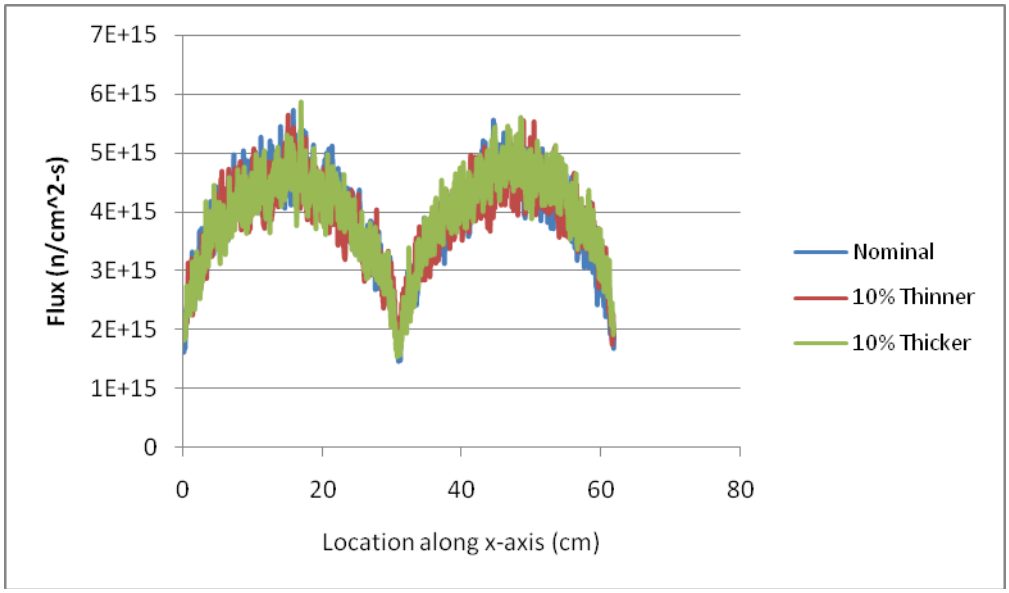

Figure 5.16: Fast neutron flux along a line that runs through fuel and perpendicularly intersects the center blade for all three control blade thicknesses.

Again, there is negligible variation noticeable in the neutron flux profiles. Table 5.9 provides the numerical results of the flux calculations.

Thermal						Normalized	
	Peak Flux Location in X-dimension (cm)	Peak Flux (n/cm^2-s)	Peak Relative % Variation	Average Flux (n/cm^2-s)	Average Relative % Variation	Variance From Nominal	Standard Deviation From Nominal
Nominal	46.69	1.7719E+15	0.00	5.4523E+14	0.00	0.0000	0.0000
10% Thinner	15.31	1.9199E+15	8.35	5.4862E+14	0.62	0.0056	0.0748
10% Thicker	15.47	1.8032E+15	1.76	5.3917E+14	-1.11	0.0048	0.0696

Epithermal						Normalized	
	Peak Flux Location in X-dimension (cm)	Peak Flux (n/cm^2-s)	Peak Relative % Variation	Average Flux (n/cm^2-s)	Average Relative % Variation	Variance From Nominal	Standard Deviation From Nominal
Nominal	15.81	2.3876E+15	0.00	1.4830E+15	0.00	0.0000	0.0000
10% Thinner	48.93	2.3294E+15	-2.44	1.4472E+15	-2.42	0.0092	0.0961
10% Thicker	18.87	2.2548E+15	-5.56	1.4845E+15	0.10	0.0106	0.1029

Fast						Normalized	
	Peak Flux Location in X-dimension (cm)	Peak Flux (n/cm^2-s)	Peak Relative % Variation	Average Flux (n/cm^2-s)	Average Relative % Variation	Variance From Nominal	Standard Deviation From Nominal
Nominal	21.03	2.9111E+15	0.00	1.8308E+15	0.00	0.0000	0.0000
10% Thinner	53.35	2.8406E+15	-2.42	1.8245E+15	-0.34	0.0080	0.0893
10% Thicker	48.13	2.9293E+15	0.62	1.8565E+15	1.40	0.0079	0.0890

Total						Normalized	
	Peak Flux Location in X-dimension (cm)	Peak Flux (n/cm^2-s)	Peak Relative % Variation	Average Flux (n/cm^2-s)	Average Relative % Variation	Variance From Nominal	Standard Deviation From Nominal
Nominal	15.81	5.7218E+15	0.00	3.8591E+15	0.00	0.0000	0.0000
10% Thinner	15.07	5.6319E+15	-1.57	3.8203E+15	-1.00	0.0044	0.0663
10% Thicker	16.93	5.8659E+15	2.52	3.8801E+15	0.55	0.0043	0.0652

Table 5.9: Flux results along a line that runs through fuel and perpendicularly intersects the center blade for all three control blade thicknesses.

Total neutron flux have relative variations of only -1.00% for the 10% thinner case and 0.55% for the 10% thicker. While peak values varied by less than 9% in all cases, peak location remained near the nominal peak location for the total flux. However, due to the symmetry of the models, the difference in the location of the peak values does not indicate serious variation in the fluxes.

5.5 Parametric Study Conclusions

SCALE-5/KENO-Va accurately modeled all tested variations in material and geometry as compared to MCNP5 results. Difference in the calculated effective multiplication factor remained below one percent for all modifications: in agreement with the work done by Johnson and Clarno [2007]. Additionally, the ability of SCALE-5/KENO-Va to calculate flux values were further validated with these variations. This is significant in that moderate and major changes were made to total neutron population of the system. More detailed neutron flux profiles were investigated using the abilities of MCNP5 but could not be compared to SCALE-5/KENO-Va because of the limitations in the mesh, as discussed in Chapter 4 and Chapter 3. Rod worth calculations were also performed, where replacing the B_4C control blades with pure graphite blades resulted in a significant change in reactivity. The resulting rod worth of $|\rho_w| = 0.22$ indicates that the F-Lattice can have a long core life.

Chapter 6: Conclusions

6.1 Summary and Conclusion

The current resurgence of interest in the nuclear power industry has led to renewed interest in new reactor designs. The GE Compact Modular Boiling Water Reactor (CM-BWR) is one such reactor. The 350 MWe CM-BWR is designed for small incremental additions to the power grid. A key feature of the CM-BWR is the use of the unique F-Lattice. The F-Lattice employs a staggered row configuration for the control blades. Additionally, the control blades are more than double the width of control blades found in most commercial boiling water reactors today. Increase in blade width and pitch allows for approximately a one-half factor decrease in the number of control blades. Reduction in control blades results in a large reduction in control rod related components. This reduces construction and maintenance costs, as well as reducing the risk of failures within the core. However, before design certification can be completed for the CM-BWR, first the tools needed to study and monitor reactor core performance must be validated.

The purpose of this thesis was to validate the SCALE packages for the F-Lattice design used in the CM-BWR core. This has been at least partially achieved in several steps. The computational cost associated with SCALE-5.1/KENO-VI, SCALE-5/KENO-VA and MCNP5 was determined. The limitations and advantages of each code were discussed. It was found that SCALE-5.1/KENO-VI is very computationally intensive for detailed analysis. Use of SCALE-5/KENO-VI, over MCNP5, for complex problems

requiring spatially detailed results is not recommended. Analysis of the F-Lattice with SCALE-5/KENO-Va and SCALE-5.1/KENO-VI showed little difference in accuracy compared to MCNP5. Therefore it was determined that SCALE-5/KENO-Va is not only able to produce accurate results (k-effective and flux distributions) for the F-Lattice, but it can do so much more efficiently than either SCALE-5.1/KENO-VI or MCNP5.

New techniques were developed to appropriately compare and validate the SCALE-5/KENO-Va flux results. Average flux values were found to be accurate (compared to MCNP5). However, only qualitative agreement was found for flux distribution between the SCALE-5/KENO-Va and MCNP5 results. Cell specific flux values may have significant error due to a "volume averaging" technique used in normalizing the SCALE-5/KENO-Va flux results to the proper units. The "volume "averaging" error was quantified by hand-calculations that produced SCALE-5 flux results with less than one percent error compared to MCNP5 results. More accurate flux results could not be achieved through mesh refinement due to memory and hard drive limitations associated with SCALE-5/KENO-Va.

Parametric design studies, on material properties and geometry, were also validated for SCALE-5/KENO-Va against MCNP5 benchmark results. The SCALE-5/KENO-Va calculated k-effective values remained within one percent of MCNP5 benchmark results, and average flux calculations also remained within an acceptable agreement of about 3%. Rod worth calculations led to a significant change in reactivity resulting from the instantaneous removal of the B_4C control blades. Therefore, gradual removal of control blades is expected to produce a relatively long fuel lifetime. Fuel

burn-up calculations are still necessary to determine the core life (preliminary burn-up results are provided in Appendix D).

In conclusion, SCALE-5/KENO-Va is found to be capable of efficient and accurate results for the F-Lattice k-effective calculations. This is important because minor variations in core configuration, such as testing different fuel compositions, can now be trusted to be accurately modeled in SCALE-5. Additionally, the first steps to validate neutron flux distributions calculated by SCALE-5 are developed in this thesis. This will allow design engineers to test many different types of modifications to the F-Lattice in a timely and efficient manner before using a more powerful and computationally costly code, such as MCNP5, for the finer details of the system.

6.2 Future Work

There are many areas relating to the F-Lattice and to code validation for the analysis of the F-Lattice that require further study. The primary suggestion for future work would be testing the flux calculations of SCALE-5/KENO-Va with an even higher level of mesh refinement. This could be done in two ways. The first would be to make an adjustment to the SCALE-5 package source code. Suggested features to enhance would be the ability to locally define the mesh size in each dimension. A restructuring of the output file format should also be examined. A second alternative for testing the accuracy of the flux calculations would be to use a supercomputer with a very large memory and hard drive space. It is believed that it is a simple hardware limitation that is preventing a more refined mesh to be analyzed with SCALE-5. Access to more powerful computers could prove both the validity of that claim, as well as allow a more meaningful comparison to the MCNP5 results. Work to eliminate the volume averaging error

discussed in this thesis should also be explored. This would require developing the tools to read the SCALE-5/KENO-Va geometry and mesh size and carry out individual volume calculations on a cell by cell basis. It is important to develop an automated tool to perform these calculations because geometry and mesh size can vary dramatically depending on the model being studied.

Additional relevant work is to explore deterministic codes for k-effective and power distribution calculations. Most likely this would start with the 4-bundle case, as it is the simplest representation of the F-Lattice. A deterministic approach may suggest an even more efficient means of parametric design studies. There are additional design parameters that need to be explored in greater detail. Significantly increased moderator pitch will affect the system thermo-hydraulics and should also be investigated more thoroughly. Finally, an investigation into isotopic burn-up and core life would provide crucial insight on the viability of the F-Lattice. A preliminary burn-up analysis of the 4-bundle case is given in Appendix D. (An "average" reactor assembly is burned for 1 month, in 1 day increments, and for 20 months, in 2 week increments. The control blades remain fully inserted for the entire duration of fuel burn.)

This thesis has provided the initial steps in validating the SCALE-5 package to analyze the F-Lattice design. K-effective and average flux values evaluated by SCALE-5 have been shown to be accurate. The package also evaluates accurate flux (power) distributions, though accurately extracting that information for comparison with MCNP5 results is not straight forward. Further validation for additional parametric studies and burn-up calculations are likely to "validate" the code for the F-Lattice design analysis.

References

Busch, R.D. and Bowman, S.M.. *KENO V.a Primer: A Primer for Criticality Calculations with SCALE/KENO V.a Using GeeWiz*. Report ORNL/TM-2005/135, Oak Ridge National Laboratory, 2005.

Challberg, R.C., "Simplified Core and Internals Design for the ESBWR," *Proceedings 6th International Conference on Nuclear Engineering,* (1998), ICONE-6066.

Clarno, K. et al., "Code-to-Code Benchmark of Coolant Void Reactivity (CVR) in the ACR-700 Reactor," *ANS Transactions* 93 (2005): 372-375.

Duderstadt, James J. and Hamilton, Louis J., *Nuclear Reactor Analysis.* New York: John Wiley and Sons, 1976.

Dupree, Stephen A. and Fraley, Stanley K, *A Monte Carlo Primer: A Practical Approach to Radiation Transport.* New York: Kluwer Academic/Plenum Publishers, 2003.

Fennern, L. et al., "Compact Modular BWR (CM-BWR)." *International Conference on Global Environment and Advanced Nuclear Power Plants* 1012: (2003).

Johnson, S. and Clarno, K. "Comparison of SCALE and MCNP Results for Computational Pebble Bed Benchmarks," *ANS Transactions* (2007).

Lamarsh, John R., *Introduction to Nuclear Reactor Theory*. Reading, Mass.: Addison - Wesley Pub. Co, 1966.

Landau, Rubin H., Páez, Manuel José and Bordeianu, Cristian C., *Computational Physics, Problem Solving with Computers,* 2nd ed. WILEY-VCH Verlag GMbH & Co. KGaA, Weinheim, 2007.

Lemey, L. and Colburn, R., *Sams Teach Yourself Perl in 21 Days,* 2nd ed. Sams Publishing, 2007.

Ragheb, M, "NPRE498 Monte Carlo Method Chapter 1," 2007, <https://netfiles.uiuc.edu/mragheb/www/> (2 September 2007).

Reis, V. et al., "Nuclear Fuel Leasing, Recycling, and Proliferation: Modeling A Global View," Nuclear Technology 150 (2005): 121-131.

SCALE: A Modular Code System for Performing Standardized Computer Analysis for Licensing Evaluations. Report ORNL/TM-2005/39, Version 5, Vols I-III, Oak Ridge National Laboratory, 2005.

SwiftGear. *Large Text File Viewer 4u*. 24 October 2005. <http://www.swiftgear.com> (3 April 2008)

Tari, Ilker. Homogenized Cross Section Determination using Monte Carlo Simulation. MS Thesis: Massachusetts Institute of Technology, 1994.

U.S. Department of Energy. Office of Nuclear Energy. Office of Fuel Cycle Management. *Global Nuclear Energy Partnership Strategic Plan*, 2007. GNEP-167312, Rev. 0.

X-5 Monte Carlo Team. *MCNP - General Monte Carlo N-paricle Transport Code, Version 5.* Los Alamos National Laboratory, 2003.

Appendix A: Efficiency Tests Sample Input Codes

SCALE-5.1/KENO-VI 10 divisions with 10,000 particles

```
'Input generated by GeeWiz SCALE 5.1 Compiled on November 9, 2006
=csas26 parm=(centrm)
kenovi blade test
238groupndf5
read composition
 uo2        1 1 300
                        92235 2
                        92238 98   end
 uo2        2 1 300
                        92235 3
                        92238 97   end
 uo2        3 1 300
                        92235 4
                        92238 96   end
 uo2        4 1 300
                        92235 5
                        92238 95   end
 h2o        5 1 300   end
end composition
read parameter
 npg=10000
 res=203
 flx=yes
 wrs=35
end parameter
read geometry
unit 1
com='2 blade'
 cuboid 1       5       0       20       0       10       0
 cuboid 2       5       0       20       0       20       0
 cuboid 3       5       0       20       0       30       0
 cuboid 4       5       0       20       0       40       0
 cuboid 5       5       0       20       0       50       0
 cuboid 6       5       0       20       0       60       0
 cuboid 7       5       0       20       0       70       0
 cuboid 8       5       0       20       0       80       0
 cuboid 9       5       0       20       0       90       0
 cuboid 10      5       0       20       0       100      0
 media 1 1 1
 media 1 1 2 -1
 media 1 1 3 -2
 media 1 1 4 -3
 media 1 1 5 -4
 media 1 1 6 -5
 media 1 1 7 -6
 media 1 1 8 -7
 media 1 1 9 -8
 media 1 1 10 -9
 boundary 10
unit 2
com='3 blade'
 cuboid 1       5       0       20       0       10       0
 cuboid 2       5       0       20       0       20       0
 cuboid 3       5       0       20       0       30       0
 cuboid 4       5       0       20       0       40       0
 cuboid 5       5       0       20       0       50       0
 cuboid 6       5       0       20       0       60       0
```

```
 cuboid 7        5       0       20      0       70      0
 cuboid 8        5       0       20      0       80      0
 cuboid 9        5       0       20      0       90      0
 cuboid 10       5       0       20      0       100     0
 media 2 1 1
 media 2 1 2 -1
 media 2 1 3 -2
 media 2 1 4 -3
 media 2 1 5 -4
 media 2 1 6 -5
 media 2 1 7 -6
 media 2 1 8 -7
 media 2 1 9 -8
 media 2 1 10 -9
 boundary 10
unit 3
com='4 blade'
 cuboid 1        5       0       20      0       10      0
 cuboid 2        5       0       20      0       20      0
 cuboid 3        5       0       20      0       30      0
 cuboid 4        5       0       20      0       40      0
 cuboid 5        5       0       20      0       50      0
 cuboid 6        5       0       20      0       60      0
 cuboid 7        5       0       20      0       70      0
 cuboid 8        5       0       20      0       80      0
 cuboid 9        5       0       20      0       90      0
 cuboid 10       5       0       20      0       100     0
 media 3 1 1
 media 3 1 2 -1
 media 3 1 3 -2
 media 3 1 4 -3
 media 3 1 5 -4
 media 3 1 6 -5
 media 3 1 7 -6
 media 3 1 8 -7
 media 3 1 9 -8
 media 3 1 10 -9
 boundary 10
unit 4
com='5 blade'
 cuboid 1        5       0       20      0       10      0
 cuboid 2        5       0       20      0       20      0
 cuboid 3        5       0       20      0       30      0
 cuboid 4        5       0       20      0       40      0
 cuboid 5        5       0       20      0       50      0
 cuboid 6        5       0       20      0       60      0
 cuboid 7        5       0       20      0       70      0
 cuboid 8        5       0       20      0       80      0
 cuboid 9        5       0       20      0       90      0
 cuboid 10       5       0       20      0       100     0
 media 4 1 1
 media 4 1 2 -1
 media 4 1 3 -2
 media 4 1 4 -3
 media 4 1 5 -4
 media 4 1 6 -5
 media 4 1 7 -6
 media 4 1 8 -7
 media 4 1 9 -8
 media 4 1 10 -9
 boundary 10
global unit 5
com='water cube'
 cuboid 1       45       0       30      0       110     0
 hole 1   origin  x=5 y=5 z=5
 hole 2   origin  x=15 y=5 z=5
 hole 3   origin  x=25 y=5 z=5
 hole 4   origin  x=35 y=5 z=5
 media 5 1 1
 boundary 1
```

```
end geometry
read bnds
  body=1
    surface(1)=mirror
    surface(2)=mirror
    surface(3)=mirror
    surface(4)=mirror
    surface(5)=vacuum
    surface(6)=vacuum
  end bnds
end data
end
=kmart6
read initial
 kunit=35
 xunit=4
 actbygrp
 rrpvol
 keno3d  40 KenoVI-10div-10.kmt
end initial
read activity
 92000 1007
 92000 1452
end activity
end
```

SCALE-5/KENO-Va 10 cm mesh with 10,000 particles

```
'Input generated by GeeWiz 5.0 Compiled on 04-30-2004
=csas25 parm=centrm
kenova 4 blade test
238groupndf5
read comp
 uo2         1 1 300 92235 2 92238 98 end
 uo2         2 1 300 92235 3 92238 97 end
 uo2         3 1 300 92235 4 92238 96 end
 uo2         4 1 300 92235 5 92238 95 end
 h2o         5 1 300 end
end comp
read parameter
 npg=10000
 res=203
 flx=yes
 plt=no
 wrs=35
 sig=0
 cfx=yes
 mfx=yes
 msh=10
 pms=yes
end parameter
read geometry
unit 1
com='2 blade'
 cuboid 1 1  5  0  20  0  100  0
unit 2
com='3 blade'
 cuboid 2 1  5  0  20  0  100  0
unit 3
com='4 blade'
 cuboid 3 1  5  0  20  0  100  0
unit 4
com='5 blade'
 cuboid 4 1  5  0  20  0  100  0
global unit 5
com='cube reactor'
 cuboid 5 1  45  0  30  0  110  0
```

```
  hole 4 35  5  5
  hole 3 25  5  5
  hole 2 15  5  5
  hole 1 5  5  5
end geometry
read bnds
 +xb=mirror
 -xb=mirror
 +yb=mirror
 -yb=mirror
 +zb=vacuum
 -zb=vacuum
end bnds
end data
end
=kmart
read initial
 kunit=35
 xunit=4
 actbygrp
 rrpvol
 keno3d  40 KenoVa-10cm10.kmt
end initial
read activity
 92000 1007
 92000 1452
end activity
end
```

MCNP5 10 cm mesh with 10,000 particles

```
4 Blade Test vs. SCALE5
C Cell Cards
1 1 -10.96 1 -2 3 -4 5 -6 imp:n=1 $ block 1
2 like 1 but mat=2 rho=-10.96 trcl=(10 0 0)
3 like 1 but mat=3 rho=-10.96 trcl=(20 0 0)
4 like 1 but mat=4 rho=-10.96 trcl=(30 0 0)
5 5 -0.9982 7 -8 9 -10 11 -12 #1 #2 #3 #4 imp:n=1
6 0 -7:8:-9:10:-11:12 imp:n=0

C Surface Cards
1 px 5.0
2 px 10.0
3 py 5.0
4 py 25.0
5 pz 5.0
6 pz 105.0
7 -7 px 0.0
8 -8 px 45.0
9 -9 py 0.0
10 -10 py 30.0
11 pz 0.0
12 pz 110.0

C Data Cards
C Material Cards
m1   92235.66c 5.1234e-5 92238.66c 0.002454
     8016.66c 0.00506
m2   92235.66c 7.6851e-5 92238.66c 0.002479
     8016.66c 0.005061
m3   92235.66c 1.02468e-4 92238.66c 0.002428
     8016.66c 0.005061
m4   92235.66c 1.28085e-4 92238.66c 0.002403
     8016.66c 0.005062
m5   1001.62c 2 8016.62c 1
mt5  lwtr.60t
C Control Cards
```

```
kcode 10000 1.0 50 203
ksrc 7.5 15 36.6 7.5 15 73.3
     17.5 15 36.6 17.5 15 73.3
     27.5 15 36.6 27.5 15 73.3
     37.5 15 36.6 37.5 15 73.3
FMESH4:n GEOM=xyz ORIGIN=0 0 0
         IMESH=50 IINTS=5
         JMESH=30 JINTS=3
         KMESH=110 KINTS=11
```

Appendix B: 4-bundle and 16-bundle Sample Input Files

SCALE-5/KENO-Va 4-bundle cell input file using a cuboid-defined global array and 3 cm mesh

```
'Input generated by GeeWiz 5.0 Compiled on 04-30-2004
=csas25 parm=centrm
4x4 kenova assembly
238groupndf5
read comp
 uo2         1 1 300 92235 2.5 92238 97.5 end
 zirc4       2 den=6.489 1 300 end
 ss304s       3 den=8 1 300 end
 h2o         4 den=1 1 300 end
 b4c         5 1 300 end
end comp
read celldata
  latticecell squarepitch fuelr=0.5544 1 gapr=0.5628 0 cladr=0.65352 2 hpitch=0.8505 4 end
    more data  szf=0.1      end more
end celldata
read parameter
 gen=800
 npg=10000
 nsk=250
 res=250
 flx=yes
 fdn=yes
 plt=no
 wrs=35
 sig=0
 cfx=yes
 pnm=0
 pmf=yes
 mfx=yes
 msh=3
 pms=yes
end parameter
read geometry
unit 1
com='fuel cell unit'
 zcylinder 1 1 0.5544  274.3  0
 zcylinder 0 1 0.5628  274.3  0
 zcylinder 2 1 0.65352  274.3  0
 cuboid 4 1  0.8505  -0.8505  0.8505  -0.8505  274.3  0
unit 2
com='bundle and canister (2,2), (2,4), (4,2) and (4,4)'
  array 1 0.1535  0.1535  0
 cuboid 4 1  13.7615  0.1535  13.7615  0.1535  274.3  0
 cuboid 3 1  13.915  0  13.915  0  274.3  0
unit 3
com='water in x (3,2) and (3,4)'
 cuboid 4 1  13.915  0  1.575  0  274.3  0
unit 4
com='water in y (2,3) and (4,3)'
 cuboid 4 1  1.575  0  13.915  0  274.3  0
unit 5
com='water in center (3,3)'
 cuboid 4 1  1.575  0  1.575  0  274.3  0
unit 6
com='left longest y cb (4,1)'
```

```
 cuboid 5 1  0.415  0  13.915  0  274.3  15.2
 cuboid 4 1  0.79  0  13.915  0  274.3  0
unit 7
com='left short y cb (3,1)'
 cuboid 5 1  0.415  0  1.575  0  274.3  15.2
 cuboid 4 1  0.79  0  1.575  0  274.3  0
unit 8
com='left medium y cb (2,1)'
 cuboid 5 1  0.415  0  11.12  0  274.3  15.2
 cuboid 4 1  0.79  0  13.915  0  274.3  0
unit 9
com='bottom longest x cb (5,2)'
 cuboid 5 1  13.915  0  0.415  0  274.3  15.2
 cuboid 4 1  13.915  0  0.79  0  274.3  0
unit 10
com='bottom short x cb (5,3)'
 cuboid 5 1  1.575  0  0.415  0  274.3  15.2
 cuboid 4 1  1.575  0  0.79  0  274.3  0
unit 11
com='bottom medium x cb ((5,4)'
 cuboid 5 1  11.12  0  0.415  0  274.3  15.2
 cuboid 4 1  13.915  0  0.79  0  274.3  0
unit 12
com='right longest y cb (2,5)'
 cuboid 5 1  0.79  0.375  13.915  0  274.3  15.2
 cuboid 4 1  0.79  0  13.915  0  274.3  0
unit 13
com='right short y cb (3,5)'
 cuboid 5 1  0.79  0.375  1.575  0  274.3  15.2
 cuboid 4 1  0.79  0  1.575  0  274.3  0
unit 14
com='right medium y cb (4,5)'
 cuboid 5 1  0.79  0.375  13.915  2.795  274.3  15.2
 cuboid 4 1  0.79  0  13.915  0  274.3  0
unit 15
com='top longest x cb (1,4)'
 cuboid 5 1  13.915  0  0.79  0.375  274.3  15.2
 cuboid 4 1  13.915  0  0.79  0  274.3  0
unit 16
com='top short x cb (1,3)'
 cuboid 5 1  1.575  0  0.79  0.375  274.3  15.2
 cuboid 4 1  1.575  0  0.79  0  274.3  0
unit 17
com='top medium x cb (1,2)'
 cuboid 5 1  13.915  2.795  0.79  0.375  274.3  15.2
 cuboid 4 1  13.915  0  0.79  0  274.3  0
unit 18
com='corner squares of water (1,1) and (5,5)'
 cuboid 4 1  0.79  0  0.79  0  274.3  0
unit 19
com='short x corner cb (lines up with 21)'
 cuboid 5 1  0.415  0  0.415  0  274.3  15.2
 cuboid 4 1  0.415  0  0.415  0  274.3  0
unit 20
com='long x corner cb (lines up with 22)'
 cuboid 5 1  0.375  0  0.415  0  274.3  15.2
 cuboid 4 1  0.375  0  0.415  0  274.3  0
unit 21
com='corner y cb (shorter than corner x) (with 19)'
 cuboid 5 1  0.415  0  0.375  0  274.3  15.2
 cuboid 4 1  0.415  0  0.375  0  274.3  0
unit 22
com='corner water square (with 20)'
 cuboid 4 1  0.375  0  0.375  0  274.3  0
unit 23
com='bottom left corner cb (5,1)'
  array 2 0  0  0
unit 24
com='top right corner cb (1,5)'
  array 3 30.195  30.195  0
```

```
global unit 25
  array 4 0  0  0
end geometry
read array
ara=1 nux=8 nuy=8 nuz=1
fill 64*1
end fill
ara=2 nux=2 nuy=2 nuz=1
fill 19 20 21 22
end fill
ara=3 nux=2 nuy=2 nuz=1
fill 22 21 20 19
end fill
ara=4 nux=5 nuy=5 nuz=1
fill 23 9 10 11 18 6 2 4 2 14 7 3 5 3 13 8 2 4 2 12 18 17 16 15 24
end fill
end array
read plot
 scr=yes
 ttl='test plot ncr'
 pic=mixtures
 xul=0
 yul=30.98
 zul=137.15
 xlr=30.98
 ylr=0
 zlr=137.15
 nax=800
 clr=1 255 0 0
     2 0 0 205
     3 0 229 238
     4 0 238 0
     5 205 205 0
 end color
 uax=1 vdn=-1
  end
end plot
read bnds
 +xb=mirror
 -xb=mirror
 +yb=mirror
 -yb=mirror
 +zb=vacuum
 -zb=vacuum
end bnds
end data
end
=kmart
read initial
 kunit=35
 xunit=4
 actbygrp
 rrpvol
 keno3d  40 3cm_MeshUpdateInUnit.kmt
end initial
read activity
 92000 1007
 92000 1452
end activity
end
```

SCALE-5/KENO-Va 16-bundle cell input file

```
'Input generated by GeeWiz 5.0 Compiled on 04-30-2004
=csas25 parm=centrm
16 bundle
238groupndf5
read comp
```

```
 uo2         1 1 300 92235 2.5 92238 97.5 end
 zirc4       2 den=6.489 1 300 end
 ss304s       3 den=8 1 300 end
 h2o         4 den=1 1 300 end
 b4c         5 1 300 end
end comp
read celldata
  latticecell squarepitch fuelr=0.5544 1 gapr=0.5628 0 cladr=0.65352 2 hpitch=0.8505 4 end
end celldata
read parameter
 gen=800
 npg=10000
 nsk=250
 res=800
 flx=yes
 fdn=yes
 wrs=35
 sig=0
 mfx=yes
 msh=10
 pms=yes
end parameter
read geometry
unit 1
com='fuel cell unit'
 zcylinder 1 1 0.5544  274.3  0
 zcylinder 0 1 0.5628  274.3  0
 zcylinder 2 1 0.65352  274.3  0
 cuboid 4 1  0.8505  -0.8505  0.8505  -0.8505  274.3  0
unit 2
com='bundle and canister (2,2), (2,4), (4,2) and (4,4)'
  array 1 0.1535  0.1535  0
 cuboid 4 1  13.7615  0.1535  13.7615  0.1535  274.3  0
 cuboid 3 1  13.915  0  13.915  0  274.3  0
unit 3
com='water in x (3,2) and (3,4)'
 cuboid 4 1  13.915  0  1.575  0  274.3  0
unit 4
com='water in y (2,3) and (4,3)'
 cuboid 4 1  1.575  0  13.915  0  274.3  0
unit 5
com='water in center (3,3)'
 cuboid 4 1  1.575  0  1.575  0  274.3  0
unit 6
com='left longest y cb (4,1)'
 cuboid 5 1  0.415  0  13.915  0  274.3  15.2
 cuboid 4 1  0.79  0  13.915  0  274.3  0
unit 7
com='left short y cb (3,1)'
 cuboid 5 1  0.415  0  1.575  0  274.3  15.2
 cuboid 4 1  0.79  0  1.575  0  274.3  0
unit 8
com='left medium y cb (2,1)'
 cuboid 5 1  0.415  0  11.12  0  274.3  15.2
 cuboid 4 1  0.79  0  13.915  0  274.3  0
unit 9
com='bottom longest x cb (5,2)'
 cuboid 5 1  13.915  0  0.415  0  274.3  15.2
 cuboid 4 1  13.915  0  0.79  0  274.3  0
unit 10
com='bottom short x cb (5,3)'
 cuboid 5 1  1.575  0  0.415  0  274.3  15.2
 cuboid 4 1  1.575  0  0.79  0  274.3  0
unit 11
com='bottom medium x cb ((5,4)'
 cuboid 5 1  11.12  0  0.415  0  274.3  15.2
 cuboid 4 1  13.915  0  0.79  0  274.3  0
unit 12
com='right longest y cb (2,5)'
 cuboid 5 1  0.79  0.375  13.915  0  274.3  15.2
```

```
 cuboid 4 1  0.79  0  13.915  0  274.3  0
unit 13
com='right short y cb (3,5)'
 cuboid 5 1  0.79  0.375  1.575  0  274.3  15.2
 cuboid 4 1  0.79  0  1.575  0  274.3  0
unit 14
com='right medium y cb (4,5)'
 cuboid 5 1  0.79  0.375  13.915  2.795  274.3  15.2
 cuboid 4 1  0.79  0  13.915  0  274.3  0
unit 15
com='top longest x cb (1,4)'
 cuboid 5 1  13.915  0  0.79  0.375  274.3  15.2
 cuboid 4 1  13.915  0  0.79  0  274.3  0
unit 16
com='top short x cb (1,3)'
 cuboid 5 1  1.575  0  0.79  0.375  274.3  15.2
 cuboid 4 1  1.575  0  0.79  0  274.3  0
unit 17
com='top medium x cb (1,2)'
 cuboid 5 1  13.915  2.795  0.79  0.375  274.3  15.2
 cuboid 4 1  13.915  0  0.79  0  274.3  0
unit 18
com='corner squares of water (1,1) and (5,5)'
 cuboid 4 1  0.79  0  0.79  0  274.3  0
unit 19
com='short x corner cb (lines up with 21)'
 cuboid 5 1  0.415  0  0.415  0  274.3  15.2
 cuboid 4 1  0.415  0  0.415  0  274.3  0
unit 20
com='long x corner cb (lines up with 22)'
 cuboid 5 1  0.375  0  0.415  0  274.3  15.2
 cuboid 4 1  0.375  0  0.415  0  274.3  0
unit 21
com='corner y cb (shorter than corner x) (with 19)'
 cuboid 5 1  0.415  0  0.375  0  274.3  15.2
 cuboid 4 1  0.415  0  0.375  0  274.3  0
unit 22
com='corner water square (with 20)'
 cuboid 4 1  0.375  0  0.375  0  274.3  0
unit 23
com='bottom left corner cb (5,1)'
  array 2 0  0  0
unit 24
com='top right corner cb (1,5)'
  array 3 30.195  30.195  0
unit 25
com='br corner'
  array 6 0  0  0
unit 26
com='tl corner'
  array 7 0  0  0
unit 27
com='br and tl assemblies'
  array 4 0  0  0
unit 28
com='tl and br assemblies'
  array 5 0  0  0
unit 29
com='unit 29'
 cuboid 5 1  0.415  0  13.915  2.795  274.3  15.2
 cuboid 4 1  0.79  0  13.915  0  274.3  0
unit 30
com='unit 30'
 cuboid 5 1  13.915  2.795  0.415  0  274.3  15.2
 cuboid 4 1  13.915  0  0.79  0  274.3  0
unit 31
com='unit 31'
 cuboid 5 1  0.79  0.375  11.12  0  274.3  15.2
 cuboid 4 1  0.79  0  13.915  0  274.3  0
unit 32
```

```
com='unit 32'
 cuboid 5 1  11.12  0  0.79  0.375  274.3  15.2
 cuboid 4 1  13.915  0  0.79  0  274.3  0
end geometry
read array
ara=1 nux=8 nuy=8 nuz=1
fill 64*1
end fill
ara=2 nux=2 nuy=2 nuz=1
fill 19 20 21 22
end fill
ara=3 nux=2 nuy=2 nuz=1
fill 22 21 20 19
end fill
ara=4 nux=5 nuy=5 nuz=1
fill 23 9 10 11 18 6 2 4 2 14 7 3 5 3 13 8 2 4 2 12 18 17 16 15 24
end fill
ara=5 nux=5 nuy=5 nuz=1
fill 18 30 10 9 25 29 2 4 2 12 7 3 5 3 13 6 2 4 2 31 26 15 16 32 18
end fill
ara=6 nux=2 nuy=2 nuz=1
fill 20 19 22 21
end fill
ara=7 nux=2 nuy=2 nuz=1
fill 21 22 19 20
end fill
ara=8 nux=2 nuy=2 nuz=1  gbl=8
fill 27 2*28 27
end fill
end array
read plot
 scr=yes
 ttl='test plot ncr'
 pic=mixtures
 xul=0
 yul=30.98
 zul=137.15
 xlr=30.98
 ylr=0
 zlr=137.15
 nax=800
 clr=1 255 0 0
     2 0 0 205
     3 0 229 238
     4 0 238 0
     5 205 205 0
 end color
 uax=1 vdn=-1
  end
end plot
read bnds
 +xb=periodic
 -xb=periodic
 +yb=periodic
 -yb=periodic
 +zb=vacuum
 -zb=vacuum
end bnds
end data
end
=kmart
read initial
 kunit=35
 xunit=4
 actbygrp
 rrpvol
 keno3d  40 16Bundle_Va_10000.kmt
end initial
read activity
 92000 1007
```

```
 92000 1452
end activity
end
```

SCALE-5.1 KENO-Va 4-bundle cell input file

```
' 'Input generated by GeeWiz SCALE 5.1 Compiled on November 9, 2006
=csas26 parm=(centrm)
4x4 bundle kenovi
238groupndf5
read composition
 uo2         1 1 300
                          92235 2.5
                          92238 97.5   end
 zirc4       2 den=6.489 1 300   end
 ss304s       3 den=8 1 300   end
 h2o         4 den=1 1 300   end
 b4c         5 1 300   end
end composition
read celldata
  latticecell squarepitch fuelr=0.5544 1 gapr=0.5628 0 cladr=0.65352 2 hpitch=0.8505 4 end
end celldata
read parameter
 gen=600
 npg=10000
 nsk=200
 res=200
 flx=yes
 wrs=35
 cfx=yes
end parameter
read geometry
unit 1
com='fuel cell unit'
 cylinder 1   0.5544    274.3        0
 cylinder 2   0.5628    274.3        0
 cylinder 3  0.65352    274.3        0
 cuboid 4   0.8505  -0.8505   0.8505  -0.8505    274.3        0
 media 1 1 1
 media 0 1 2 -1
 media 2 1 3 -2
 media 4 1 4 -3
 boundary 4
unit 2
com='8x8 bundle'
 cuboid 1  13.7615   0.1535  13.7615   0.1535    274.3        0
 cuboid 2   13.915        0   13.915        0    274.3        0
 array 1 1  place 1 1 1 1.004 1.004 0
 media 3 1 2 -1
 boundary 2
unit 3
com='y tall control balde'
 cuboid 1    0.415        0     27.4        0    259.1        0
 media 5 1 1
 boundary 1
unit 4
com='x long control blade'
 cuboid 1   26.985        0    0.415        0    259.1        0
 media 5 1 1
 boundary 1
global unit 5
com='4x4 bundle'
 cuboid 1    30.98        0    30.98        0    274.3        0
 hole 2   origin  x=0.79 y=0.79 z=0
 hole 2   origin  x=0.79 y=16.28 z=0
 hole 2   origin  x=16.28 y=16.28 z=0
 hole 2   origin  x=16.28 y=0.79 z=0
```

```
 hole 3   origin  x=0 y=0 z=15.2
 hole 4   origin  x=0.415 y=0 z=15.2
 hole 3   origin  x=30.565 y=3.58 z=15.2
 hole 4   origin  x=3.58 y=30.565 z=15.2
 media 4 1 1
 boundary 1
end geometry
read array
ara=1 nux=8 nuy=8 nuz=1 typ=square
 com='8x8 bundle'
 fill
    1    1    1    1    1    1    1    1
    1    1    1    1    1    1    1    1
    1    1    1    1    1    1    1    1
    1    1    1    1    1    1    1    1
    1    1    1    1    1    1    1    1
    1    1    1    1    1    1    1    1
    1    1    1    1    1    1    1    1
    1    1    1    1    1    1    1    1
 end fill
end array
read plot
 scr=yes
 ttl='test plot vi'
 pic=mixtures
 xul=0
 yul=30.98
 zul=137.15
 xlr=30.98
 ylr=0
 zlr=137.15
 nax=800
 clr=1 255 0 0
     2 0 0 205
     3 0 229 238
     4 0 238 0
     5 205 205 0
 end color
 uax=1 vdn=-1
  end
end plot
read bnds
  body=1
    surface(1)=mirror
    surface(2)=mirror
    surface(3)=mirror
    surface(4)=mirror
    surface(5)=vacuum
    surface(6)=vacuum
  end bnds
end data
end
=kmart6
read initial
 kunit=35
 xunit=4
 actbygrp
 rrpvol
 keno3d  40 4x4VInewRhob4c.kmt
end initial
read activity
1092235 1
1092238 1
1008016 1
 92000 1452
end activity
end
```

SCALE-5.1 KENO-Va 16-bundle cell input file

```
'Input generated by GeeWiz SCALE 5.1 Compiled on November 9, 2006
=csas26 parm=(centrm)
4x4 bundle kenovi
238groupndf5
read composition
 uo2         1 1 300
                          92235 2.5
                          92238 97.5   end
 zirc4       2 den=6.489 1 300   end
 ss304s      3 den=8 1 300   end
 h2o         4 den=1 1 300   end
 b4c         5 1 300   end
end composition
read celldata
  latticecell squarepitch fuelr=0.5544 1 gapr=0.5628 0 cladr=0.65352 2 hpitch=0.8505 4 end
end celldata
read parameter
 gen=600
 npg=10000
 nsk=200
end parameter
read geometry
unit 1
com='fuel cell unit'
 cylinder 1   0.5544    274.3        0
 cylinder 2   0.5628    274.3        0
 cylinder 3  0.65352    274.3        0
 cuboid 4   0.8505  -0.8505   0.8505  -0.8505    274.3        0
 media 1 1 1
 media 0 1 2 -1
 media 2 1 3 -2
 media 4 1 4 -3
 boundary 4
unit 2
com='8x8 bundle'
 cuboid 1  13.7615   0.1535  13.7615   0.1535    274.3        0
 cuboid 2   13.915        0   13.915        0    274.3        0
 array 1 1  place 1 1 1 1.004 1.004 0
 media 3 1 2 -1
 boundary 2
unit 3
com='y tall control balde'
 cuboid 1    0.415        0     27.4        0    259.1        0
 media 5 1 1
 boundary 1
unit 4
com='x long control blade'
 cuboid 1   26.985        0    0.415        0    259.1        0
 media 5 1 1
 boundary 1
unit 5
com='4x4 bundle bottom left'
 cuboid 1    30.98        0    30.98        0    274.3        0
 hole 2   origin  x=0.79 y=0.79 z=0
 hole 2   origin  x=0.79 y=16.28 z=0
 hole 2   origin  x=16.28 y=16.28 z=0
 hole 2   origin  x=16.28 y=0.79 z=0
 hole 3   origin  x=0 y=0 z=15.2
 hole 4   origin  x=0.415 y=0 z=15.2
 hole 3   origin  x=30.565 y=3.58 z=15.2
 hole 4   origin  x=3.58 y=30.565 z=15.2
 media 4 1 1
 boundary 1
unit 6
com='4x4 bundle bottom right'
 cuboid 1    30.98        0    30.98        0    274.3        0
```

```
 hole 2   origin  x=0.79 y=0.79 z=0
 hole 2   origin  x=0.79 y=16.28 z=0
 hole 2   origin  x=16.28 y=16.28 z=0
 hole 2   origin  x=16.28 y=0.79 z=0
 hole 3   origin  x=0 y=3.58 z=15.2
 hole 4   origin  x=0.415 y=30.565 z=15.2
 hole 3   origin  x=30.565 y=0 z=15.2
 hole 4   origin  x=3.58 y=0 z=15.2
 media 4 1 1
 boundary 1
global unit 7
com='4 assemblies'
 cuboid 1    61.96        0    61.96        0    274.3        0
 array 2 1  place 1 1 1 0 0 0
 boundary 1
end geometry
read array
ara=1 nux=8 nuy=8 nuz=1 typ=square
 com='8x8 bundle'
 fill
    1    1    1    1    1    1    1    1
    1    1    1    1    1    1    1    1
    1    1    1    1    1    1    1    1
    1    1    1    1    1    1    1    1
    1    1    1    1    1    1    1    1
    1    1    1    1    1    1    1    1
    1    1    1    1    1    1    1    1
    1    1    1    1    1    1    1    1
 end fill
ara=2 nux=2 nuy=2 nuz=1 typ=square
 com='1 assembly array'
 fill
    5    6
    6    5
 end fill
end array
read plot
 scr=yes
 ttl='test plot vi'
 pic=mixtures
 xul=0
 yul=30.98
 zul=137.15
 xlr=30.98
 ylr=0
 zlr=137.15
 nax=800
 plt=no
 clr=1 255 0 0
     2 0 0 205
     3 0 229 238
     4 0 238 0
     5 205 205 0
 end color
 uax=1 vdn=-1
  end
end plot
read bnds
  body=1
    surface(1)=periodic
    surface(2)=periodic
    surface(3)=periodic
    surface(4)=periodic
    surface(5)=vacuum
    surface(6)=vacuum
  end bnds
end data
end
```

MCNP5 4-bundle cell input file using a 3 cm mesh

```
F-Lattice Design with 3cm mesh 100,000 parts. b4c
C Cell Cards
1 1 -10.96 -1 4 -5 u=1 imp:n=1 $ Fuel
2 0        1 -2 4 -5 u=1 imp:n=1 $ Gap
3 2 -6.489 2 -3 4 -5 u=1 imp:n=1 $ Clad
4 3 -1.0 3 6 -7 8 -9 4 -5 u=1 imp:n=1 $ Water cell
5 0 -7 6 -9 8 -5 4 lat=1 fill=1 u=2 imp:n=1 $ Unit Cell
6 0 -10 11 -14 15 -5 4 fill=2 u=3 imp:n=1 $ Assembly - *Edit for Non-fuel cells*
7 4 -8.0 10 -12 17 -16 4 -5 u=3 imp:n=1 $ Canister right side
8 4 -8.0 13 -11 17 -16 4 -5 u=3 imp:n=1 $ Canister left side
9 4 -8.0 17 -15 11 -10 4 -5 u=3 imp:n=1 $ Cansiter y bottom
10 4 -8.0 14 -16 11 -10 4 -5 u=3 imp:n=1 $ Canister y top
11 0 -12 13 -16 17 -5 4 lat=1 fill=3 u=4 imp:n=1 $ Assembly/Canister
12 0 -12 13 -16 17 -5 4 fill=3 imp:n=1 $ Main assembly (2,2)
13 like 12 but trcl (0 -15.49 0)   $ assemblies
14 like 12 but trcl (-15.49 -15.49 0)
15 like 12 but trcl (-15.49 0 0)
C Control Blades
16 5 -2.52 (20 -23 28 -29 30 -5):(22 -23 26 -29 30 -5) imp:n=1 $ tr
17 5 -2.52 (18 -19 24 -27 30 -5):(18 -21 24 -25 30 -5) imp:n=1 $ bl
C Water
18 3 -1.0 18 -23 24 -29 4 -5
     #1 #2 #3 #4 #5 #6 #7 #8 #9 #10 #11 #12 #13 #14 #15 #16
     #17 imp:n=1
19 0        -4:5:-18:23:-24:29 imp:n=0

C Surface Cards
1 c/z 0.8505 0.8505 0.5544  $ fuel
2 c/z 0.8505 0.8505 0.5628  $ gap
3 c/z 0.8505 0.8505 0.65352  $ clad
4 pz 0.0  $ bottom z of fuel pin
5 pz 274.3  $ top z of fuel pin
6 px 0.0  $ left side of fuel cell
7 px 1.701  $ right side of fuel cell
8 py 0.0  $ bottom y side of fuel cell
9 py 1.701  $ top y side of fuel cell
C Main Assembly 1.535 mm Canister
10 px 6.804 $ right side assembly
11 px -6.804 $ left side assembly
12 px 6.9575 $ right side canister
13 px -6.9575 $ left side canister
14 py 6.804 $ top y side assembly
15 py -6.804 $ bottom y side assembly
16 py 6.9575 $ top y side canister
17 py -6.9575 $ bottom y side canister
C Main Control Blade
18 -18 px -23.235 $ left side of bl blade
19 px -22.82 $ right side of bl blade
20 px -19.655 $ = left side tr control blade
21 px 4.165 $ = right side of bl blade
22 px 7.33 $ || left side of tr control blade
23 -23 px 7.745 $ || right side of tr control blade
24 -24 py -23.235 $ bottom y of bl blade
25 py -22.82 $ top y of bl blade
26 py -19.655 $ || bottom y side tr blade
27 py 4.165 $ top y side bl blade
28 py 7.33 $ = top y side tr blade
29 -29 py 7.745 $ = top y side tr control blade
30 pz 15.2 $ bottom Z of control blade 6" above bottom Z fuel

C Data Cards
C Material Cards
C m1   92235.66c 0.025 92238.66c 0.975
C      8016.66c 2
m1   92235.66c 6.40638e-5 92238.66c 0.0024467
     8016.66c 0.005062
```

```
C m2   40000 -98.25 50000 -1.45 24000 -0.1   density =-0.400527
C     26000 -0.135 28000 -0.055 72000 -0.01
m2  24050.60c    -4.17e-005  $Zircaloy-4 (with ENDF-VI)
     24052.60c    -0.0008371 24053.60c    -9.67e-005 24054.60c    -2.45e-005
     26054.60c    -8.55e-005 26056.60c    -0.001378 26057.60c    -3.21e-005
     26058.60c     -4.4e-006 40000.60c       -0.9825 50000.42c        -0.015
m3   1001.62c 2 8016.62c 1
mt3  lwtr.60t
m4  6000.60c        -0.0003  $SS-304,SS-304L (with ENDF-VI)
     14000.60c        -0.005 15031.60c     -0.000225 16000.60c      -0.00015
     24050.60c      -0.00793 24052.60c     -0.159031 24053.60c     -0.018378
     24054.60c     -0.004661 25055.60c         -0.01 26054.60c     -0.039996
     26056.60c     -0.644764 26057.60c     -0.015026 26058.60c     -0.002039
     28058.60c      -0.06234 28060.60c     -0.024654 28061.60c     -0.001085
     28062.60c     -0.003504 28064.60c     -0.000917
m5   5010.60c 1.10847e-2 5011.60c 4.46176e-2 6000.60c 1.39256e-2 $ b4c
C Control Cards
kcode 100000 1.0 250 800
ksrc 0.8505 0.8505 137.15 -0.8505 0.8505 137.15 -0.8505 -0.8505 137.15
    0.8505 -0.8505 137.15 -14.6395 0.8505 137.15 -16.3405 0.8505 137.15
    -16.3405 -0.8505 137.15 -14.6395 -0.8505 137.15 0.8505 -14.6395 137.15
    -0.8505 -14.6395 137.15 -0.8505 -16.3405 137.15 0.8505 -16.3405 137.15
    -14.6395 -14.6395 137.15 -16.3405 -14.6395 137.15
    -16.3405 -16.3405 137.15 -14.6395 -16.3405 137.15
FMESH4:n GEOM=xyz ORIGIN=-23.235 -23.235 0 $ Flux on bottom z cross section
       IMESH=9.765 IINTS=11
       JMESH=9.765 JINTS=11
       KMESH=276   KINTS=92
       EMESH 0.225E-6 0.1 20 EINTS 1 1 1
```

MCNP5 16-bundle cell input file with flux profiles

```
F-Lattice Design 16 bundles. b4c. Cross Section Meshes
C Cell Cards
1 1 -10.96 -1 4 -5 u=1 imp:n=1 $ Fuel
2 0        1 -2 4 -5 u=1 imp:n=1 $ Gap
3 2 -6.489 2 -3 4 -5 u=1 imp:n=1 $ Clad
4 3 -1.0 3 6 -7 8 -9 4 -5 u=1 imp:n=1 $ Water cell
5 0 -7 6 -9 8 -5 4 lat=1 fill=1 u=2 imp:n=1 $ Unit Cell
6 0 -10 11 -14 15 -5 4 fill=2 u=3 imp:n=1 $ Assembly - *Edit for Non-fuel cells*
7 4 -8.0 10 -12 17 -16 4 -5 u=3 imp:n=1 $ Canister right side
8 4 -8.0 13 -11 17 -16 4 -5 u=3 imp:n=1 $ Canister left side
9 4 -8.0 17 -15 11 -10 4 -5 u=3 imp:n=1 $ Cansiter y bottom
10 4 -8.0 14 -16 11 -10 4 -5 u=3 imp:n=1 $ Canister y top
11 0 -12 13 -16 17 -5 4 lat=1 fill=3 u=4 imp:n=1 $ Assembly/Canister
12 0 -12 13 -16 17 -5 4 fill=3 imp:n=1 $ Main assembly (2,2)
13 like 12 but trcl (0 -15.49 0)   $ assemblies
14 like 12 but trcl (0 15.49 0)
15 like 12 but trcl (0 30.98 0)
16 like 12 but trcl (-15.49 -15.49 0)
17 like 12 but trcl (-15.49 0 0)
18 like 12 but trcl (-15.49 15.49 0)
19 like 12 but trcl (-15.49 30.98 0)
20 like 12 but trcl (15.49 -15.49 0)
21 like 12 but trcl (15.49 0 0)
22 like 12 but trcl (15.49 15.49 0)
23 like 12 but trcl (15.49 30.98 0)
24 like 12 but trcl (30.98 -15.49 0)
25 like 12 but trcl (30.98 0 0)
26 like 12 but trcl (30.98 15.49 0)
27 like 12 but trcl (30.98 30.98 0)
C Control Blades
28 5 -2.52 (18 -19 24 -25 26 -5):(22 -23 20 -21 26 -5) imp:n=1 $ center
29 5 -2.52 (27 -28 33 -35 26 -5):(27 -29 33 -34 26 -5) imp:n=1 $ bl
30 5 -2.52 (27 -28 36 -38 26 -5):(27 -29 37 -38 26 -5) imp:n=1 $ tl
31 5 -2.52 (30 -32 33 -34 26 -5):(31 -32 33 -35 26 -5) imp:n=1 $ br
32 5 -2.52 (30 -32 37 -38 26 -5):(31 -32 36 -38 26 -5) imp:n=1 $ tr
```

```
C Water
33 3 -1.0 27 -32 33 -38 4 -5
     #1 #2 #3 #4 #5 #6 #7 #8 #9 #10 #11 #12 #13 #14 #15 #16
     #17 #18 #19 #20 #21 #22 #23 #24 #25 #26 #27 #28 #29
     #30 #31 #32 imp:n=1
34 0        -4:5:-27:32:-33:38 imp:n=0

C Surface Cards
1 c/z 0.8505 0.8505 0.5544  $ fuel
2 c/z 0.8505 0.8505 0.5628  $ gap
3 c/z 0.8505 0.8505 0.65352  $ clad
4 pz 0.0  $ bottom z of fuel pin
5 pz 274.3  $ top z of fuel pin
6 px 0.0  $ left side of fuel cell
7 px 1.701  $ right side of fuel cell
8 py 0.0  $ bottom y side of fuel cell
9 py 1.701  $ top y side of fuel cell
C Main Assembly 1.535 mm Canister
10 px 6.804 $ right side assembly
11 px -6.804 $ left side assembly
12 px 6.9575 $ right side canister
13 px -6.9575 $ left side canister
14 py 6.804 $ top y side assembly
15 py -6.804 $ bottom y side assembly
16 py 6.9575 $ top y side canister
17 py -6.9575 $ bottom y side canister
C Main Control Blade
18 px 7.33 $ || left side main control blade
19 px 8.16 $ || right side main control blade
20 px -19.655 $ = left side main control blade
21 px 35.145 $ = right side main control blade
22 py 7.33 $ = bottom y side main control blade
23 py 8.16 $ = top y side main control blade
24 py -19.655 $ || bottom y side main control blade
25 py 35.145 $ || top y side main control blade
26 pz 15.2 $ bottom Z of control blade 6" above bottom Z fuel
C Border Control Blades
27 -32 px -23.235 $ left side of left blades
28 px -22.82 $ right side of left blades
29 px 4.165 $ right side of left top/bottom blades
30 px 11.335 $ left side of right top/bottom blades
31 px 38.31 $ left side of right blades
32 -27 px 38.725 $ right side of right blades
33 -38 py -23.235 $ bottom y of bottom blades
34 py -22.82 $ top y of bottom blades
35 py 4.165 $ top y side bottom blades
36 py 11.335 $ bottom y of top side blades
37 py 38.31 $ bottom y of top blades
38 -33 py 38.725 $ top y of top blades

C Data Cards
C Material Cards
C m1   92235.66c 0.025 92238.66c 0.975
C     8016.66c 2
m1   92235.66c 6.40638e-5 92238.66c 0.0024467
     8016.66c 0.005062
C m2   40000 -98.25 50000 -1.45 24000 -0.1   density =-0.400527
C     26000 -0.135 28000 -0.055 72000 -0.01
m2  24050.60c    -4.17e-005  $Zircaloy-4 (with ENDF-VI)
      24052.60c    -0.0008371 24053.60c    -9.67e-005 24054.60c    -2.45e-005
      26054.60c    -8.55e-005 26056.60c     -0.001378 26057.60c    -3.21e-005
      26058.60c     -4.4e-006 40000.60c       -0.9825 50000.42c        -0.015
m3   1001.62c 2 8016.62c 1
mt3  lwtr.60t
m4  6000.60c        -0.0003  $SS-304,SS-304L (with ENDF-VI)
      14000.60c       -0.005 15031.60c     -0.000225 16000.60c      -0.00015
      24050.60c      -0.00793 24052.60c     -0.159031 24053.60c     -0.018378
      24054.60c     -0.004661 25055.60c         -0.01 26054.60c     -0.039996
      26056.60c     -0.644764 26057.60c     -0.015026 26058.60c     -0.002039
      28058.60c      -0.06234 28060.60c     -0.024654 28061.60c     -0.001085
```

```
     28062.60c     -0.003504 28064.60c     -0.000917
m5   5010.60c 1.10847e-2 5011.60c 4.46176e-2 6000.60c 1.39256e-2 $ b4c
C Control Cards
kcode 50000 1.0 250 600
ksrc 0.8505 0.8505 137.15 -0.8505 0.8505 137.15 -0.8505 -0.8505 137.15
    0.8505 -0.8505 137.15 -14.6395 0.8505 137.15 -16.3405 0.8505 137.15
    -16.3405 -0.8505 137.15 -14.6395 -0.8505 137.15 0.8505 -14.6395 137.15
    -0.8505 -14.6395 137.15 -0.8505 -16.3405 137.15 0.8505 -16.3405 137.15
    -14.6395 -14.6395 137.15 -16.3405 -14.6395 137.15
    -16.3405 -16.3405 137.15 -14.6395 -16.3405 137.15
    0.8505 31.8305 137.15 -0.8505 31.8305 137.15 -0.8505 30.1295 137.15
    0.8505 30.1295  137.15 -14.6395 31.8305 137.15 -16.3405 31.8305 137.15
    -16.3405 30.1295 137.15 -14.6395 30.1295 137.15 0.8505 14.6395 137.15
    -0.8505 14.6395 137.15 -0.8505 16.3405 137.15 0.8505 16.3405 137.15
    -14.6395 14.6395 137.15 -16.3405 14.6395 137.15 -16.3405 16.3405 137.15
    -14.6395 16.3405 137.15
    31.8305 0.8505 137.15 31.8305 -0.8505 137.15 30.1295 -0.8505 137.15
    30.1295 0.8505 137.15 31.8305 -14.6395 137.15 31.8305 -16.3405 137.15
    30.1295 -16.3405 137.15 30.1295 -14.6395 137.15 14.6395 0.8505 137.15
    14.6395 -0.8505 137.15 16.3405 -0.8505 137.15 16.3405 0.8505 137.15
    14.6395 -14.6395 137.15 14.6395 -16.3405 137.15 16.3405 -16.3405 137.15
    16.3405 -14.6395 137.15
    31.8305 31.8305 137.15 31.8305 31.8305 137.15 30.1295 30.1295 137.15
    30.1295 30.1295 137.15 31.8305 31.8305 137.15 31.8305 31.8305 137.15
    30.1295 30.1295 137.15 30.1295 30.1295 137.15 14.6395 14.6395 137.15
    14.6395 14.6395 137.15 16.3405 16.3405 137.15 16.3405 16.3405 137.15
    14.6395 14.6395 137.15 14.6395 14.6395 137.15 16.3405 16.3405 137.15
    16.3405 16.3405 137.15
FMESH4:n GEOM=xyz ORIGIN=-23.235 -23.235 0
       IMESH=38.725 IINTS=30
       JMESH=38.725 JINTS=30
       KMESH=274.3   KINTS=274
       EMESH 0.225E-6 0.1 20 EINTS 1 1 1
FMESH14:n GEOM=xyz ORIGIN=-23.235 7.3715 136.4
       IMESH=38.725 IINTS=3098
       JMESH=8.1185 JINTS=1
       KMESH=137.4  KINTS=1
       EMESH 0.225E-6 0.1 20 EINTS 1 1 1
FMESH24:n GEOM=xyz ORIGIN=-23.235 .3505 136.4
       IMESH=38.725 IINTS=3098
       JMESH=1.3505 JINTS=1
       KMESH=137.5  KINTS=1
       EMESH 0.225E-6 0.1 20 EINTS 1 1 1
FMESH34:n GEOM=xyz ORIGIN=-23.235 -16.8405 136.4
       IMESH=38.725 IINTS=3098
       JMESH=-15.8405 JINTS=1
       KMESH=137.5  KINTS=1
       EMESH 0.225E-6 0.1 20 EINTS 1 1 1
```

Appendix C: FluxParse.pl

FluxParse.pl is a Perl script that operates on SCALE-5/KENO-Va output files containing superimposed mesh flux results. Flux results are organized to a per cell basis and reported in Flux.txt normalized to "per starting particle." A "volume averaging" error is present because only the model's total unit volume and total cell occurrences are reported. Individual cell "region volumes" are required to eliminate this error.

The DOS command to run this code, while in the same directory as the output file, is:

: > FluxParse.pl ScaleOutpitName.out

FluxParse.pl Script

```
#!/usr/bin/perl -w

#  Steven Weiss
#  FluxParse.pl
#  This data will find, organize and add up the fluxes for each location
# produced from a Scale5 - KenoV.a output for arbitrary Mesh Size in the
# x,y and z dimensions

# Output will be a tab delimited text file (Flux.txt) that can be easily
# converted into an Excel Worksheet format.

# Command Line:  > FluxParse.pl ScaleOutputName.out
# Make sure to have both files in the same directory or to correctly reference
# location.  Output will be to current directory

($scale_file) = @ARGV;

open(SCALE, $scale_file) or die "Cannot open $!";

@flux=[ [ [ ] ] ]; #initialize 3-dimensional array
@Vol=[ [ ] ]; #initialize 2-d array for volume info
$xmax=0;  # Used to keep track of length of each dimension
$ymax=0;
$zmax=0;

#Volume Info Finder
while (<SCALE>) {
   $line = $_;
```

```
    chomp($line);
    @test = split (' ',$line);
    if (@test > 3){
       if ("$test[1]" =~ "msh"){
          if ("$test[2]" =~ "mesh"){
          $mshVol = $test[8]*$test[8]*$test[8];
          }
       }
       if ("$test[0]" =~ "sum"){
          if ("$test[1]" =~ "of"){
             if ("$test[2]" =~ "mesh") {
                $line = <SCALE>;  #Skip down 4 lines from "sum of mesh
                $line = <SCALE>;   #volumes" to Data Desired
                $line = <SCALE>;
                $line = <SCALE>;
                chomp($line);
                @volume = split (' ',$line);
                $volume = @volume;
                $temp = 1; #pre-declare for scope reasons
                while ($volume < 9){
                   if ($volume == 7){ #First region of a unit
                      $unit = $volume[0];
                      $temp = $unit;
                      $region = $volume[2];
                      $Tvolume = $volume[4];
                      $NumUsed = $volume[6];
                   }
                   if ($volume == 6){ #First region of a unit no Mix #
                      $unit = $volume[0];
                      $temp = $unit;
                      $region = $volume[2];
                      $Tvolume = $volume[3];
                      $NumUsed = $volume[5];
                   }
                   if ($volume == 5){ #2nd+ region of a unit
                      $unit = $temp;
                      $region = $volume[0];
                      $Tvolume = $volume[2];
                      $NumUsed = $volume[4];
                   }
                   $Vol[$unit][$region] = $Tvolume / $NumUsed;
                   $line = <SCALE>;
                   @volume = split (' ',$line);
                   $volume = @volume;
                }
                if ($volume > 8){
                   goto MESH
                }

             }
          }
       }
    }
}
```

```
#Read output line by line searching for Mesh Fluxes
MESH: while (<SCALE>) {
   $line = $_;
   chomp($line);
   if ("$line" =~ "Mesh Fluxes") {
      $line = <SCALE>;  #Skip down 4 lines from "Mesh Fluxes" to Data Desired
      $line = <SCALE>;
      $line = <SCALE>;
      $line = <SCALE>;
      chomp($line);  #  Remove the \n or RETURN from end of line
      INNER: for ($count=1; $count<239; $count++) {
         @data = split (' ',$line);  #break line into individual columns
         #$energy = $data[0];
         $unit = $data[1];
         $region = $data[2];
         $xvalue = $data[3];
         $yvalue = $data[4];
         $zvalue = $data[5];
         $value = $data[6];
         #print($energy);print("\n");
         #print($unit);print("\n");
         #print($region);print("\n");
         #print($Leth[$energy]);print("\n");
         #print($Vol[$unit][$region]);print("\n");
         #print($value);print("\n");
         #$AddValue = (($value)*($Leth[$energy])*($Vol[$unit][$region]))/($Leth[0]);
         $AddValue = ($value) * ($Vol[$unit][$region])/($mshVol);
         #print($AddValue);print("\n");
         #$AddValue = 0;
         $flux[$xvalue][$yvalue][$zvalue]+= $AddValue; #add up fluxes at (x,y,z)
         if ($xvalue > $xmax){
            $xmax = $xvalue;
         }
         if ($yvalue > $ymax){
            $ymax = $yvalue;
         }
         if ($zvalue > $zmax){
            $zmax = $zvalue;
         }
         $line = <SCALE>;
         chomp($line);
      }
      $line = <SCALE>;  #skip blank lines after Energy Group 238
      $line = <SCALE>;
      chomp($line);
      @Size = split (' ',$line);
      # Here @Size > 0 implies not a blank line, meaning there is still
      # data for this region of the current unit
      # If @Size <0 then it is a blank line and code will search for the
      # next location of "Mesh Fluxes", ie, the next unit and region
      if (@Size > 0) {
         goto INNER
      }
   }
}
```

```
close(SCALE);
# output code in tab delimited format to be easily converted to Excel Format
open(OUTPUT, ">Flux.txt");
printf OUTPUT "X     Y      Z       Flux\n";
for($i=1; $i <= $xmax; $i++){
   for($j=1; $j <= $ymax; $j++) {
      for($k=1; $k <= $zmax; $k++){
         printf OUTPUT "$i     $j   $k          $flux[$i][$j][$k]\n";
      }
   }
}

close(OUTPUT);
```

Simple Test Case Verification

Two simple cases were used to test the results of FluxParse.pl before it was applied to the F-Lattice. The first test case was a homogeneous cube, 10 cm on each side, of UO_2 that is enriched to five weight percent Uranium-235. The second case tested was the simple plate fuel reactor described in Chapter 3 for use in the computational cost comparisons. The plate fuel geometry provides a multiple region problem, which introduces varying "region volume" sizes (and thus the volume averaging error) discussed in Chapter 4. The results are shown in Table C.1 and Table C.2 for the homogeneous cube and the slab geometries respectively. Accurate results are obtained for the average flux values; however there is some error in specific peak values due to the volume averaging error discussed in Chapter 4. The different (x, y, z) locations for the peak flux values in Table C.1 can be accounted for by the symmetry in the system.

Homogeneous Cube 1.0 cm Mesh							
	X	Y	Z	Peak Flux (n/cm^2-s)	% Error Relative to MCNP	Average Flux (n/cm^2-s)	% Error Relative to MCNP
MCNP	8.5	2.5	5.5	6.8192E+18	0.00	6.6782E+18	0.00
SCALE	1.5	7.5	4.5	6.7980E+18	-0.31	6.6590E+18	-0.29

Homogeneous Cube 5.0 cm Mesh							
	X	Y	Z	Peak Flux (n/cm^2-s)	% Error Relative to MCNP	Average Flux (n/cm^2-s)	% Error Relative to MCNP
MCNP	7.5	7.5	2.5	6.6880E+18	0.00	6.6782E+18	0.00
SCALE	2.5	7.5	7.5	6.6651E+18	-0.34	6.6590E+18	-0.29

Table C.1: Flux results for a simple homogeneous cube system.

Fuel plate Geometry 2 cm Mesh							
	X	Y	Z	Peak Flux (n/cm^2-s)	% Error Relative to MCNP	Average Flux (n/cm^2-s)	% Error Relative to MCNP
MCNP	23	17	55	6.4046E+16	0.00	2.7132E+16	0.00
SCALE	2	7	25	8.5171E+16	32.98	2.6685E+16	-1.65

Fuel plate Geometry 5 cm Mesh							
	X	Y	Z	Peak Flux (n/cm^2-s)	% Error Relative to MCNP	Average Flux (n/cm^2-s)	% Error Relative to MCNP
MCNP	22.5	17.5	57.5	5.7662E+16	0.00	2.7734E+16	0.00
SCALE	32.5	17.5	57.5	5.8576E+16	1.58	2.7132E+16	-2.17

Table C.2: Flux results for a slab geometry system.

Appendix D: Burn-up Calculations

Burn-up analysis is important to determine the core life, as well as how the power distribution changes with time. During operation, fuel composition changes in terms of quantity of fissile, fertile and poisoning isotopes. Fissile isotopes are consumed continuously as fissions take place, while fertile isotopes are transformed into additional isotopes. The production of poisonous isotopes, such as Xe-135, quickly accumulates and achieves an equilibrium state, which in turn helps regulate the reactivity of the system. At the same time, fission products, such as Cs-137, are produced. All of these reactions have an effect on core life, power distribution and reactivity. How the core changes with time is an important aspect of any reactor and must be investigated in detail.

A preliminary study of core burn-up was performed on the F-Lattice (4 bundle case). These results are given to provide preliminary insight into additional analysis of the F-Lattice that still must be carried out. The software used to carry out these calculations was the Oak Ridge National Laboratory codes, Origen 2.2 [Croff 1983] and Monteburns 2.0 [Poston and Trellue 2003]. Origen is an isotopic processing code for burn-up and decay of point reactors. Monteburns is capable of producing criticality and burn-up results by linking MCNP and Origen in an iterative loop. MCNP calculations are first performed on a problem to determine basic criticality properties (cross-section processing, power distribution, k-effective, etc…). Monteburns then collapses these results into a single point reactor, which is fed into Origen, where burn-up calculations are performed. Once a burn-up cycle has been completed, Monteburns edits the original MCNP input file with the new material compositions and cross-section information. MCNP is run again for the new iteration and this entire process (MCNP – Monteburns –

Origen – Monteburns – MCNP) is repeated for the desired number of time steps. For more information on Origen and Monteburns, refer to the documentation provided by Croff [1983] and by Poston and Trellue [2003], respectively.

Two tests were carried out on the F-Lattice, assuming a fresh core with an average burn rate of 9.80 MWt (control blades remain fully inserted over the entire duration of burn). The first burn-up calculation was performed for 1 month (31 days). Monteburns performed 31 outer burn steps (1 day intervals), which refers to the time step in which neutron fluxes are actualized with an MCNP simulation. 60 internal steps are performed with Origen between every out step. The Monteburns input file is included below for more details. The second test was performed for 20 months with 40 outer steps (2 week time steps) and 40 internal steps. K-effective calculations and important isotopic abundances were tracked. (For a preliminary study, and due to time constraints, MCNP5 simulations were run with reduced accuracy, using only 10,000 particles for 150 inactive cycles and 150 active cycles.)

Preliminary Burn-up Study Results

The results of the 1 month burn-up calculation with 1 day time steps are given in Figure D.1 – 7.

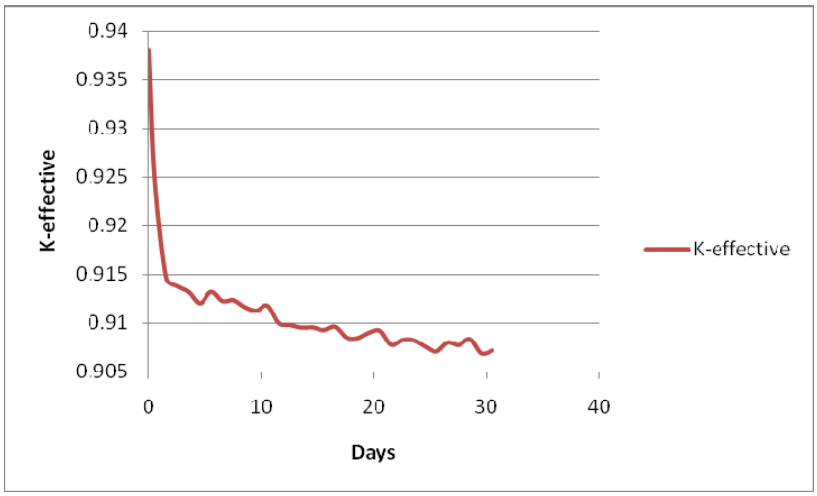

Figure D.1: K-effective results for 31 day burn with 1 day time steps.

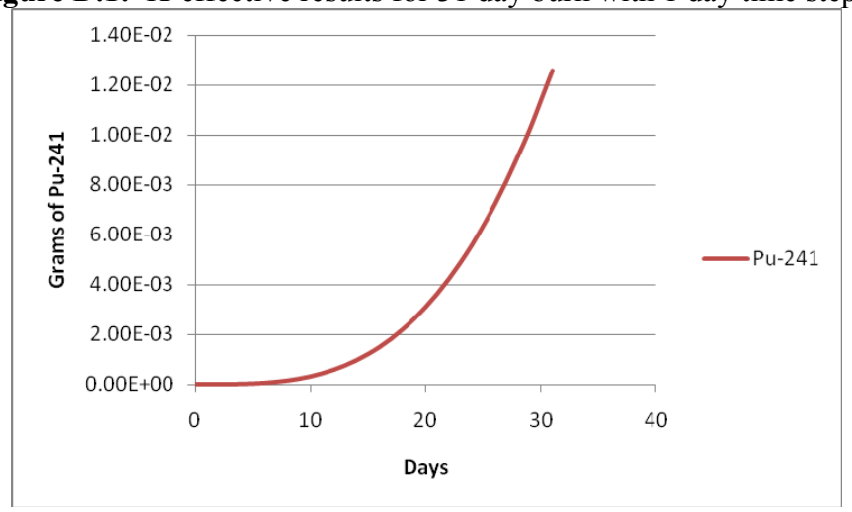

Figure D.2: Grams of Pu-241 in the reactor over 31 days with 1 day time steps.

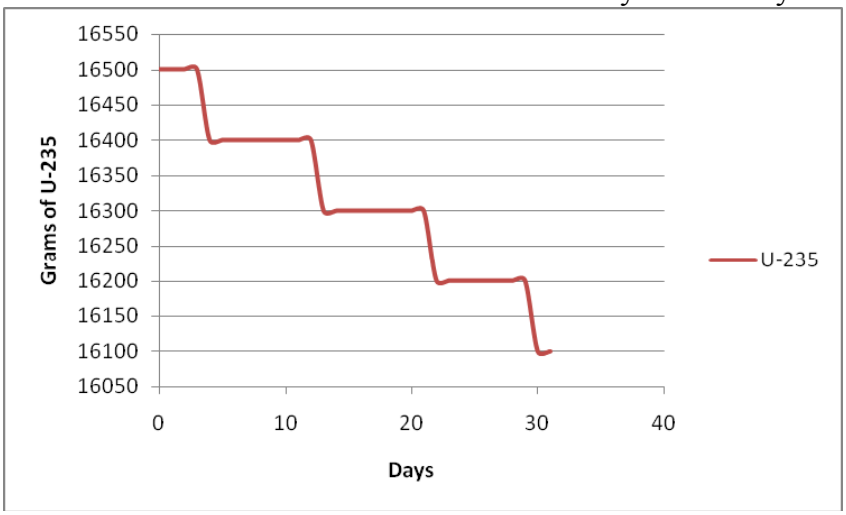

Figure D.3: Grams of U-235 in the reactor over 31 days with 1 day time steps.

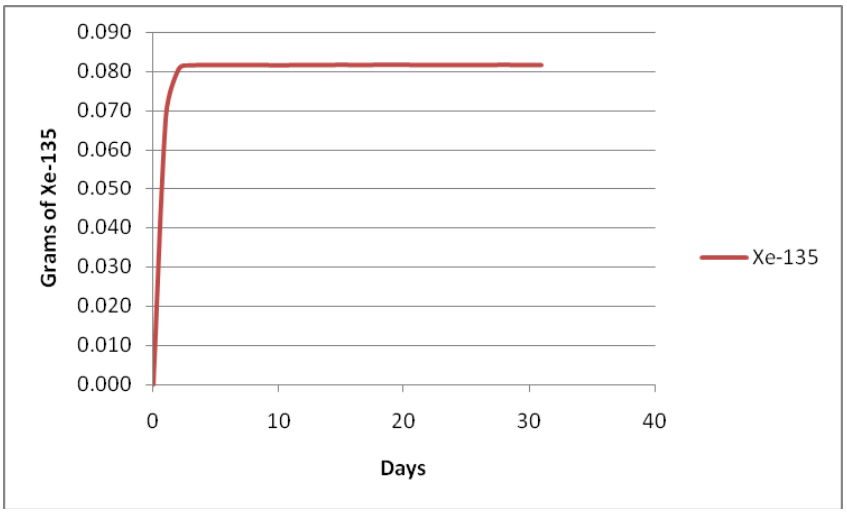

Figure D.4: Grams of Xe-135 in the reactor over 31 days with 1 day time steps.

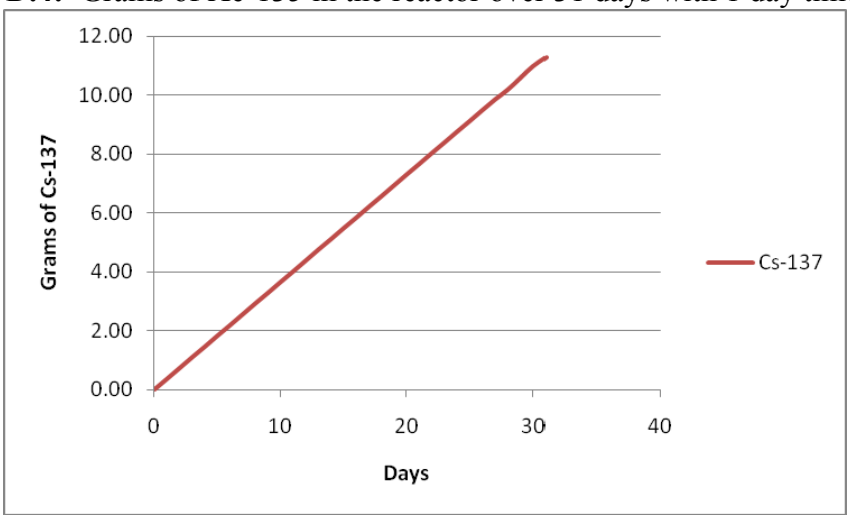

Figure D.5: Grams of Cs-137 in the reactor over 31 days with 1 day time steps.

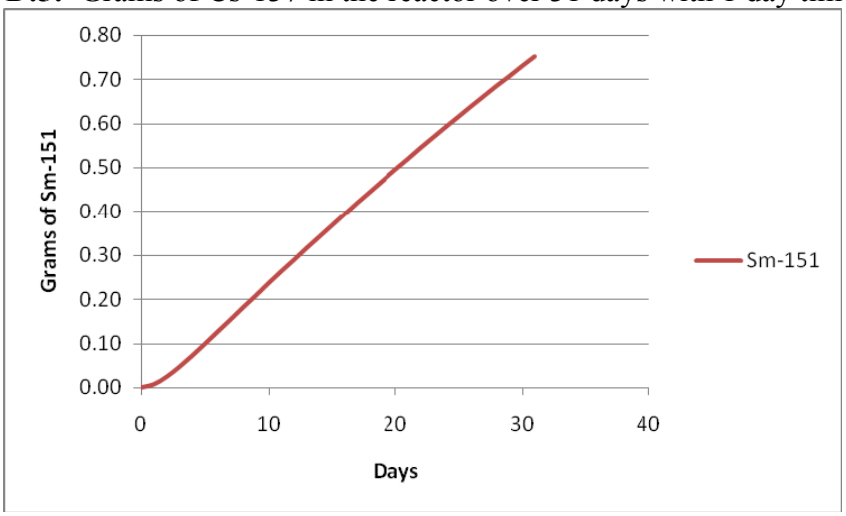

Figure D.6: Grams of Sm-151 in the reactor over 31 days with 1 day time steps.

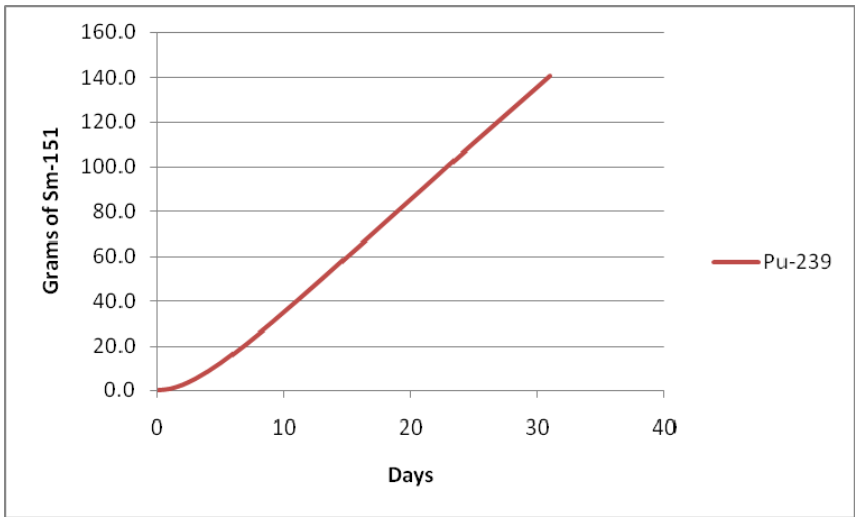

Figure D.7: Grams of Pu-239 in the reactor over 31 days with 1 day time steps.

The large drop in k-effective on the first day of burn is a result of the jump in Xe-135 present in the reactor. This well known Xenon posioning has a fast and dramatic effect on the core reactivity before it reaches an equilibrium state. Fission product accumulation of Pu-239, Cs-137 and Sm-151 are all linear. Grams of Pu-241 are produced at an increasingly faster rate as the burn continues. The quantity of U-235 decreases linearly but because of a lack of significant figures (only 2 decimal points are reported), Figure D.3 appears to change in step-wise fashion. Results for the 20 month burn with 2 week time steps show a more linear U-235 burn (Figure D.10). The final k-effective, at the end of 31 days, is 0.9072, a 3.3% decrease from the initial value of 0.9380.

Results for the 20 month burn, with 2 week time steps, are given in Figure D.8-14.

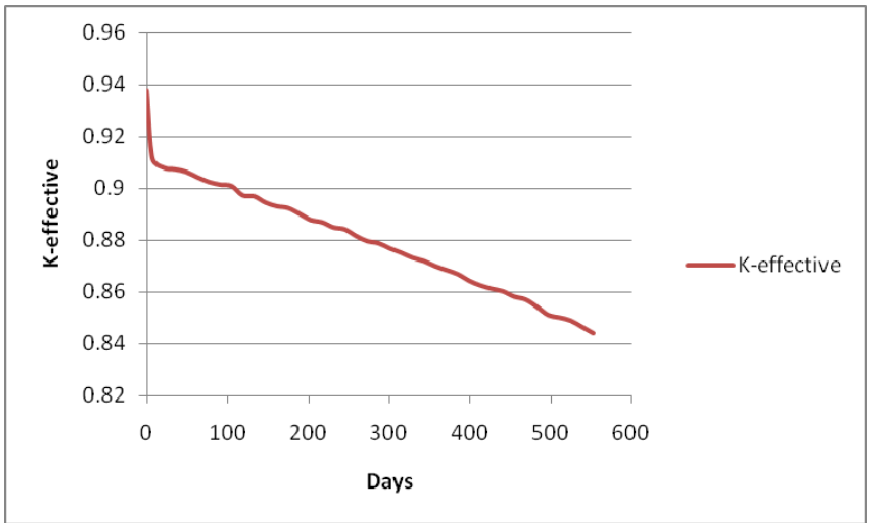

Figure D.8: K-effective results for 20 months burn with 2 week time steps.

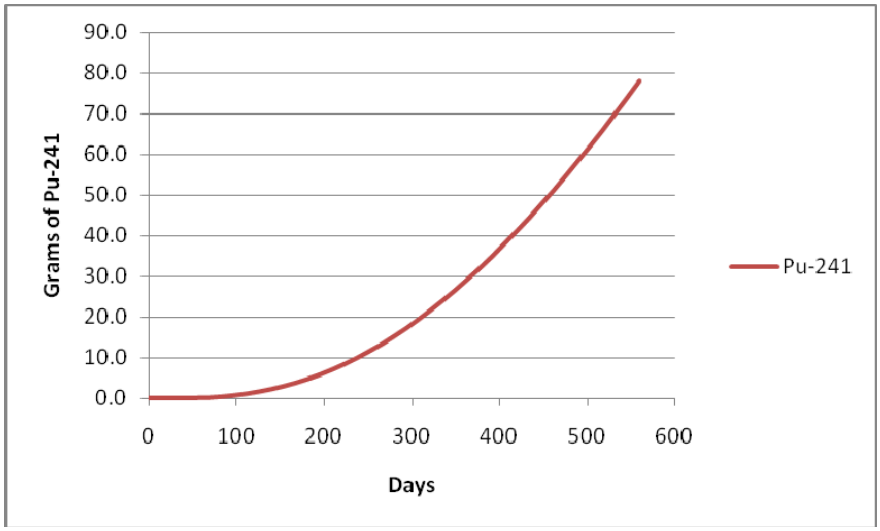

Figure D.9: Grams of Pu-241 in the reactor over 20 months with 2 week time steps.

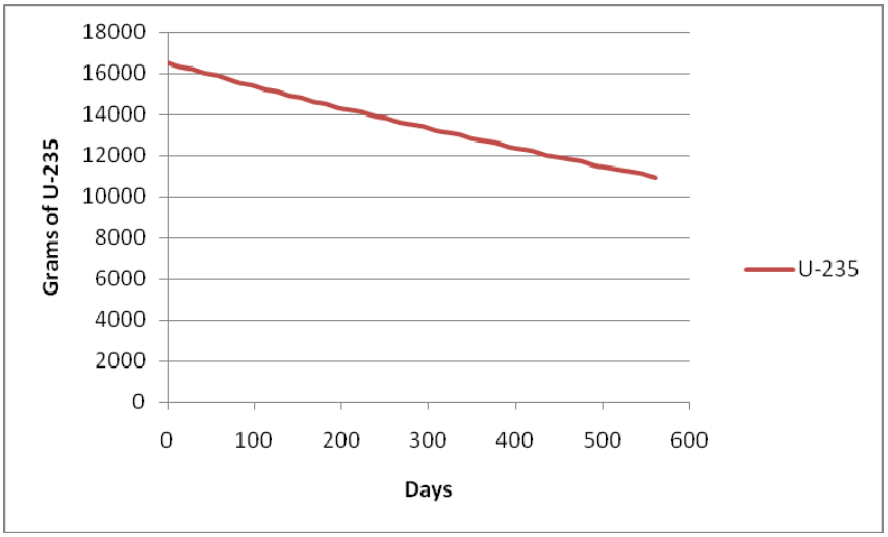

Figure D.10: Grams of U-235 in the reactor over 20 months with 2 week time steps.

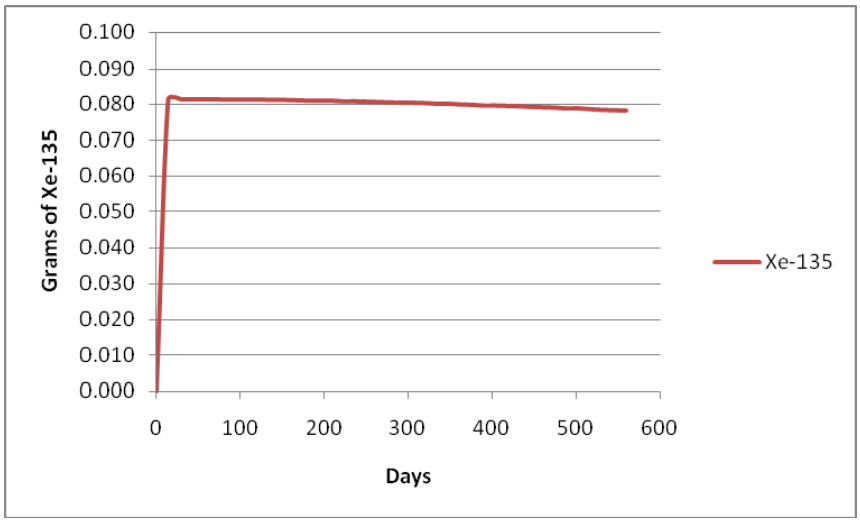

Figure D.11: Grams of Xe-135 in the reactor over 20 months with 2 week time steps.

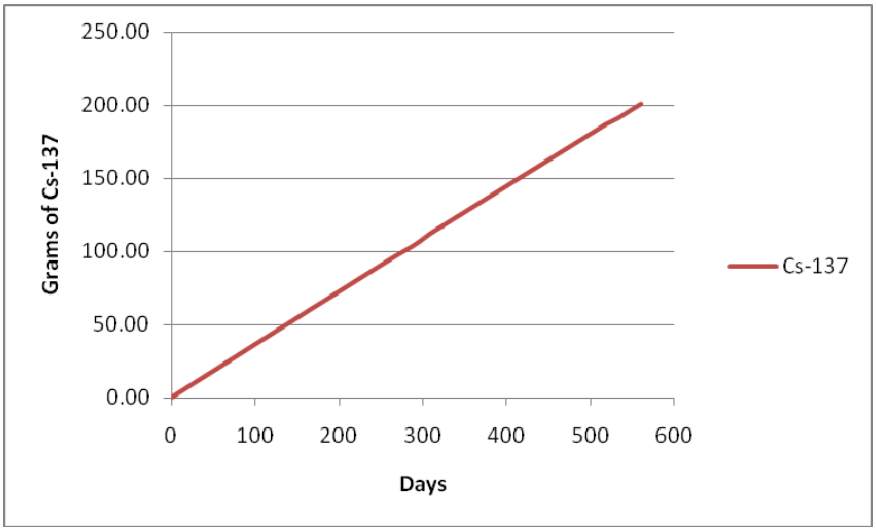

Figure D.12: Grams of Cs-137 in the reactor over 20 months with 2 week time steps.

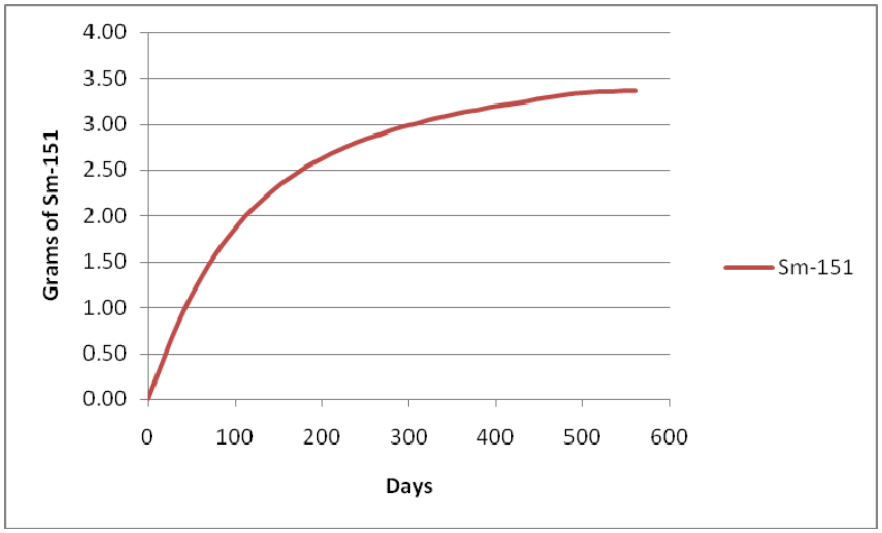

Figure D.13: Grams of Sm-151 in the reactor over 20 months with 2 week time steps.

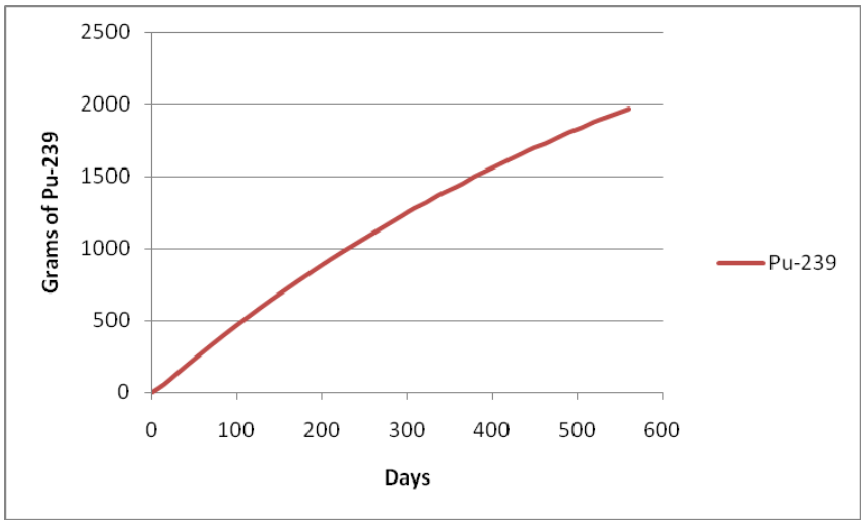

Figure D.14: Grams of Pu-239 in the reactor over 20 months with 2 week time steps.

Xenon posioning acheives and maintains an equilibrium of 0.08 grams present in the reactor after one burn step. Grams of Sm-151 no longer accumulate in a linear fashion for a core burn beyond 31 days (Figure D.13). U-235 decreases in a linear fashion for the entire burn. The final k-effective value is 0.8441, a 10.0% decrease from the initial value of 0.9380.

31 day burn Monteburns input file

```
Heatpipe Power System (HPS) 12 module core, 10 yr burn @ 750 kW
PC        ! Type of Operating System
1         ! Number of MCNP materials to burn
1         ! MCNP material number #1 (will burn all cells with this mat)
67805.1      ! Material #1 volume (cc), input 0 to use mcnp value (if exists)
2.45      ! Power in MWt (for the entire system modeled in mcnp deck)
-200.     ! Recov. energy/fis (MeV); if negative use for U235, ratio other isos
31.0     ! Total number of days burned (used if no feed)
31         ! Number of outer burn steps
60        ! Number of internal burn steps (multiple of 10)
1         ! Number of predictor steps (+1 on first step), 1 usually sufficient
0         ! Step number to restart after (0=beginning)
BWRU      ! number of default origen2 lib - next line is origen2 lib location
c:/origen22/libs
.001      ! fractional importance (track isos with abs,fis,atom,mass fraction)
0         ! Intermediate keff calc. 0) No 1) Yes
8         ! Number of automatic tally isotopes, followed by list.
92235.66c
92238.66c
54135.50c
55137.60c
48113.66c
```

62151.50c
94239.66c
94241.66c

20 month burn Monteburns input file

```
Heatpipe Power System (HPS) 12 module core, 10 yr burn @ 750 kW
PC        ! Type of Operating System
1         ! Number of MCNP materials to burn
1         ! MCNP material number #1 (will burn all cells with this mat)
67805.1      ! Material #1 volume (cc), input 0 to use mcnp value (if exists)
2.45      ! Power in MWt (for the entire system modeled in mcnp deck)
-200.     ! Recov. energy/fis (MeV); if negative use for U235, ratio other isos
560.0     ! Total number of days burned (used if no feed)
40        ! Number of outer burn steps
40        ! Number of internal burn steps (multiple of 10)
1         ! Number of predictor steps (+1 on first step), 1 usually sufficient
0         ! Step number to restart after (0=beginning)
BWRU      ! number of default origen2 lib - next line is origen2 lib location
c:/origen22/libs
.001      ! fractional importance (track isos with abs,fis,atom,mass fraction)
0         ! Intermediate keff calc. 0) No 1) Yes
8         ! Number of automatic tally isotopes, followed by list.
92235.66c
92238.66c
54135.50c
55137.60c
48113.66c
62151.50c
94239.66c
94241.66c
```

Author's Biography

Steven Weiss was born in Oak Park, Illinois on June 20th, 1985. He graduated from Downers Grove South High School in the spring of 2003. In the fall of 2003 he began his studies at the University of Illinois at Urbana-Champaign. In the summer of 2005, Steven took part in a study abroad program with the Hiroshima Institute of Technology in Hiroshima, Japan. In the spring of 2007 he graduated with a Bachelors of Science in nuclear engineering and minor in computer science and immediately began graduate school at the University of Illinois. Following the completion of this thesis, Steven will be joining Westinghouse Electric Company as a Nuclear Core Design Engineer, starting in the summer of 2008.